

IN-19

64272

NASA Contractor Report 189569

P.94

Final STS-35 "Columbia" Descent BET Products  
and Results for LaRC OEX Investigations

Kevin F. Oakes  
John T. Findlay  
Rachel A. Jasinski  
James S. Wood

**Flight Mechanics & Control, Inc.**  
47 East Queen's Way  
Hampton, VA 23669

CONTRACT NAS1-18937  
November 1991



National Aeronautics and  
Space Administration

**Langley Research Center**  
Hampton, Virginia 23665

(NASA-CR-189569) FINAL STS-35 COLUMBIA  
DESCENT BET PRODUCTS AND RESULTS FOR LaRC  
OEX INVESTIGATIONS (Flight Mechanics and  
Control) 94 p

N92-16013

CSCL 22B

Unclass

G3/19 0064272



## PREFACE

This is the first Orbiter Experiments (OEX) flight since the Challenger accident for which FM&C has been enjoined under Task Agreement Contract NAS1-18937 to provide NASA Langley Research Center (LaRC) with research quality descent Best Estimate Trajectory products. FM&C's prior efforts, as subcontractor to the Bionetics Corporation on their LaRC Contract NAS1-18267, involved archival and development of the trajectory reconstruction software, ENTREE, and the associated pre- and post-processing tools to enable this continued activity. The ENTREE System of Software, Reference 1 herein, was published as a comprehensive user's manual and the various output files were rigorously redefined to facilitate researchers in their post-flight data reduction activities. It is noted that the report was intended to be published as a four part manual but the tracking data pre-processors, planned as Part II, were never published since the ground tracking data interface had never been re-established after the stand-down. However, the file structure enabling use of the C-band tracking data via Johnson Space Center (JSC) has since been defined. In fact, sample data were obtained from the previous OEX flight (STS-32) as part of the software development and check-out. Consequently, FM&C was able to generate BET products for this earlier flight. This additional information has been made available to LaRC. We will publish these results, resources permitting, after completion of the next planned OEX flight, STS-40.

It should also be noted that our efforts on these two flights involved the first use of coherent Doppler data from the Tracking and Data Relay Satellite System (TDRSS) during descent to enable BET generation. This capability was developed for the Aeroassist Flight Experiment (AFE) project, more specifically, in support of the Aerodynamic Performance Experiment (APEX). These data provide an excellent alternative since ground-based S-band tracking data are no longer expected to be available via the Ground Spaceflight Tracking and Data Network (GSTDN) during descent. The support of the past (Mr. Chris Cerimele, EG3) and current (Mr. Matt Ondler, EG3) APEX Principal Investigator (PI) at JSC in the development of this capability is acknowledged. In addition, Mr. Paul Siemers of NASA LaRC must be acknowledged for his interest and support of this effort, both as Principal Investigator for the OEX Shuttle Entry Air Data System (SEADS), as well as his more recent dual role as AFE Project Scientist and co-PI on the Pressure Data/Air Data System (PD/ADS) experiment for that project. Also, the support of the LaRC OEX Data Manager (Ms. Joanne Hudgins) and her supporting Unisys contractors (Messrs. Glenn Bittner and Jim Rowe) is acknowledged. The efforts of these latter persons assured the prompt delivery and conversion of the necessary input data products received from JSC.

Finally, pursuant to the tracking data, one must acknowledge the support provided by JSC as well as the continued support by Goddard Space Flight Center (GSFC) personnel in the delivery of the TDRSS data. The C-band data were made available via the JSC BET contractor, RSOC. This activity is headed by Don Cooper, whose team provides operational BETs in support of the Navigation Section of the Orbit Analysis Branch. Consultation provided by Jon Weaver of that Section in resolving the appropriate identification and location for the high-rate Kwajalein station is acknowledged. To that end, the consultation provided by J. J. Blackburn (Bendix contractor at JSC), and both Jerry Wolfe and Pieter Hoffman-Heyden (network operations personnel at Kennedy Space Center) was greatly appreciated. GSFC personnel who have provided both data and invaluable consultations for this and past activities include: Osvaldo Cuevas of the Mission and Network Support Section (Code 553) and his Section Head, Kate Hartman, for the TDRSS ephemeris; J. A. Jackson, Head of the Trajectory and Tracking Analysis Section (Code 554) for the data delivery; Verna Reamy of Bendix for her invaluable insights; and, both J. B. Joyce (who has since moved on from his previous position as Head, Mission and Network Support Section) and J. Teles (Head, Flight Dynamics Branch) for their past and continued consultations.

## TABLE OF CONTENTS

SECTION	PAGE
PREFACE .....	i
LIST OF FIGURES AND TABLES .....	iv
LIST OF SYMBOLS, ACRONYMS AND SUBSCRIPTS .....	v
SUMMARY .....	1
I. INERTIAL TRAJECTORY RECONSTRUCTION .....	3
I. A. DYNAMIC DATA PROCESSING .....	3
I. B. TRACKING DATA PROCESSING .....	12
I. C. RECONSTRUCTION RESULTS .....	19
II. EXTENDED BET DEVELOPMENT .....	31
III. AERODYNAMIC BET DEVELOPMENT .....	38
IV. SUMMARY RESULTS .....	43
REFERENCES .....	52
APPENDIX A - FINAL C-BAND RESIDUALS FOR STS-35 TRAJECTORY RECONSTRUCTION .....	53
APPENDIX B - LISTING OF TRAJECTORY AND AIR-DATA PARAMETERS FOR THE STS-35 COLUMBIA OEX ENTRY MISSION .....	65

## LIST OF FIGURES AND TABLES

Figure No.	Page
I-1. Differences in derived body-axis dynamics, IMU1-IMU2 .....	6
I-2. Differences in derived body-axis dynamics, IMU1-IMU3 .....	7
I-3. Differences in derived body-axis dynamics, IMU2-IMU3 .....	8
I-4. STS-35 derived body-axis dynamics from IMU1 .....	9
I-5. STS-35 ground track and metric tracking coverage .....	17
I-6. STS-35 altitude profile and tracking timelines .....	18
I-7. Final TDRS1 Doppler residuals for STS-35 .....	26
I-8. Composite range residuals for STS-35 entry reconstruction .....	27
I-9. Composite azimuth residuals for STS-35 entry reconstruction .....	28
I-10. Composite elevation residuals for STS-35 entry reconstruction .....	29
I-11. KPTC residuals based on final BET for STS-35 .....	30
II-1. STS-35 temperature profile .....	33
II-2. Density profile for STS-35 .....	34
II-3. STS-35 pressure profile .....	35
II-4. Horizontal wind components versus altitude for STS-35 .....	36
II-5. STS-35 density and temperature comparisons .....	37
III-1. STS-35 RCS jet activity during entry .....	41
III-2. Time history of STS-35 control surface deflections .....	42
IV-1. Spacecraft angular rates versus Mach number during STS-35 entry .....	45
IV-2. STS-35 body-axis accelerations versus Mach number .....	46
IV-3. STS-35 control surface deflections versus Mach number .....	47
IV-4. STS-35 center-of-gravity versus Mach number .....	48
IV-5. STS-35 air-relative attitude angles versus Mach number .....	49
IV-6. STS-35 flight/databook lift, drag and L/D comparisons for which the predicted values are rectified by the FAD26 incrementals .....	50
IV-7. STS-35 axial force, normal force and pitching moment comparisons (databook rectified by FAD26, $C_m$ referenced to 65% X/L) .....	51

Table No.	Page
1. IMU matrices for STS-35 .....	4
2. STS-35 tracking station locations, refraction and other information .....	14
3. C-band biases determined for STS-35 .....	21
4. Final ENTREE parameter estimates for STS-35 .....	22
5. Summary of fit statistics for STS-35 .....	25
6. STS-35 mass properties .....	40

## LIST OF SYMBOLS, ACRONYMS AND SUBSCRIPTS

A	acceleration
ADDB	Aerodynamic Design Data Book
ADS	Air Data System (Orbiter side-probes)
AEROBET	Aerodynamic Best Estimate Trajectory
AFE	Aeroassist Flight Experiment
AF'78	1978 Air Force Reference Atmospheres
ALTAIR	ARPA Long-range Tracking, Acquisition and Instrumentation Radar
APEX	AFE Aerodynamic Performance Experiment
ARL	aerodynamic reference line
ARPA	Advanced Research Projects Agency
BET	Best Estimate Trajectory
C	computed tracking observables
$C_A$	axial force coefficient
$C_D$	drag coefficient
$C_L$	lift coefficient
$C_m$	pitching moment coefficient
$C_N$	normal force coefficient
CDC	Control Data Corporation
CG	center-of-gravity (also c.g.)
DFRF	NASA Dryden Flight Research Facility
EAFB	Edwards Air Force Base
EFFC	FPS-16 C-band radar at EAFB (see Table 2, p. 14)
EI	entry interface
ENTREE	Entry Trajectory Estimation Program
F	flight computed aerodynamic parameter
FAD	Flight Assessment Deltas
FM&C	Flight Mechanics and Control, Inc.
FPS	C-band radar type
fps	feet per second
FRCC	FPS-16 C-band radar at NASA DFRF (see Table 2, p. 14)
FRFC	FPS-16 C-band radar at NASA DFRF (see Table 2, p. 14)
g	gravitational acceleration
GMT	Greenwich Mean Time
GRAM	MSFC Global Reference Atmospheric Model
GSFC	NASA Goddard Space Flight Center
GSTDN	Ground Spaceflight Tracking and Data Network
h	altitude above Fischer ellipsoid (ALTDE in Appendix B)
HAIR	High Accuracy Instrumentation Radar
HiRAP	High Resolution Accelerometry Package

## LIST OF SYMBOLS, ACRONYMS AND SUBSCRIPTS (continued)

Hz	Hertz (Doppler units, cycles per second)
I	moment (or product) of inertia
IMU	Inertial Measurement Unit
JSC	NASA Johnson Space Center
kft	kilofeet
KMACH	Kwajalein P-Band ALTAIR radar (high-rate, see Table 2 herein)
KMACL	Kwajalein P-Band ALTAIR radar (low-rate, see Table 2 herein)
KPTC	FPQ-14 C-Band radar at Kaena Point, Hawaii
KSC	NASA Kennedy Space Center
LAIRS	Langley Atmospheric Information Retrieval System
LaRC	NASA Langley Research Center
LHDF	down-firing RCS jets, left side
LHUF	up-firing RCS jets, left side
L/D	lift-to-drag ratio
L7	body-axis version of final pre-operational ADDB
M	Mach number (MACH in Appendix B)
MSFC	NASA Marshall Space Flight Center
M50	Mean Equator and Equinox of 1950 inertial coordinate system
NASA	National Aeronautics and Space Administration
N/A	not applicable
NOAA	National Oceanic and Atmospheric Administration
O	tracking measurements
OEX	Orbiter Experiments
OI	Operational Instrumentation
P	roll rate
P	predicted aerodynamic parameter
PI	Principal Investigator
PMFC	FPS-16 C-band radar at Point Mugu, California (see Table 2, p. 14)
ppm	parts per million
PTPC	FPQ-6 C-band radar at Point Pillar, California
Q	pitch rate
q	dynamic pressure (QBAR in Appendix B)
R	yaw rate
RCS	Reaction Control System
REFSMMAT	Reference matrix, stable member to Mean 1950 (Table 1, pp. 4, 5)
RHDF	down-firing RCS jets, right side
RHUF	up-firing RCS jets, right side
RMS	root-mean-square

## LIST OF SYMBOLS, ACRONYMS AND SUBSCRIPTS (continued)

$R_N$	Reynolds number (RNUM in Appendix B)
RSOC	Rockwell Space Operations Company
SEADS	Shuttle Entry Air Data System
SILTS	Shuttle Infrared Leeside Temperature Sensing
SNFC	FPS-16 C-band radar on San Nicolas Island (see Table 2, p. 14)
STS	Space Transportation System
SUMS	Shuttle Upper Atmosphere Mass Spectrometer
S/C	spacecraft
T	atmospheric temperature
t	time from epoch
TDRSS	Tracking and Data Relay Satellite System
TDRS1	supporting satellite during STS-35 mission
TDSR	TDRSS south ground station at White Sands, New Mexico
TPQ	C-band radar type
u	southward wind component
v	westward wind component
VAFB	Vandenberg Air Force Base
VDBC	TPQ-18 C-band radar at VAFB (see Table 2, p. 14)
VDFC	FPS-16 C-band radar at VAFB (see Table 2, p. 14)
VDHC	C-band HAIR radar at VAFB (see Table 2, p. 14)
VDSC	FPS-16 C-band radar at VAFB (see Table 2, p. 14)
$V_A$	air relative velocity (VEL A, Appendix B)
$V_{bar}$	hypersonic viscous interaction parameter (VBAR in Appendix B)
$V_R$	Earth relative velocity
WONG	vehicle weight on nose gear
WOW	vehicle weight on wheels (main gear touchdown)
YAWN	RCS yaw jets firing to produce negative yaw
YAWP	RCS yaw jets firing to produce positive yaw

## GREEK SYMBOLS

$\alpha$	angle-of-attack (ALPHA in Appendix B)
$\beta$	sideslip angle (BETA in Appendix B)
$\gamma$	flight-path angle (GAM A in Appendix B)
$\delta$	control surface deflection
$\Delta$	denotes difference

## GREEK SYMBOLS (continued)

$\theta$	Euler pitch angle
$\lambda$	longitude
$\mu$	mean
$\rho$	atmospheric density
$\rho_{C_N}$	Shuttle-derived density
$\rho_{76}$	U.S. 1976 Standard Atmosphere density
$\sigma$	roll angle about velocity vector (SIGMA, Appendix B)
$\sigma$	standard deviation
$\phi$	Euler roll angle
$\Phi$	latitude
$\psi$	Euler yaw angle
$\Psi$	heading angle (HDG A in Appendix B)

## SUBSCRIPTS

$A$	aileron
$A$	air-relative parameter
$B$	body-axis parameter
$b$	bias
$BF$	bodyflap
$D$	geodetically referenced
$E$	elevator
$R$	planet-relative parameter
$R_A$	rudder, with respect to ARL
$SB_A$	speedbrake, with respect to ARL
$W$	weighted parameter
$X$	x-body axis
$Y$	y-body axis
$Z$	z-body axis

## SUMMARY

Presented herein are the final post-flight results from the Shuttle Columbia entry segment of the STS-35 mission, the fourth such mission to carry the full complement of the following Orbiter Experiments (OEX); the Shuttle Entry Air-Data System (SEADS), an upper-altitude mass spectrometer (SUMS), an infrared thermal-mapping experiment (SILTS), and the micro-g accelerometer package (HiRAP).

The inertial Best Estimate Trajectory (BET), IBETF35, was obtained based on the considerable C-band tracking data available during the flight, enhanced by the use of coherent 1 Hz TDRSS Doppler measurements available from Entry Interface (EI) to approximately 79 kft. Since no cinetheodolite data were available due to the lighting conditions at landing, processing of pseudo altimeter and Doppler data during roll-out on Runway 22 were also included. Tracking data considerations and problems peculiar to this mission are further discussed in Section I of this report. In summary, resolving the appropriate tracker locations for both the high- and low-rate Kwajalein data, as well as quantifying the apparent bad measurements from the Hawaii and Point Pillar passes are discussed. Other editing considerations, to include inconsistencies between the upper altitude data and the coastal radars, and the rather large C-band angular bias determinations, are discussed as part of the actual trajectory reconstruction (refer to Section I. C). Inertial Measurement Unit (IMU) data processing and the resultant selection of IMU1 as the dynamic data source for the reconstruction are also discussed as part of Section I herein. Though the derived, equivalent body-axis dynamics suggested by each of the IMUs compared well as expected, it is noted that instrument parameters were necessarily included in the final trajectory determination to obtain the best, contiguous, top-down reconstruction.

The Inertial BET solution was anchored at an epoch of 19,200<sup>s</sup> GMT on December 11, 1990. At this epoch, the corresponding altitude was approximately 513 kft. As previously stated, the final estimate required the use of an expanded solution set to obtain a maximum-likelihood estimate that best fit the measurements throughout the entire descent time frame. In addition to solving for the usual Shuttle position, velocity, and attitude at epoch, three accelerometer scale-factors and three gyro biases were incorporated. The expanded state was necessary, even after inclusion of the aforementioned C-band biases, because the more simple, state-only estimate did not yield a reasonable fit to the entire complement of tracking data. Section I. C herein presents further details as to the nature of and goodness-of-fit obtained for the final estimate.

The only available STS-35 atmospheric data source was the National Oceanic and Atmospheric Administration (NOAA) "totem-pole" profile data usurped from the Johnson Space Center (JSC) BET generated by RSOC. Upper altitude density comparisons between Shuttle-derived results and model data were made to substantiate the NOAA profile. This atmosphere was utilized for the generation of both the Extended BET (EBETF35) and the Aerodynamic BET (ABETF35). Extended BET discussions are included in Section II of this report.

In Section III, AEROBET considerations and development of same are discussed. Summary results are presented in Section IV. Shown are Shuttle configuration data and longitudinal aerodynamic performance comparisons. For the latter, percentage differences between the flight-derived and predicted coefficients are shown, where the predicted results are based on the final pre-operational data book values. In some instances, configuration data and aerodynamic comparisons are correlated versus past ensemble results from previous Shuttle entry flights, up to and including STS 61-C, the first OEX mission. Where aerodynamic performance comparisons are presented versus the equivalent flight-derived parameters, the predicted coefficients based on the final pre-operational databook are updated based on the final published Flight Assessment Deltas (FAD26).

The Inertial BET, Extended BET, and AEROBET are all available to LaRC researchers as semi-private files under User Catalog 274885C on the NASA LaRC Control Data Corporation (CDC) computers. Due to size considerations, the AEROBET is a direct access file whereas the other two files are indirect access files. Two Appendices are included which present the final tracking data residual plots (Appendix A) and a listing of relevant AEROBET state vector and air-data parameters (Appendix B).

## I. INERTIAL TRAJECTORY RECONSTRUCTION

### I. A. DYNAMIC DATA PROCESSING

The OI-1 data containing the tri-redundant IMU data for this flight were received from LaRC (converted by Unisys for CDC use) as nine-track physical reel NX0513. These data were reformatted using PREOI1 and edited using the PRETMS utility prior to deriving the equivalent "strapped-down" data using the PREIMUS cubic-spline algorithms. Readers can refer to the software discussions presented in Part I of the ENTREE System of Software user's manual (Reference 1) for further insights as to the need for, and extent of, IMU pre-processing.

It is noted herein that the data for this flight were essentially devoid of any significant time gaps, apart from the occasional 1.12 and 1.92 second skips that are expected due to the incompatibility between the downlist rate and the fundamental 6.25 Hz operating frequency of the IMUs. Though each IMU compared favorably, IMU1 was selected as the source for STS-35 reconstruction. This choice was substantiated by comparing the equivalent body-axes data derived from the accumulated sensed velocity changes and attitude quaternions separately measured by each IMU during entry. Differences between the equivalent (derived) body-axes data from the three sources are presented in Figures I-1 through I-3. Figure I-1 shows the differences (derived at the IMU downlist rate for this analysis) between IMU1 and IMU2. Annotated thereon are the computed mean ( $\mu$ ) and standard deviation ( $\sigma$ ) in the differences for each component. Similarly, Figure I-2 shows comparisons between the derived IMU1 and IMU3 results, and Figure I-3 depicts similar results between IMU2 and IMU3. Time zero on these plots corresponds to the selected processing epoch for this mission (19,200 GMT seconds). It can be seen that there are only subtle discrepancies between the various IMUs. For the most part, though certainly not critical, the isolated "spikes" can be identified as more germane to the data from IMU2 and IMU3, indicating that the data from IMU1 were better.

As information, Figure I-4 is included to show the actual body-axes rates and accelerations derived from the IMU1 measurements. Presented are the spacecraft roll rate ( $P_B$ ), pitch rate ( $Q_B$ ), yaw rate ( $R_B$ ), and accelerations along the X, Y, and Z body axes. These data are plotted from epoch throughout the entire entry phase, subdivided into three 700 second intervals to show the ongoing dynamics. It is noted that the acceleration data shown thereon are below the IMU measurement threshold ( $\approx 1$  milli-g) for the first 300 seconds.

For completeness, as well as satisfy archival requirements, the following table (Table 1) is included which defines the various IMU matrices for STS-35. These are the Columbia orbiter-unique transformation between the navigation base and the body axes, and the IMU specific matrices which define transformations between the navigation base and the outer roll gimbal (the stable member) and the so-called REFSMMATs which orient the stable platform to the inertial M50 system. Inspection of these matrices indicates that both IMU 1 and 3 were changed-out since the last Columbia mission (STS-32). Again, readers are referred to Part I of Reference 1 for more information concerning the rigorous IMU treatment utilizing these matrices.

---

Navigation base to body matrix

0.982956500000	0.000436332300	- 0.183837900000
- 0.000452950800	0.999999900000	- 0.000048404800
0.183837900000	0.000130849300	0.982956600000

Navigation base to outer roll gimbal matrices

IMU1

0.999999615063	0.000834364233	- 0.000271495562
- 0.000834364202	0.999999651918	0.000000226526
0.000271495657	0.000000000000	0.999999963145

IMU2

0.999995413970	0.002305187539	0.001961801379
- 0.002305210043	0.999997338223	0.000009252310
- 0.001961774830	- 0.000013774632	0.999998075741

IMU3

0.999991103679	0.004149357326	- 0.000754459966
- 0.004149344094	0.999991388317	0.000019031280
0.000754532435	- 0.000015900597	0.999999715378

**Table 1. IMU matrices for STS-35.**

Reference matrices: stable member to Mean of 1950

IMU1

0.051770310849	- 0.757755279541	0.650481879711
- 0.259236693382	0.618830084801	0.741515696049
- 0.964425265789	- 0.207017302513	- 0.164400935173

IMU2

- 0.772230446339	0.147799253464	0.617912113667
0.564199090004	- 0.287655889988	0.773907840252
0.292129099369	0.946260750294	0.138748407364

IMU3

0.408958375454	0.401200652122	0.819628596306
- 0.616607129574	- 0.540627181530	0.572291731834
0.672717332840	- 0.739432334900	0.026289150119

Table 1. IMU matrices for STS-35 (concluded).

---

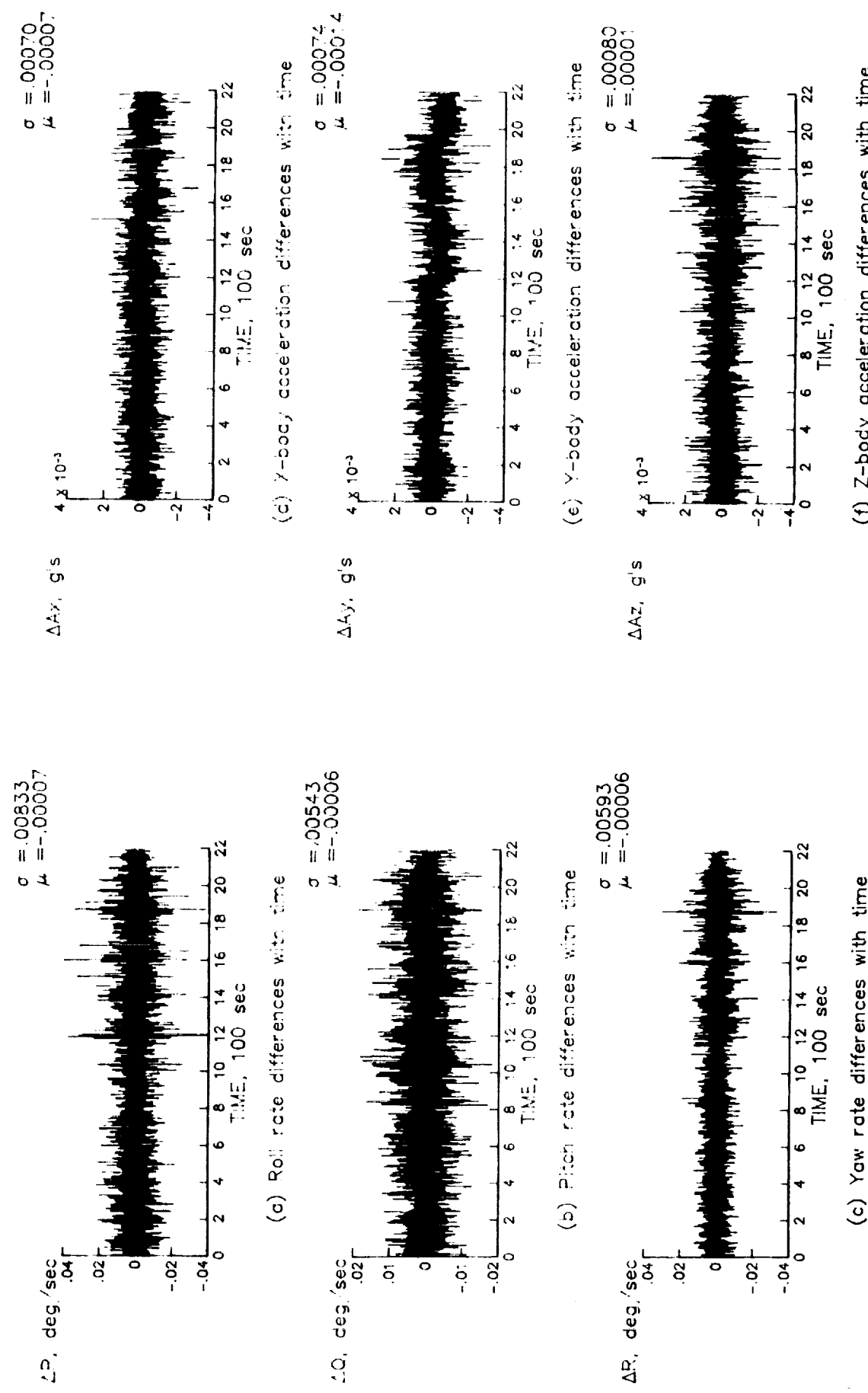


Figure I-1. Differences in derived body-axis dynamics, IMU1 - IMU2.

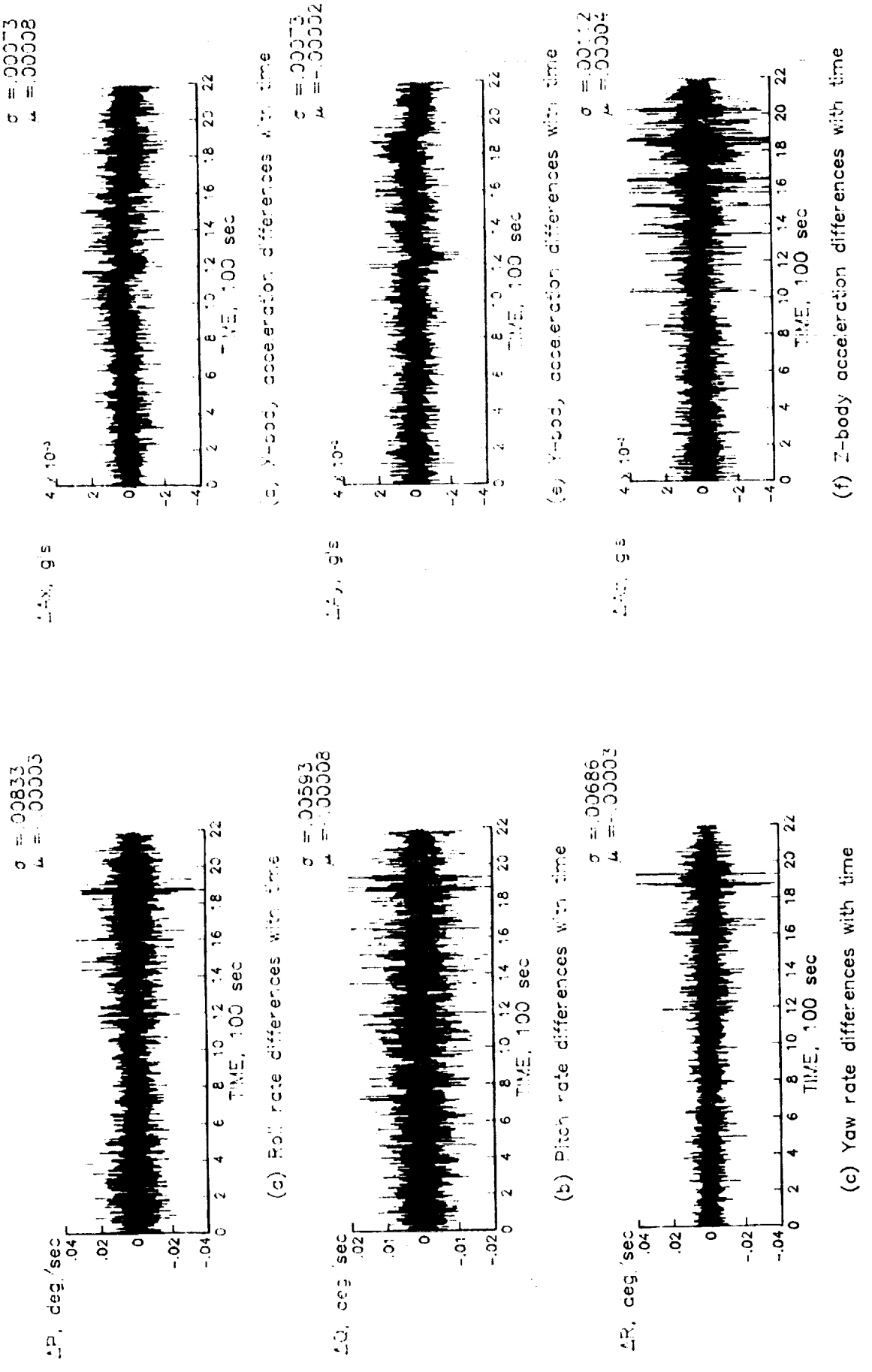
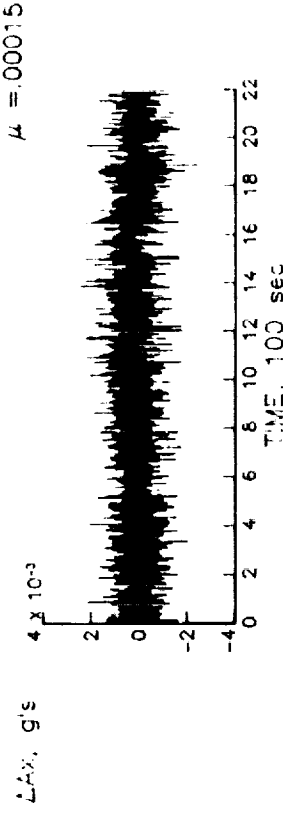
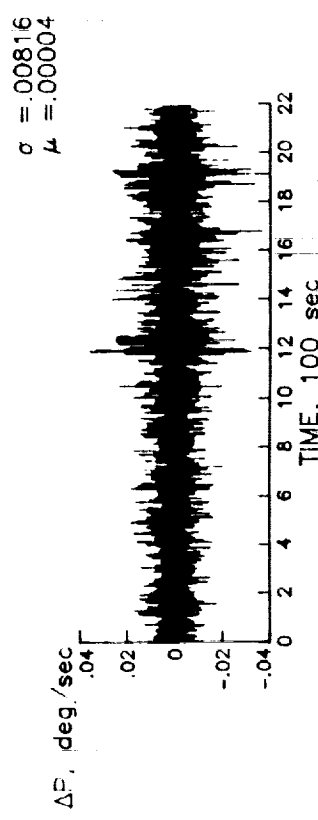
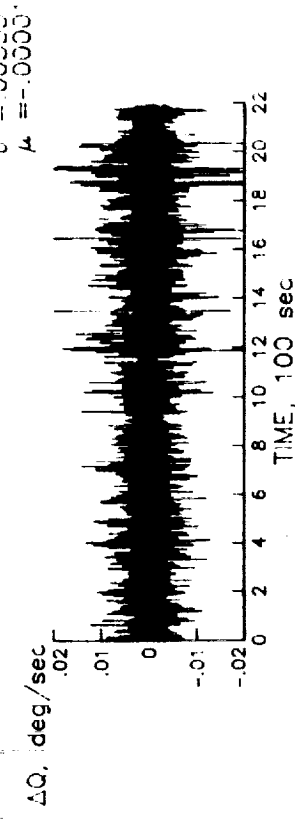


Figure I-2. Differences in derived body-axis dynamics, IMU1 - IMU3.

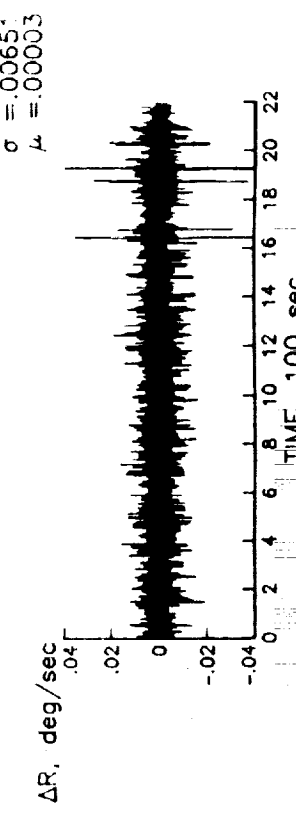
ORIGINAL PAGE IS  
OF POOR QUALITY



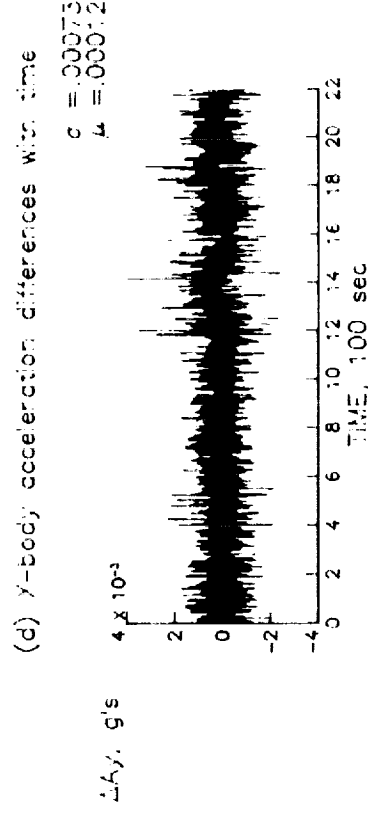
(a) Roll rate differences with time



(b) Pitch rate differences with time



(e) γ-body acceleration differences with time



(f) Z-body acceleration differences with time

Figure I-3. Differences in derived body-axis dynamics, IMU2 - IMU3.

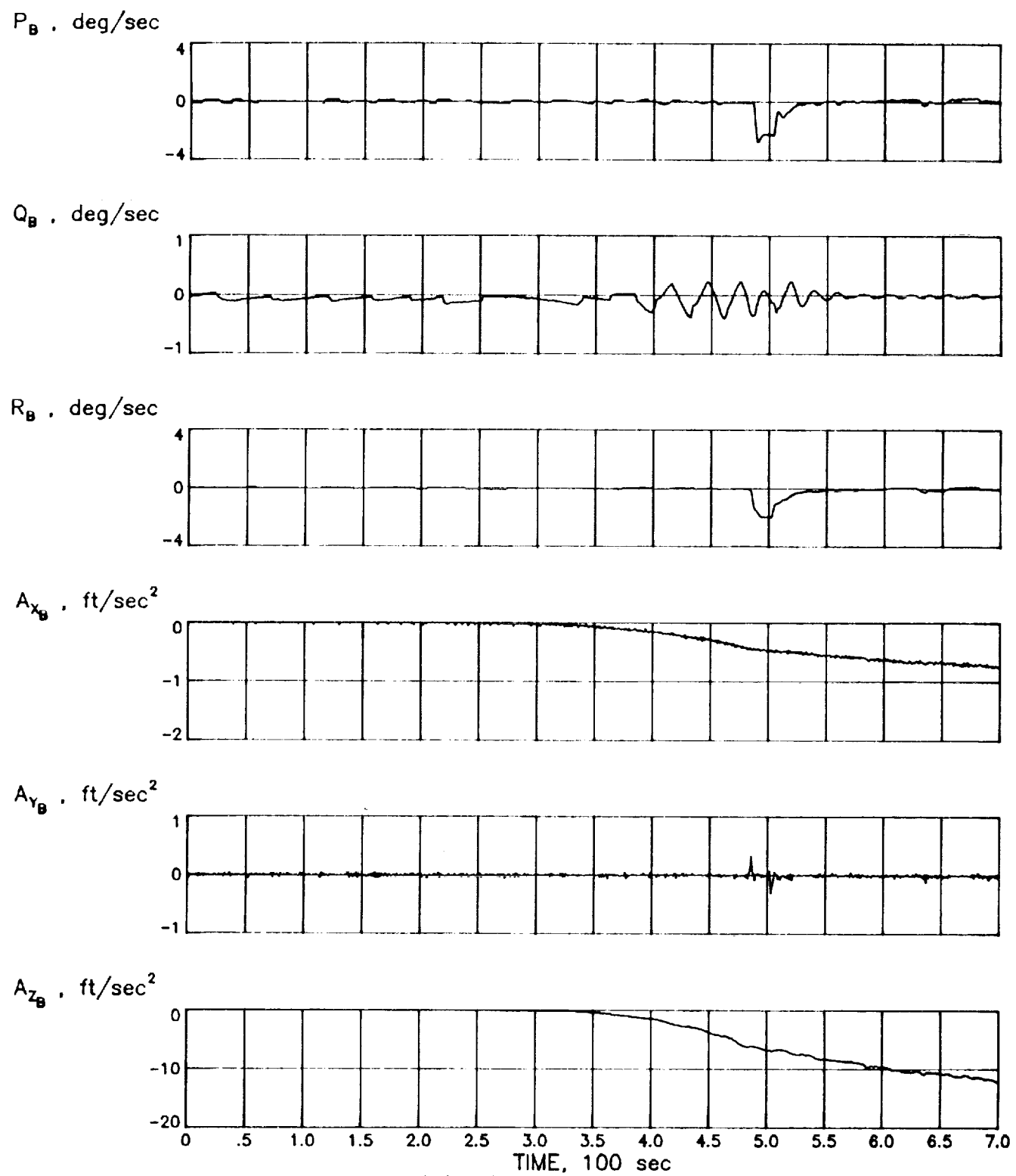


Figure I-4. STS-35 derived body-axis dynamics from IMU1.

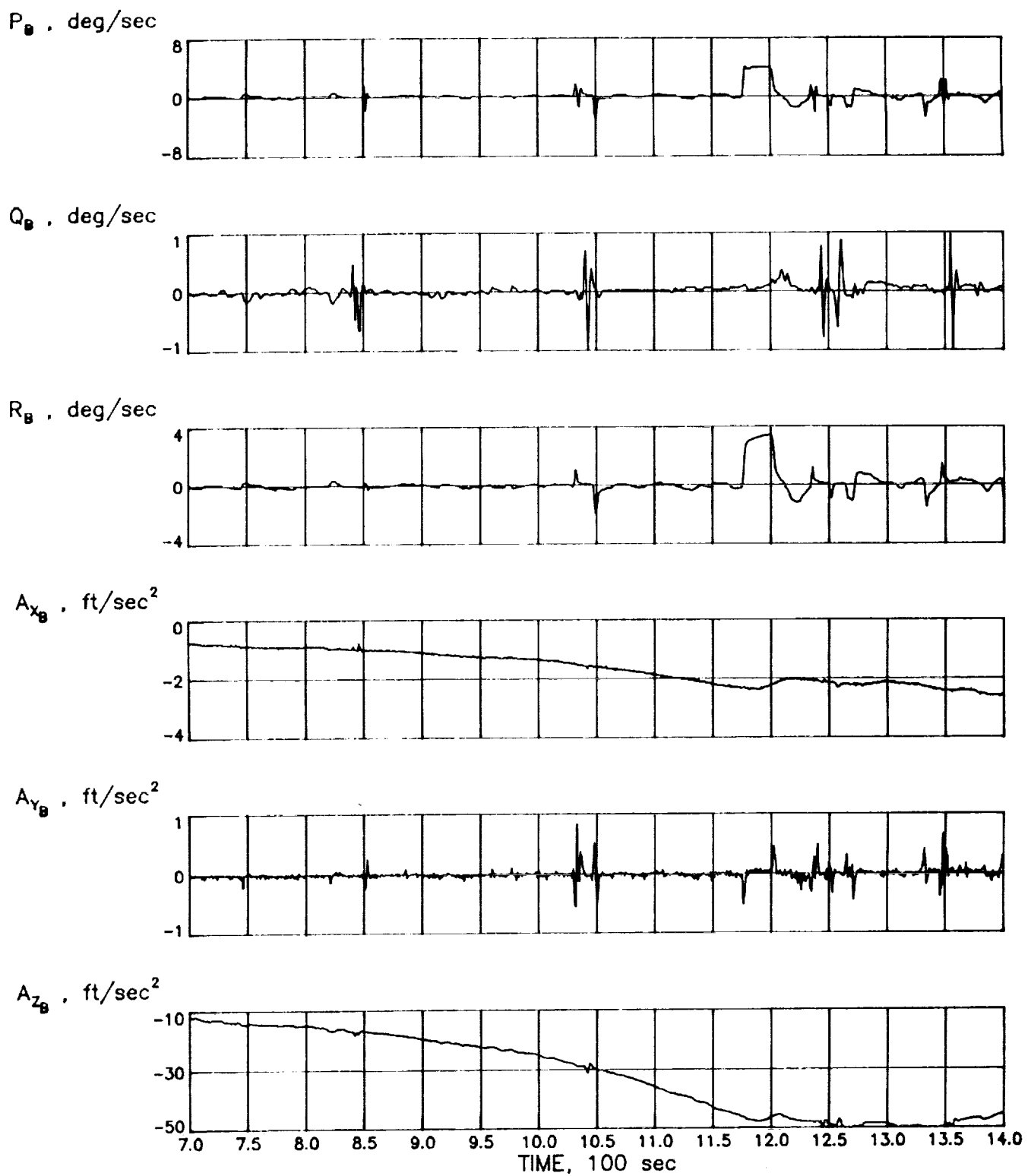


Figure I-4. (continued)

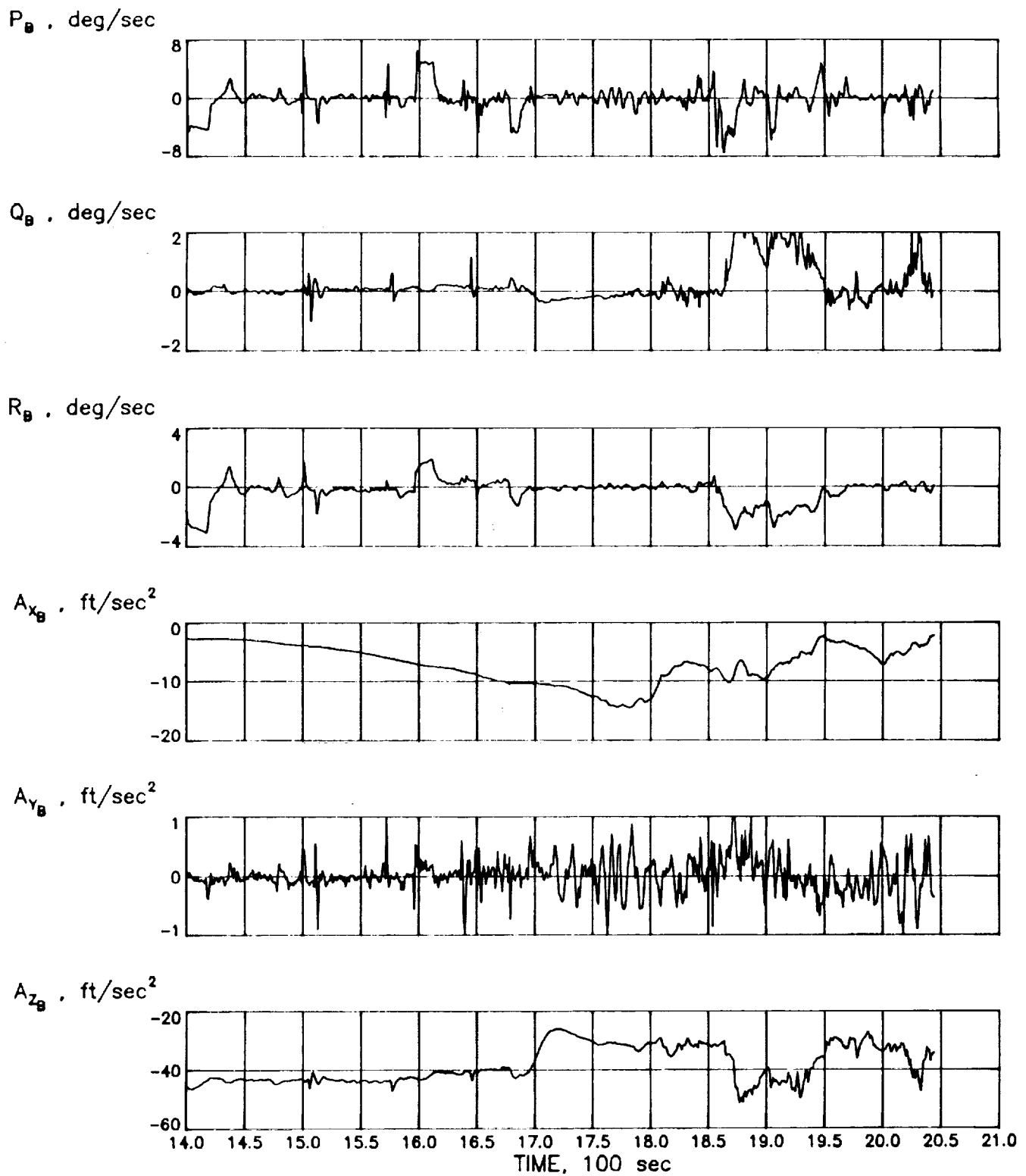


Figure I-4. (concluded)

## I. B. TRACKING DATA PROCESSING

Historically, C-band tracking information via JSC, high-speed play-back S-band data from GSFC, and cinetheodolite tracking from EAFB have been employed for trajectory reconstruction at LaRC. Since the TDRSS has become operational, coherent S-band tracking from the GSTDN are no longer expected during Shuttle entries. Recognizing this as a potential limitation, particularly for entry reconstruction on future missions such as the AFE, FM&C has developed the necessary software to utilize the TDRSS data in lieu of the more conventional ground-based tracking (Reference 2). Moreover, C-band tracking data have not routinely been obtained from JSC since the Shuttle stand-down. Consequently, this interface was recently reestablished in anticipation of the OEX post-flight data processing requirements.

The revised C-band interface has been satisfied via the so-called ADDLOG tape provided by JSC's current BET contractor, RSOC. They also provided (informally) accompanying documentation usurped from an official JSC publication which completely described the contents of this deliverable. Three ADDLOG tapes were received for this flight, namely JP359 (entry playback), JP3510 (real time ADDLOG), and JP3511 (real time KMACL). These data were also converted by Unisys for use at LaRC. The output of that activity resulted in four separate CDC compatible files (35HSR1, 35HSR2, 35HSR3, and 35LSR1). These files were accessed, archived under user catalog UN=U446631, analyzed, edited for "blunder" points, and combined and reformatted for use in ENTREE. The combined C-band data file is a semi-private indirect access file (CBNDF35) under the above mentioned user catalog. This file contains the high- and low-rate C-band measurements available throughout entry for this mission. These data were combined using PREOBS (unpublished) for use in the ENTREE software. In addition, the two-way coherent TDRSS measurements (received from LaRC via GSFC on physical reel JHP353) were included thereon. These data, Doppler only, were taken at a one per second rate pursuant to a request from the APEX PI at JSC. The final combined ENTREE observations file for trajectory reconstruction is T35OBS, a semi-private indirect access file under user catalog U446631.

Figure I-5 shows the Shuttle entry ground-track for STS-35 on which are superimposed the locations of the various tracking stations (complexes). Figure I-6 shows the altitude profile along with annotated bar graphs depicting the available coverage (above an assumed 5°

elevation mask angle) during the entry time frame. At first glance, it is quite apparent that there was considerable tracking available during this mission. However, as a consequence of some of the early editing, it was determined that the Hawaii data (KPTC) were questionable. Even though this was a low elevation pass (maximum of 5.3 degrees), one is always reluctant to give up on these mid-range data. However, it was quite apparent that the range measurements were disjoint in the middle of the pass, suggesting more than a shift from/to either leading-edge or trailing-edge skin tracking phenomena; the elevation data exhibited a sawtooth, searching pattern over the latter half of the pass; and the azimuth component, excluding the last minute of tracking, was marginal. These residual signatures will again be reviewed as part of the final trajectory estimate discussions in Section I. C.

Other C-band editing involved the exclusion of the range component from San Nicolas Island (SNFC) which was visibly segmented as if to suggest a multiplicity of range ambiguities, and the deletion of the Point Pillar pass (PTPC). Neither of the latter deletions are considered significant since there was ample overlap coverage from the remaining stations throughout this same time frame. In fact, the PTPC data might well have been good data if, contrary to published station characteristics information, it had already been corrected for refraction. A similar discrepancy occurred with one of the Vandenberg stations (VDBC) but, in that instance, there was sufficient data to substantiate that these measurements had in fact been corrected for refraction despite information to the contrary. Again, the Point Pillar coverage was a low elevation pass with a maximum elevation of only 6.1 degrees.

It is noted that both high- and low-rate tracking data were available from the Kwajalein Atoll complex, apparently to satisfy a request by JSC navigation personnel to provide simultaneous data for a planned Kalman filtering exercise, ostensibly as part of the descent validation process. Both sets of data were presumably referenced to the master Tradex site. Early results clearly indicated that this was not the case. A preliminary assessment suggested that the low-rate data had been transformed as reported. The actual location of the sensor for the high-rate data remained in question. FM&C consulted with both JSC and KSC to clarify the actual sensor location for the high-rate data. It was learned that only one sensor was operable during the STS-35 descent mission. Consequently, since the low-rate data (KMACL herein) was apparently data from the KMAC radar (properly transformed to the master site), one should expect that the high-rate data (KMACH herein) were also KMAC measurements, though, in this instance, consistent with the actual sensor location. After iterating with both JSC and KSC, the KSC recommended sensor location was utilized.

Pursuant to the aforestated commentary, the actual C-band trackers utilized for the trajectory reconstruction on this flight are given in Table 2 below.

---

Radar Type	Acronym	Geod. Lat. (degrees)	Longitude (degrees)	Altitude (feet)	Modulus of Refraction	Scale Hgt (feet)	Max. Elev. (degrees)
ALTAIR	KMACH	9.3954318	167.479288	206.37	382	18650	13
ALTAIR	KMACL	9.3987028	167.481992	86.02	382	18650	13
FPS-16	PMFC	34.123011	240.845125	-197.05	318	22455	29
FPS-16	SNFC	33.247708	240.479350	725.49	311	22924	14
TPQ-18	VDBC	34.665867	239.418650	202.36	317	22573	44
FPS-16	VDFC	34.583053	239.438981	1974.15	299	23613	52
HAIR	VDHC	34.758258	239.372886	10.69	320	22395	37
FPS-16	VDSC	34.582761	239.438525	1974.11	299	23613	52
FPS-16	EFFC	34.970458	242.068583	2540.39	287	24306	56
FPS-16	FRCC	34.960828	242.088561	2481.36	288	24252	59
FPS-16	FRFC	34.957753	242.088153	2462.07	289	24169	60

**Table 2. STS-35 tracking station locations, refraction and other information.**

---

Included above are the relevant parameters required for the refraction calculations, i. e., the modulus of refraction and the atmospheric scale height. Refraction corrections are only applied for those stations not otherwise corrected. However, even for those stations whose data are already corrected, the computations are made. The data from all stations are down-weighted at the limbs accordingly (as a percentage, nominally 10%, of the magnitude of the refraction correction) to minimize the dependence on any refraction algorithms employed. The maximum radar elevation angle which occurred over each station is also presented as additional information. Note that the ALTAIR station which provides both the high- and low-rate Kwajalein data is actually specified as P-band. Though not completely understood, perhaps the radar is so designated because this frequency band lies in the mid-range of the ALTAIR dual-frequency radar capability. In any event, these data

are properly treated herein as a conventional C-band skin-tracking radar which provides the usual measurements of range, azimuth and elevation. As readers will observe in the next sub-section, additional editing in terms of significant bias determinations and removal of same was also required to enable the BET for STS-35.

It is noted that the TDRSS data were requested by the APEX PI from deorbit throughout entry. Due to computer equipment problems at the TDRSS ground-station (White Sands, New Mexico) data were not enabled until (approximately) entry interface. However, apart from the loss which occurred during the first roll reversal, the TDRSS data were essentially contiguous throughout entry upon reacquisition, at least down to an altitude of approximately 79 kft. The TDRSS data were from one of the westerly located satellites which, consistent with the GSFC notation, corresponds to the first satellite launched (TDRS1). The necessary ephemeris information for this satellite was received separately from GSFC. At the time of this mission, this satellite was nominally located at approximately  $4^{\circ}$  south latitude,  $171^{\circ}$  west longitude and, of course, at geosynchronous altitude. However, since the satellite position is not actually fixed, the TDRS1 radius, declination, and longitude were specified by GSFC at ten (10) minute intervals. The reconstruction software uses this detailed ephemeris information and employs cubic spline interpolation to satisfy the data processing requirements. It should also be stated that the White Sands ground station utilized during this mission was the southerly site, TDSR.

Readers are reminded that TDRSS data represent a relatively new S-band Doppler observable type for orbit determination and its use for endo-atmospheric trajectory reconstruction is most unique. Consequently, at least for these early Shuttle entry reconstruction applications, it is utilized herein to augment the solution without constraining the estimate to actually fit the TDRSS data commensurate with its own measurement accuracy. This down-weighting, as it were, amounts to fitting the data with an equivalent 1 Hz presumed accuracy rather than the virtually zero RMS noise expected. The "looser" tolerance compensates for the fact that it is almost impossible to compute this observable as accurate as the measurements themselves (refraction considerations in the atmosphere, tracking satellite ephemeris uncertainties, etc.); it de-sensitizes the filter to the limited geometry afforded by such a pass (particularly since the Shuttle transponder does not provide ranging via TDRSS); and it accommodates the considerable signal resulting as a consequence of spacecraft angular motion during the rather lengthy, certainly dynamic entry flight. These limitations having been stated, one should still understand that the accuracy of any Shuttle entry trajectory reconstruction can be further substantiated by these TDRSS

data. FM&C's use of these data for Shuttle applications is tantamount to providing a quality assessment, i.e., an independent verification of the accuracy of the reconstructed trajectory that might otherwise be obtained by using data from the ground-based radars only.

In addition to the C-band and TDRSS data, pseudo observables were incorporated to enhance the trajectory estimate during the final landing phase. This has commonly been done at LaRC whenever cinetheodolite data are not available, as was the case due to the night-time lighting conditions commensurate with the STS-35 landing. These pseudo observables included theoretical measurements of altitude during rollout (referenced to the vehicle center-of-gravity after nose gear contact) and null Doppler measurements after the known stop-time. Three pseudo Doppler stations collocated around the runway are used to control the post-stop Shuttle north, east, and vertical velocities to essentially zero values.

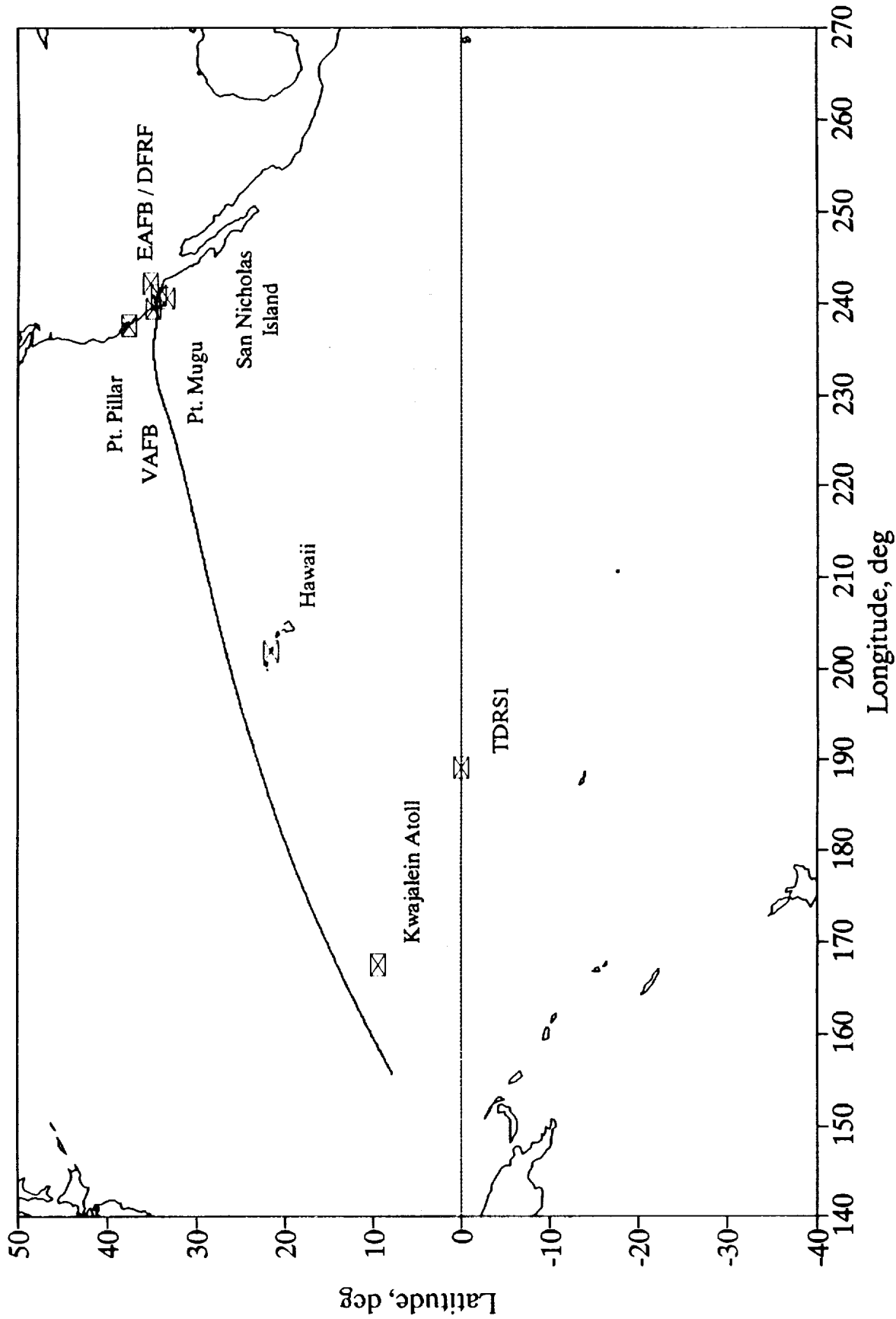
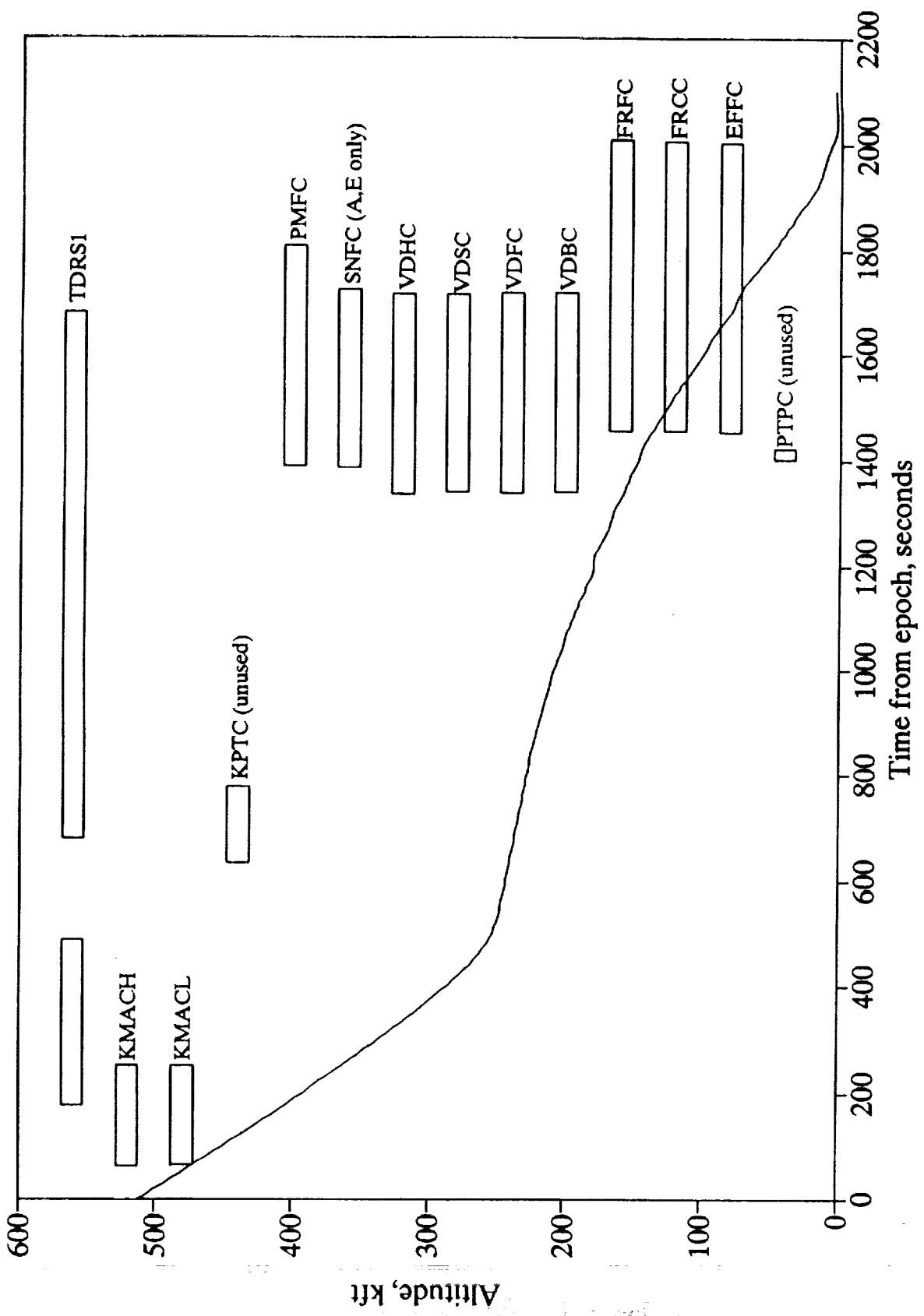


Figure I-5. STS-35 ground track and metric tracking coverage.



**Figure I-6.** STS-35 altitude profile and tracking timelines.

### I. C. RECONSTRUCTION RESULTS

Early ENTREE reconstruction activities for STS-35 concentrated on state-only estimates, where state-only refers to the nine state variables which completely describe the Shuttle position, velocity and attitude histories during descent. Such methodology has been successfully employed on previous missions, to include the last Columbia mission, STS-32, during January 1990. This is the preferred method since the trajectory estimate is felt to be more unique. Historically, extended parameters have been included into the solution set (IMU parameters mostly) as required to enable a better fit. However, one can never be sure that the resultant parameters determined are actually real calibrations or a "sink" to absorb other discrepancies (perhaps some other IMU errors, observational biases, etc.).

It was anticipated that a state-only solution would be satisfactory for STS-35, particularly since the IMUs compared so favorably and there was ample tracking available for the trajectory determination. Even if the state-only solution was not sufficient, such an estimate would, by inference, provide one with a measure of the enhanced fit to be expected when incorporating instrument parameters or radar biases into an expanded solution set.

The first results obtained clearly indicated that state-only estimation resulted in a miscompare between the uppermost altitude tracking and that from the coastal radars. The ensemble statistics were satisfactory, indicative of an essentially zero mean estimate fit to within a  $2\sigma$  weighted root-mean-square. However, there was considerable structure in the associated residual plots from any given station. Also, comparisons versus the TDRSS data were degraded. Moreover, results from ESOLVES (a stand-alone solve utility which evaluates the relative improvement of fit to be gained by inclusion of additional solve-fors) indicated that there was virtually little improvement to be expected. As a point of interest, the indicated altitude correction at epoch was somewhat higher ( $\approx 4,500$  feet) than expected.

Recalling the previous discussions and concerns with some of the tracking data, additional reviews and editing were conducted. The presumed locations for the Kwajalein sensors were substantiated by obtaining a state estimate using these data only. Here, the attitude angle corrections were suppressed since determinations of same are impossible over this uppermost altitude (low density) interval. A reasonable fit was obtained which

substantiated both sensor locations. The Hawaii data were reconsidered and again removed as part of the ensemble data set for reasons previously discussed. Once again, the initial altitude estimate seemed to be higher than expected (by some 6,000 feet in this instance) and the TDRSS comparisons degraded. Moreover, this solution, when passed through the remaining data, resulted in first pass residuals in excess of  $100\sigma$ .

Clearly, adequate state-only estimation for the STS-35 descent was not to be realized. Given the extent of the miscompare between the up-range and down-range radars, far greater than ever observed on any of the previous flights reduced at LaRC, and, further, assuming that the data from each radar were accurate, the discrepancies must occur as a result of state propagation errors. Since ENTREE uses dynamic data from the selected IMU in a deterministic integration algorithm to propagate the state throughout entry, the IMU data must be questioned. Such a statement can be made even though it has already been shown that the actual measurements from each of the tri-redundant IMUs compared as well as one could expect. Nevertheless, errors well below the IMU measurement threshold can be significant in the deterministic prediction scheme.

As the data processing evolved, it became clear that there were some biases visible in the C-band data. In part, these biases were responsible for the fact that the ESOLVES analysis did not suggest any significant improvement to the overall fit when additional solution parameters were investigated. Consequently, prior to finalizing the BET for this flight, which knowingly would require inclusion of IMU parameters in the final estimate, it was felt that these biases, where significant, should be removed. Separately, bias values were determined for both Kwajalein sensors as well as for the coastal radars. The biases were determined by selectively processing data over the upper and lower altitude intervals, respectively. The residual means were computed from these short arc reductions and adopted as biases since, other than the apparent biases, excellent fits were otherwise obtained. The following table (Table 3) is included to show these determinations. As a point of reference, each bias is compared to the expected RMS measurement accuracy to show the extent of the levels determined. Only radar angle biases are shown in the table since these were the most obvious determinations. Other small (range and angle) biases were not removed since they were not felt to be significant in the final analysis.

---

STATION	COMPONENT	BIAS (degrees)	WEIGHTED BIAS ( $\approx\sigma$ level)
KMACL	AZIMUTH	-0.01353	-1.18
KMACL	ELEVATION	-0.00573	-0.5
KMACH	AZIMUTH	-0.01382	-1.21
PMFC	ELEVATION	-0.01276	-1.11
SNFC	AZIMUTH	-0.00756	-0.66
SNFC	ELEVATION	0.01139	0.99
VDHC	ELEVATION	0.00826	0.72
VDSC	ELEVATION	-0.01710	-1.49
VDFC	ELEVATION	-0.01578	-1.38

**Table 3. C-band biases determined for STS-35.**

---

The above observational biases were incorporated and estimates were generated for which a variety of solution parameters were investigated. As a result of this analysis, the final ENTREE estimate included, in addition to the nine state, some six IMU parameters. These latter parameters were gyro biases (3) and accelerometer scale-factors (3). The software solves for these parameters in the platform axes, i. e., the axes consistent with the actual measurements, to provide for a more rigorous model. However, the software assumes that there are three independent accelerometers per platform rather than the two that actually exist. This approximation is not felt to be significant and is consistent with the modeling done on all previous flights. The final ENTREE estimate is presented in Table 4. It should be noted that the initial estimate of the nine state parameters conform to the RSOC values at epoch. The initial values assumed for the IMU parameters represent perfect instrumentation. As a point of reference, gyro biases of approximately 0.022 deg/hr are commensurate with the  $1\sigma$  expected accuracy. This is the fixed-drift component and does not include the potential for an additional g-sensitive drift component of 0.025 deg/hr/g. In addition, the scale-factors shown are expressed as errors from a perfect 1.0 value. An expected level of 100 ppm is consistent with the accelerometer specifications.

---

PARAMETER	INITIAL	FINAL
Velocity ( $V_R$ ), fps	24358.99	24357.56
Flight path angle ( $\gamma_R$ ), deg	-1.5116	-1.5147
Heading angle ( $\Psi_R$ ), deg	60.7434	60.7438
Altitude (h), ft	512680	513594
Latitude ( $\Phi_D$ ), deg	7.7759	7.7771
Longitude ( $\lambda$ ), deg	155.6030	155.6038
Euler yaw angle ( $\psi$ ), deg	60.4417	60.4936
Euler pitch angle ( $\theta$ ), deg	38.0809	38.0749
Euler roll angle ( $\phi$ ), deg	0.0789	0.0411
IMU roll gyro bias ( $P_b$ ), deg/hr	0.0	0.034
IMU pitch gyro bias ( $Q_b$ ), deg/hr	0.0	-0.094
IMU yaw gyro bias ( $R_b$ ), deg/hr	0.0	0.058
IMU X-accelerometer scale-factor error, ppm	0.0	278
IMU Y-accelerometer scale-factor error, ppm	0.0	200
IMU Z-accelerometer scale-factor error, ppm	0.0	-10

**Table 4. Final ENTRÉE parameter estimates for STS-35.**

---

Clearly, the error coefficients determined for the IMU parameters are quite large, particularly when compared to levels determined on prior flights at LaRC. However, as stated previously, the relative inconsistency between the upper altitude and coastal radar data was more significant than ever observed such that these results are not surprising. Nonetheless, these determinations should not be construed as exact IMU calibrations which, in this particular instance, would imply calibrations for the selected IMU1 measurements. Past experience has shown that such determinations, though indicative, are not unique. It was previously demonstrated that the IMU1 measurements agreed favorably with those from the other IMUs but, it was also stated, differences at levels implied by the above error correction coefficients might well go undetected in the direct IMU comparison analyses.

Moreover, it was pointed out that IMU1 was changed out since the last Columbia mission. Again, readers should not interpret that the replacement is of lesser quality or, perhaps, is not as well aligned within the spacecraft. Suffice it to say that, for the ensemble tracking data available, the above solution set best fits these observables and, though (perhaps) not unique, some IMU correction terms must be incorporated.

Separate discussions with personnel at JSC vindicated the assessment that IMU1 had performed the best overall during the STS-35 descent. Indeed, the feeling was that the overall onboard navigation performance during this mission was essentially nominal. Their post-flight analyses had quantified the performance as an approximate  $1\sigma$  (or better) flight. Despite this apparent quandary, FM&C is comfortable with the fact that some instrument determinations must be included if one is going to fit the ensemble of tracking data available for this mission. Though the determinations herein may not be unique, the final trajectory that results agrees quite well with the JSC BET throughout the entire entry time frame and, as next shown, the final fit to the tracking data is excellent.

Final residual plots showing the goodness-of-fit to the C-band tracking data are given in Appendix A. Plotted are the residuals as well as the weighted residuals. Annotated on each plot are the residual mean and standard deviation computed for each component. The TDRSS Doppler residuals are presented as Figure I-7 as part of this sub-section. As previously discussed, these data, though down-weighted heavily, were incorporated to obtain the final estimate.

Table 5 herein summarizes the overall fit quality. Whereas some small biases remain, the most notable being the  $-0.56\sigma$  weighted mean in the range component from VDBC, it is obvious that an excellent fit has been obtained. In fact, the overall ensemble statistics (computed based on 12,345 observations) reflect a weighted mean of  $-0.04$  and an ensemble weighted standard deviation of  $0.756$ . However, close inspection of the individual residual charts in Appendix A does show some signal remaining. The range and azimuth from the Kwajalein stations still exhibit a modest ramp signature in the respective residuals. The Vandenberg data suggest, at least in the elevation component, that there might be some refraction considerations remaining, though, admittedly, some of this signature could be spacecraft related. The elevation residuals from the Edwards/Dryden stations exhibit a sharp, unexplained ramp increase near the end of each of their respective passes. Finally, the TDRSS residuals still exhibit considerable structure. The long period variation between  $\pm 2$  Hz is either Shuttle trajectory or tracking satellite ephemeris related, i. e., this spread is

probably consistent with the accuracy of either since 1 Hz at S-band frequencies corresponds to an extremely accurate (0.22 fps) line-of-sight velocity measurement. The higher frequency, more dominant structure is directly related to Shuttle rotational motion during entry. As can be seen, each of these contributions totally mask any apparent measurement noise.

Composite residuals by component for the C-band trackers are shown in Figure I-8 through I-10 herein. Composite range residuals are presented as Figure I-8. Composite azimuth and elevation residuals are given in Figures I-9 and I-10, respectively. Individual station signatures cannot be gleaned from these figure but such plots best reflect the overall fit to the tracking data throughout the entire entry. Though the weighted residuals are not shown, the weighted mean and weighted standard deviation are annotated on each figure along with the actual dimensional values for each component. Lastly, strictly as information, Figure I-11 is included to show the previously discussed Hawaii pass. Though not included as part of the fitting process, these data have been passed through the final estimate to show the measurement discrepancies. The jump discontinuity in ranging and the considerable signal remaining in the angular data can readily be seen. For the latter, the elevation residuals vary between (approximately)  $-2\sigma$  and  $7\sigma$ .

The final inertial BET for this flight, derived as just described, is available on the LaRC CDC machines as a semi-private indirect access file (IBETF35) under User Catalog UN=274885C. Approximate event times of interest are listed below in terms of seconds from epoch. The remaining sections of this report discuss the Extended and Aerodynamic BETs derived from this inertial product.

<b>Entry Interface (EI)</b>	185
<b>Main Gear Deployment</b>	2030
<b>Weight on Wheels (WOW)</b>	2046
<b>Weight on Nose Gear (WONG)</b>	2060
<b>Stop time</b>	2106

TYPE	STATION	ACCEPTED	MEAN	WEIGHTED MEAN	STD. DEV.	WEIGHTED STD. DEV.
DOPPLER	TDRS1	1079 of 1247	0.14	0.14	1.16	1.16
RANGE	KMACI	31 of 31	-14.5	-0.37	31.4	0.79
	KMACHI	183 of 183	2.1	0.05	32.6	0.82
	PMFC	360 of 379	-6.8	-0.17	34.2	0.86
	VDHC	358 of 358	1.9	0.05	26.8	0.68
	VDSC	336 of 345	6.0	0.15	21.0	0.53
	VDFC	351 of 358	-11.1	-0.28	28.9	0.73
	VDBC	349 of 355	-22.4	-0.56	20.0	0.51
	FRFC	527 of 537	14.4	0.36	23.2	0.59
	FRCC	520 of 527	-1.5	-0.04	24.5	0.62
	EFFC	519 of 531	8.9	0.23	25.3	0.64
AZIMUTH	KMACL	31 of 31	-0.0008	-0.07	0.0061	0.53
	KMACHI	184 of 184	-0.0008	-0.07	0.0065	0.57
	PMFC	389 of 389	0.0040	0.35	0.0063	0.55
	SNFC	291 of 294	-0.0002	-0.02	0.0045	0.4
	VDHC	376 of 376	-0.0005	-0.04	0.0038	0.33
	VDSC	348 of 363	-0.0042	-0.36	0.0061	0.53
	VDFC	348 of 371	-0.0016	-0.14	0.0071	0.62
	VDBC	371 of 372	0.0009	0.08	0.0050	0.44
	FRFC	461 of 540	-0.0005	-0.04	0.0088	0.76
	FRCC	447 of 534	0.0043	0.38	0.0096	0.84
ELEVATION	EFFC	486 of 545	-0.0023	-0.20	0.0086	0.75
	KMACL	30 of 30	-0.0031	-0.18	0.0074	0.45
	KMACHI	184 of 184	-0.0016	-0.07	0.0082	0.47
	PMFC	387 of 387	-0.0020	-0.16	0.0050	0.35
	SNFC	238 of 241	-0.0055	-0.38	0.0071	0.46
	VDHC	374 of 374	-0.0022	-0.13	0.0067	0.49
	VDSC	359 of 363	-0.0021	-0.10	0.0101	0.74
	VDFC	331 of 369	-0.0031	-0.16	0.0131	0.98
	VDBC	370 of 371	0.0001	0.01	0.0059	0.44
	FRFC	467 of 541	-0.0047	-0.32	0.0123	0.97
	FRCC	521 of 536	-0.0009	-0.10	0.0094	0.75
	EFFC	522 of 542	-0.0052	-0.37	0.0110	0.84

Units are Hz, ft, and degrees

Table 5. Summary of fit statistics for STS-35.

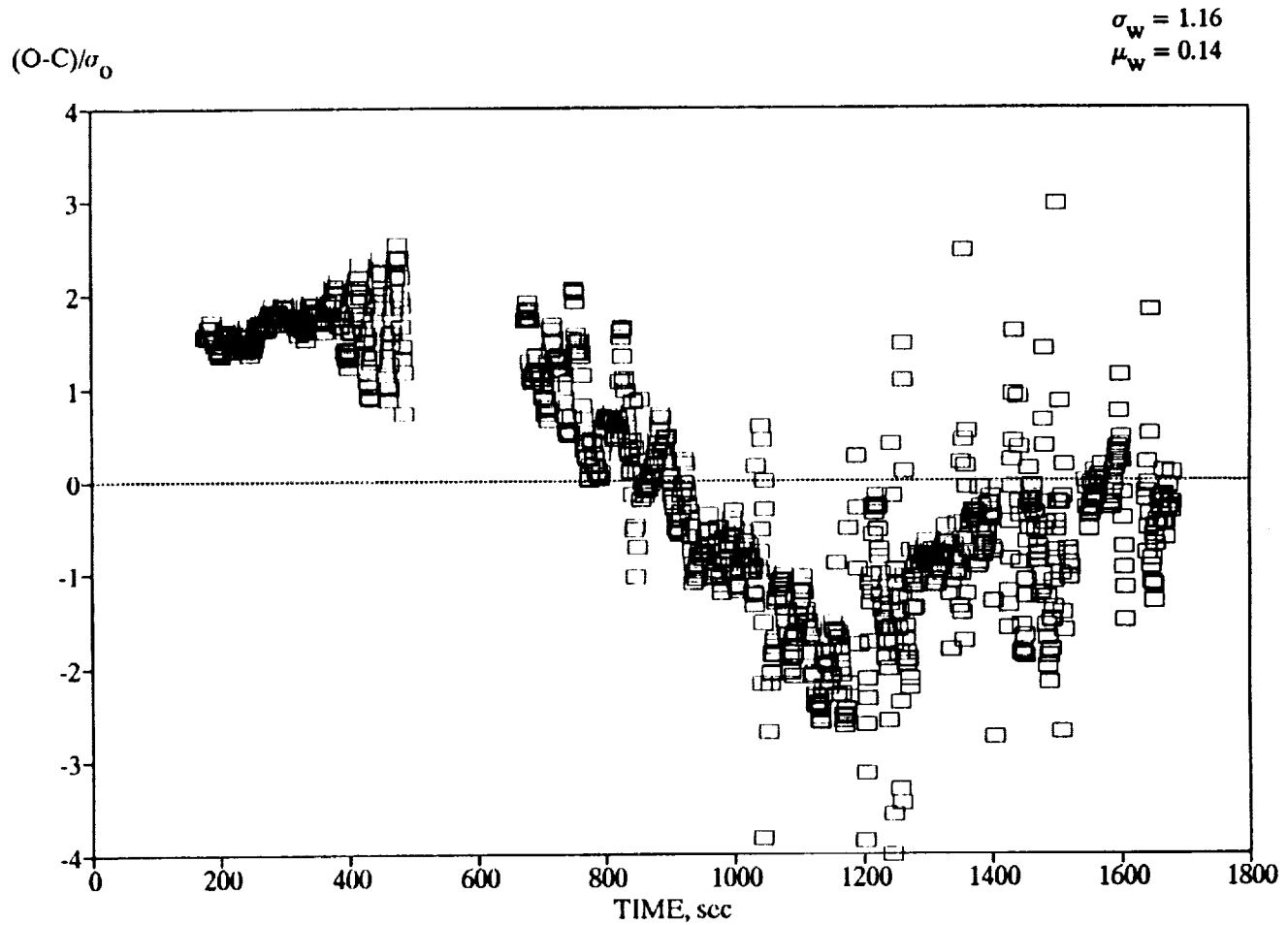


**Figure I-7. Final TDRS1 Doppler residuals for STS-35.**

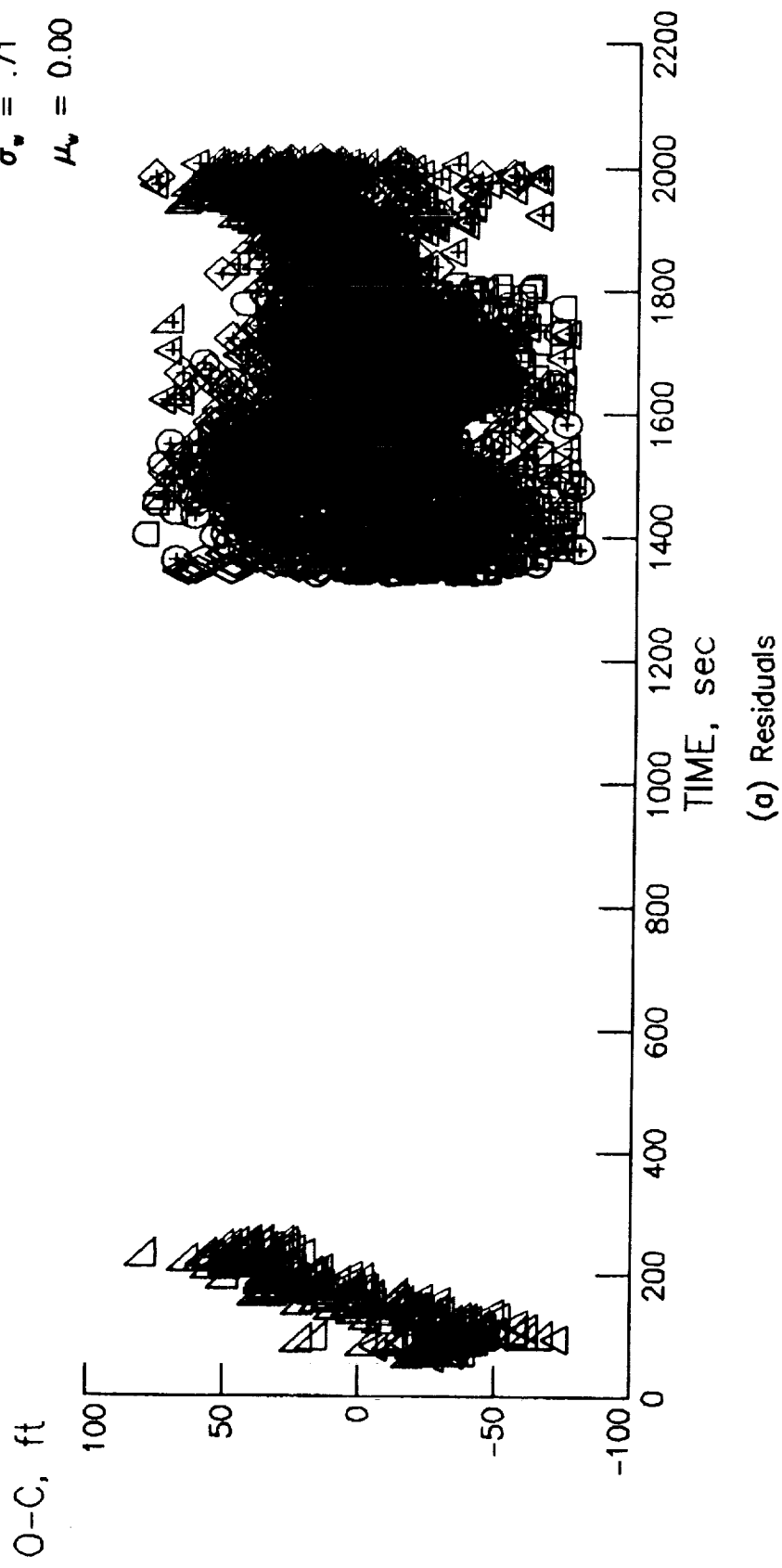


Figure I-8. Composite range residuals for STS-35 entry reconstruction.

$$\begin{aligned}\sigma &= .008 \\ \mu &= 0.000 \\ \sigma_* &= .66 \\ \mu_* &= 0.00\end{aligned}$$

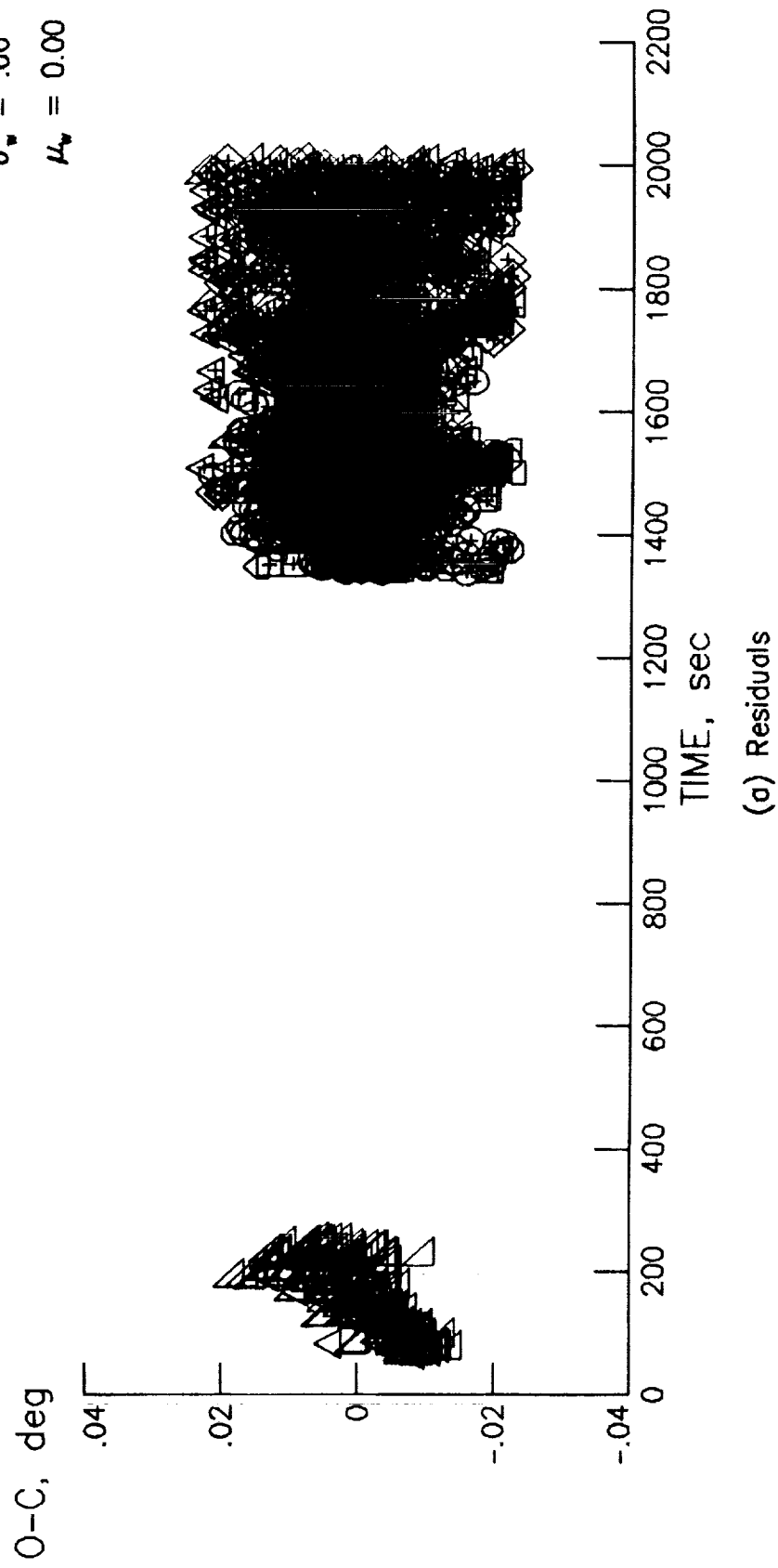


Figure I-9. Composite azimuth residuals for STS-35 entry reconstruction.

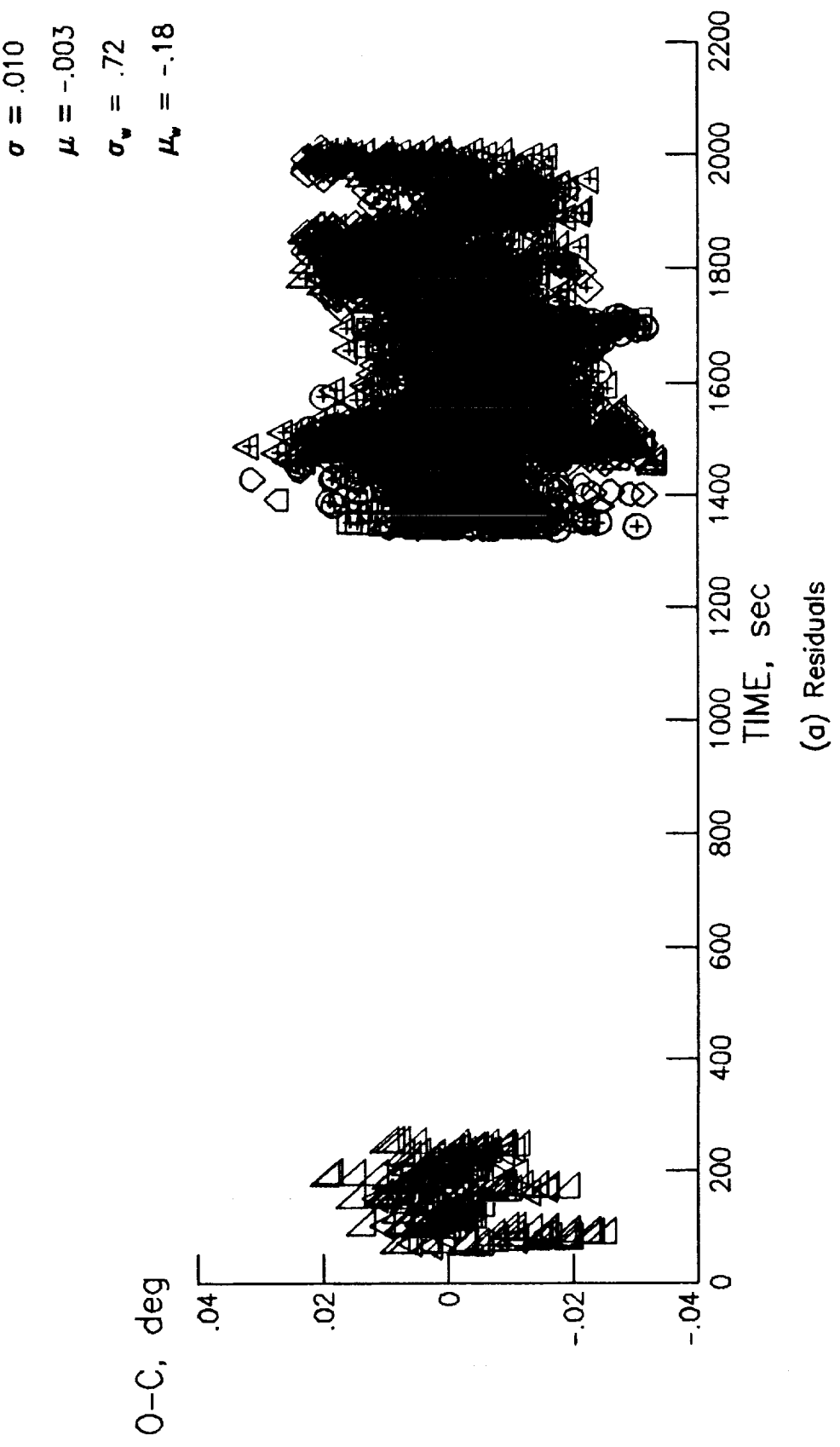
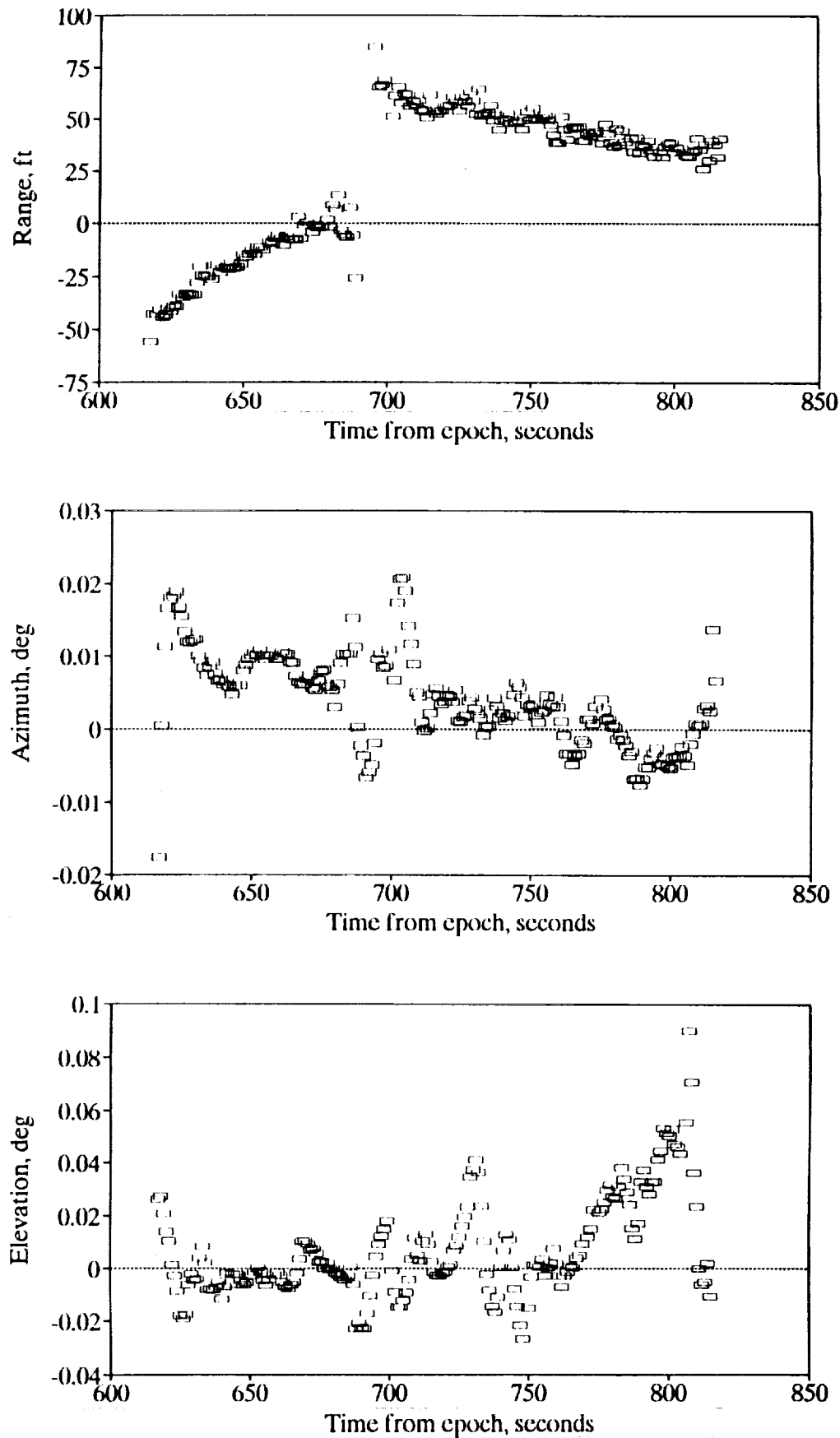


Figure I-10. Composite elevation residuals for STS-35 entry reconstruction.



**Figure I-11.** KPTC residuals based on final BET for STS-35.

## II. EXTENDED BET DEVELOPMENT

Development of the 66-word Extended BET for STS-35 was rather straightforward in view of the limited options available. Past activities at LaRC involved the development of LAIRS files based on the available NOAA remote sounding information taken in support of a specific entry flight. These data, along with the equivalent "totem-pole" atmospheres extracted from the JSC BET files, permitted optional analyses to select that atmosphere deemed most appropriate for the mission. In view of the fact that the LAIRS activity has ceased, the only option remaining is the JSC data. For readers unfamiliar with the "totem-pole" atmospheres, it is relevant to state that these data are derived by Mr. Mel Gelman of the Climatology Branch of the National Weather Service. They are based on the same remote sensing data which were the source for the LAIRS file generation. Gelman spatially locates vertical profiles in the vicinity of a representative ground-track for the Shuttle. These data are cross interpolated versus altitude, latitude and longitude, resulting in a single Shuttle specific atmosphere. Extraction of these data using RELAIRS is a rather simple process. The extracted results are rewritten to conform to the usual LAIRS file format and combined with the inertial trajectory data to generate the Extended BET.

Atmospheric parameters obtained from the JSC STS-35 data are presented as Figures II-1 through II-4, respectively. As seen thereon, temperature, density, pressure, and horizontal wind components are plotted versus altitude. These data are plotted over the lowermost 400 kft since results above this altitude are not particularly meaningful.

As a measure of confidence in the JSC data, the upper altitude atmospheric density and temperature were compared versus that which would be expected based on Shuttle-derived results as well as elaborate model considerations. These comparisons are presented in Figure II-5 where, it can readily be seen, metric units are employed. This is commensurate with the available software which has been utilized on past missions to develop an atmospheric database for JSC (Reference 3). It is noted that the density for each of the atmospheric sources has been normalized to the 1976 Standard Atmosphere. The Shuttle-derived density profile is computed using the predicted (L7 pre-operational databook), flight-substantiated (FAD26, Reference 4), normal force coefficient and the in situ normal acceleration profile sensed by IMU1. Temperature is computed from the perfect gas law after integration of the hydrostatic equation to obtain the pressure profile. Model data included are the Marshall Space Flight Center (MSFC) Global Reference Atmospheric Model (GRAM, Reference 5) and the 1978 Air Force Reference

Atmospheres (AF'78, Reference 6). Whereas there are some differences noted, particularly near 70 km, the Shuttle-derived density profile compares quite favorably with the JSC data. Moreover, based on past experience, the Shuttle-derived profile is representative of a reasonably smooth density, devoid of any major density shears or other abrupt structure. Data from both models tend to be more dense below approximately 85 km but such comparisons are not atypical.

On the basis of the limited analysis just presented, the JSC data appear to be adequate for this flight. The final Extended BET for this flight is available on the LaRC CDC machines as EBETF35 under user catalog UN=274885C. Appendix B contains a listing (at a 2 second spacing) of pertinent parameters from the Extended BET. Included are the air-relative velocity, flight path and heading angles, altitude, attitude angles with respect to the air-relative velocity vector, Mach number, dynamic pressure, and both the hypersonic viscous parameter (VBAR) and Reynolds number (RNUM). Readers should note that labels utilized conform to word definitions employed on the Aerodynamic BET file later presented. Actually, Reynolds number and the hypersonic viscous parameter were extracted from the AEROBET since these data are not written to the Extended BET. As a final note, QBAR, VBAR and RNUM are only computed below entry interface where meaningful atmospheric information is available. In the case of VBAR, no computations are included below a value of 0.005, i. e., below the minimum value utilized in the aerodynamic databook formulation as discussed in the next section.

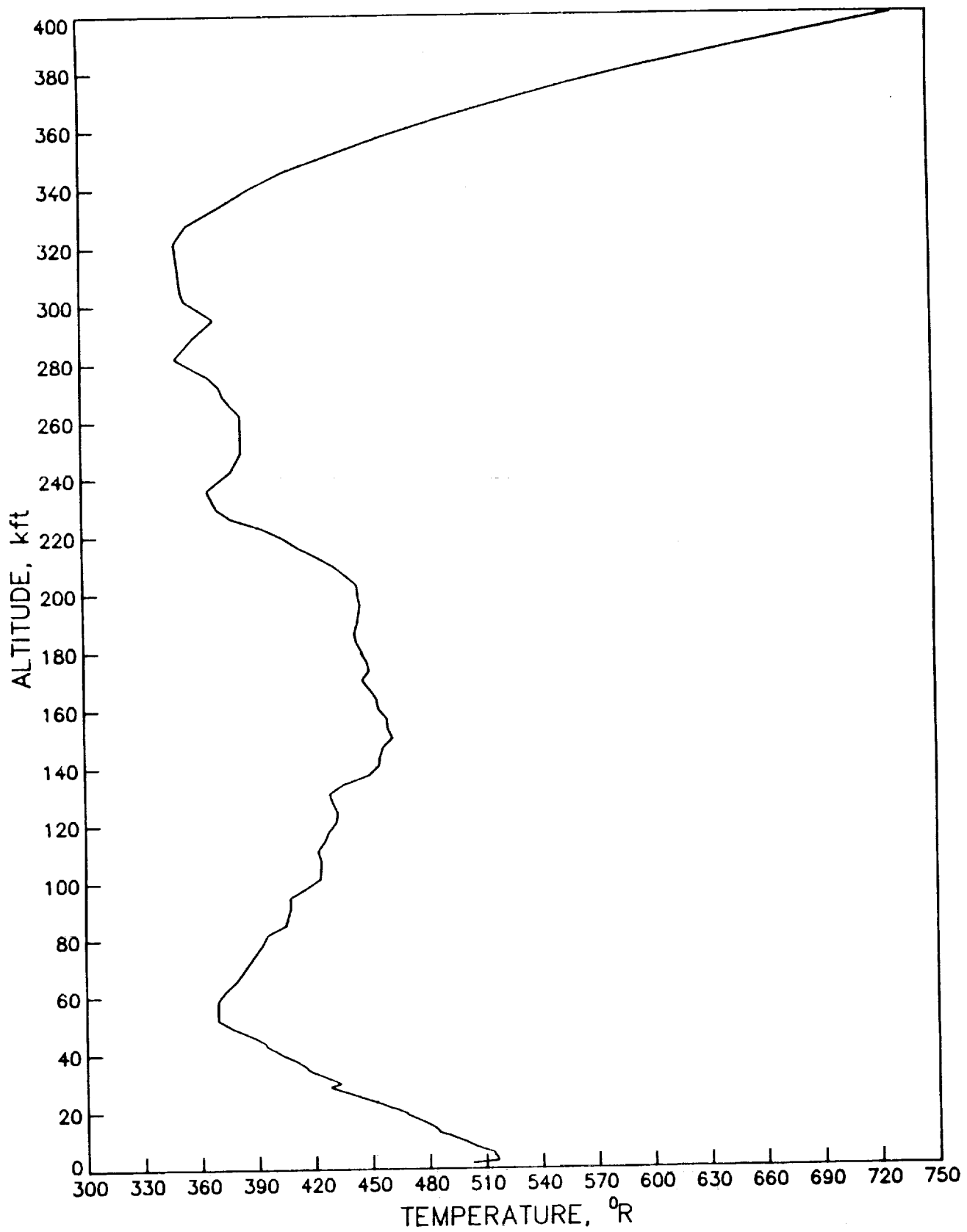


Figure II-1. STS-35 temperature profile.

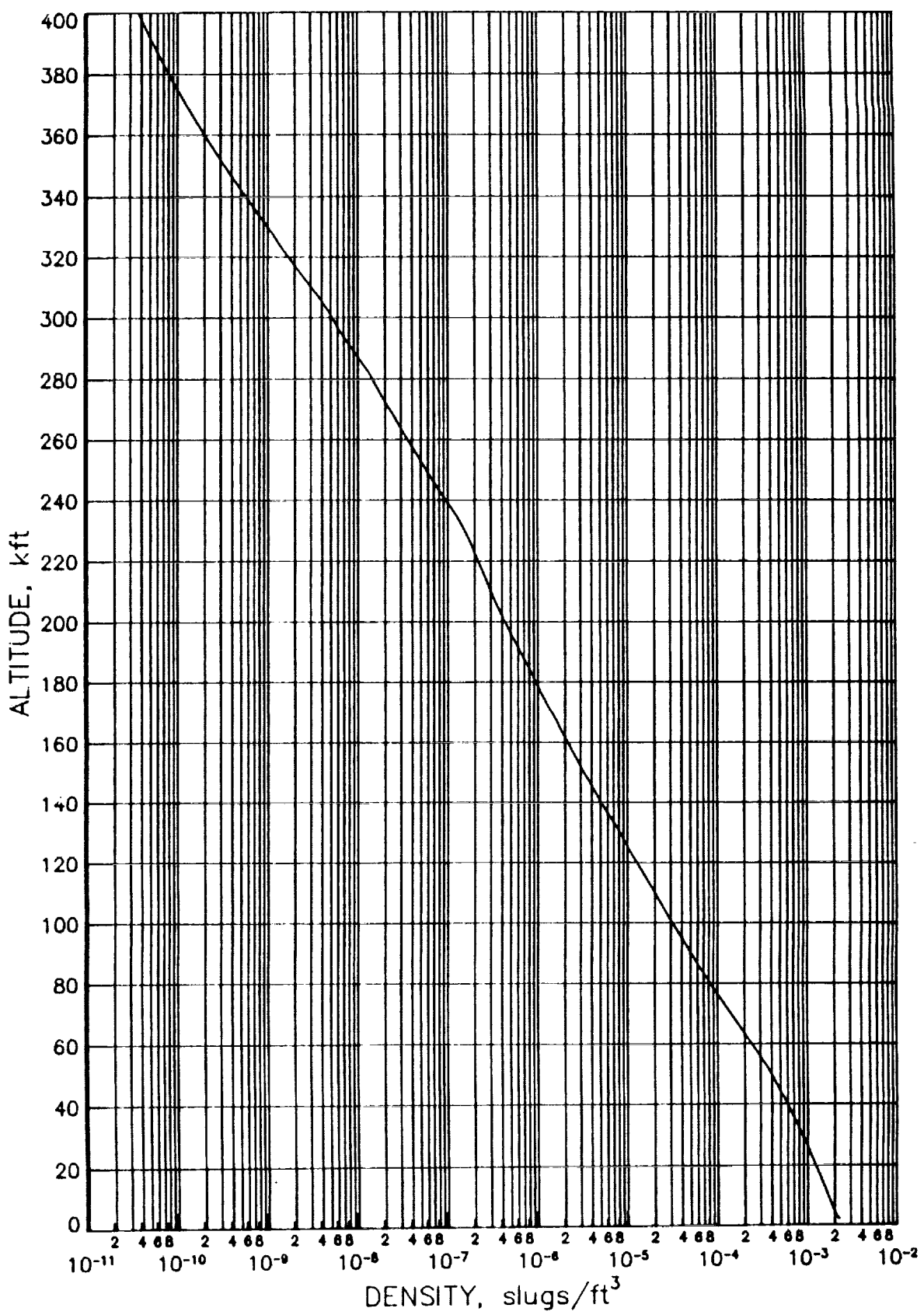


Figure II-2. Density profile for STS-35.

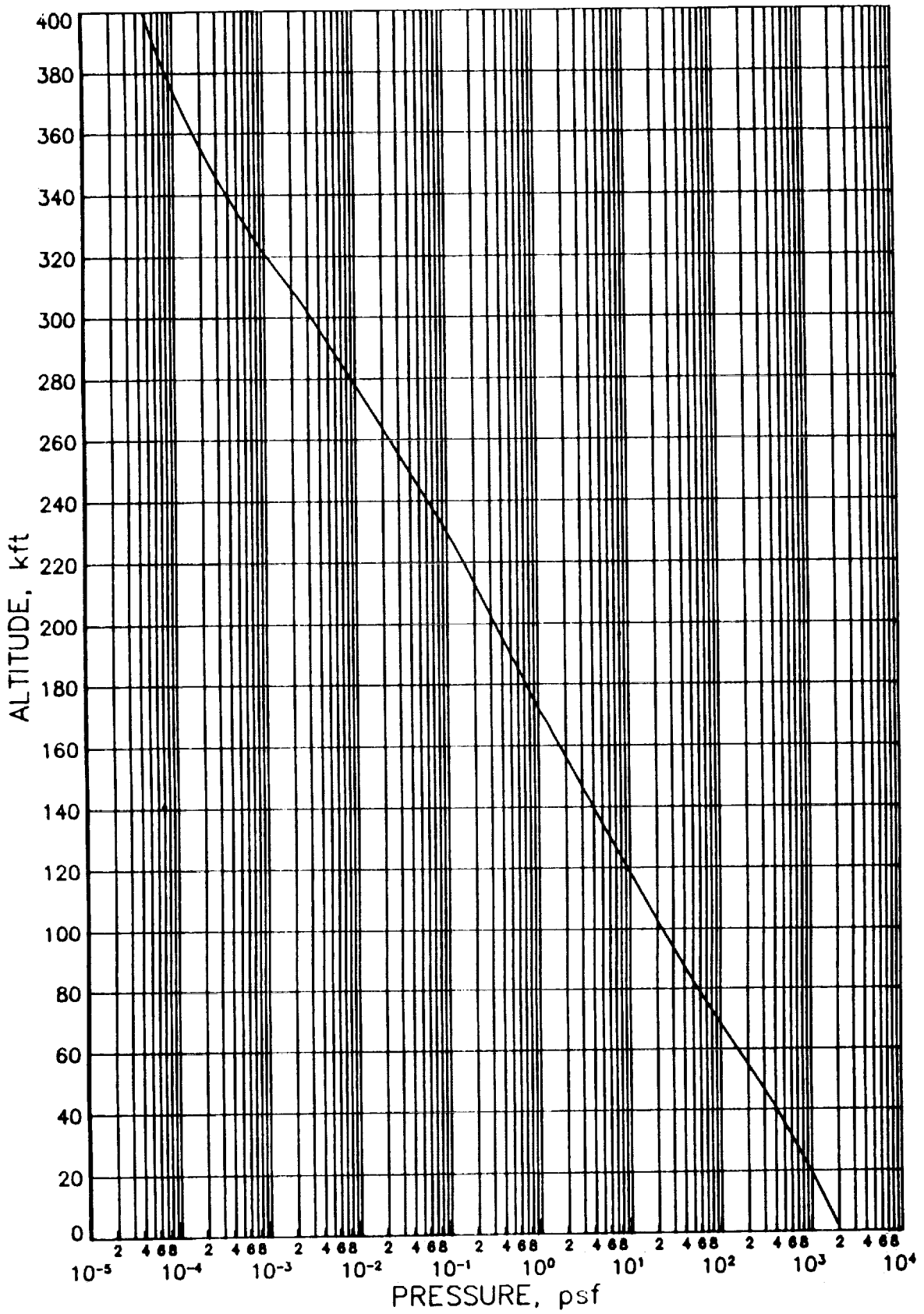


Figure II-3. STS-35 pressure profile.

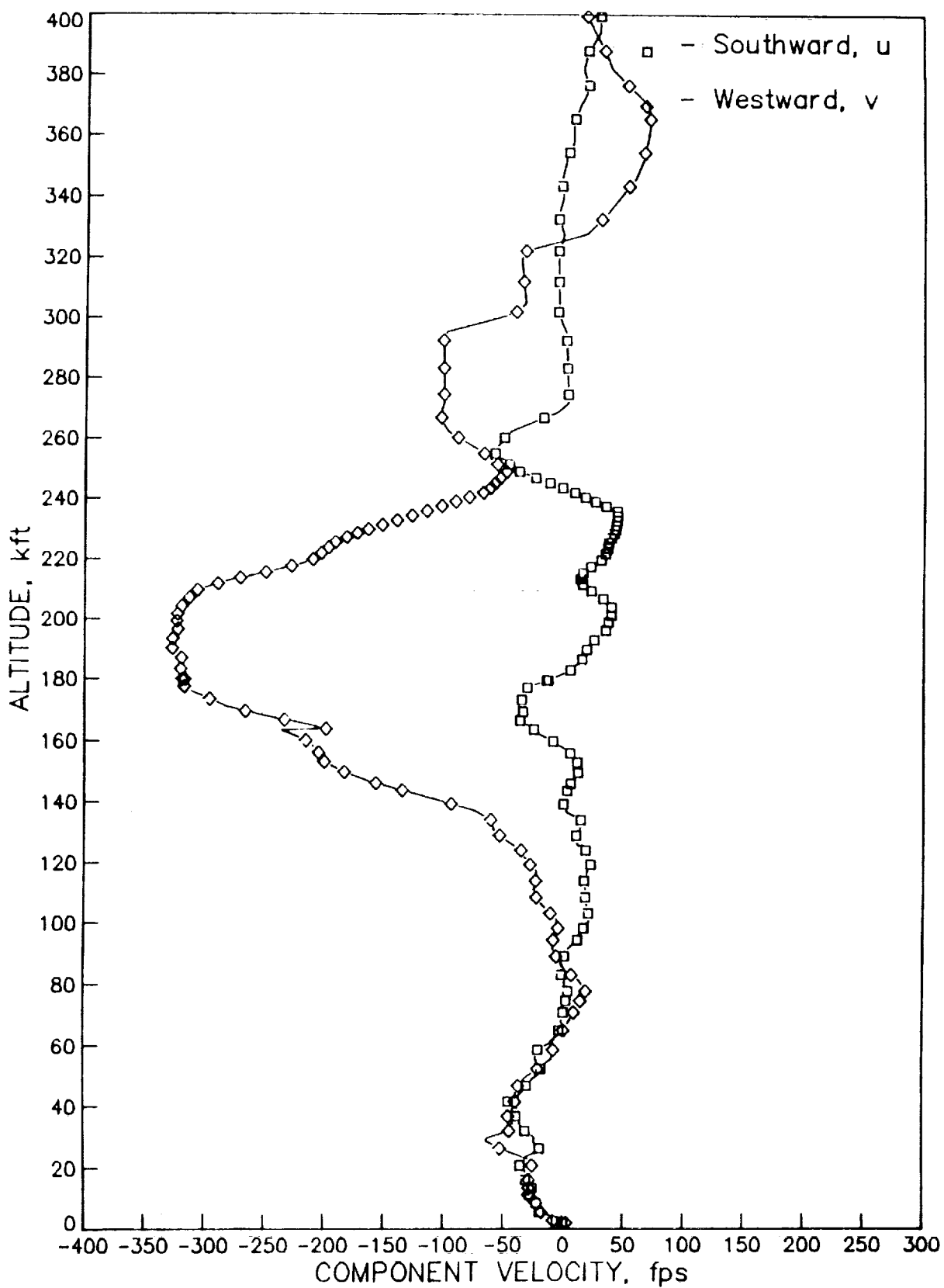


Figure II-4. Horizontal wind components versus altitude for STS-35.

December 11, 1990

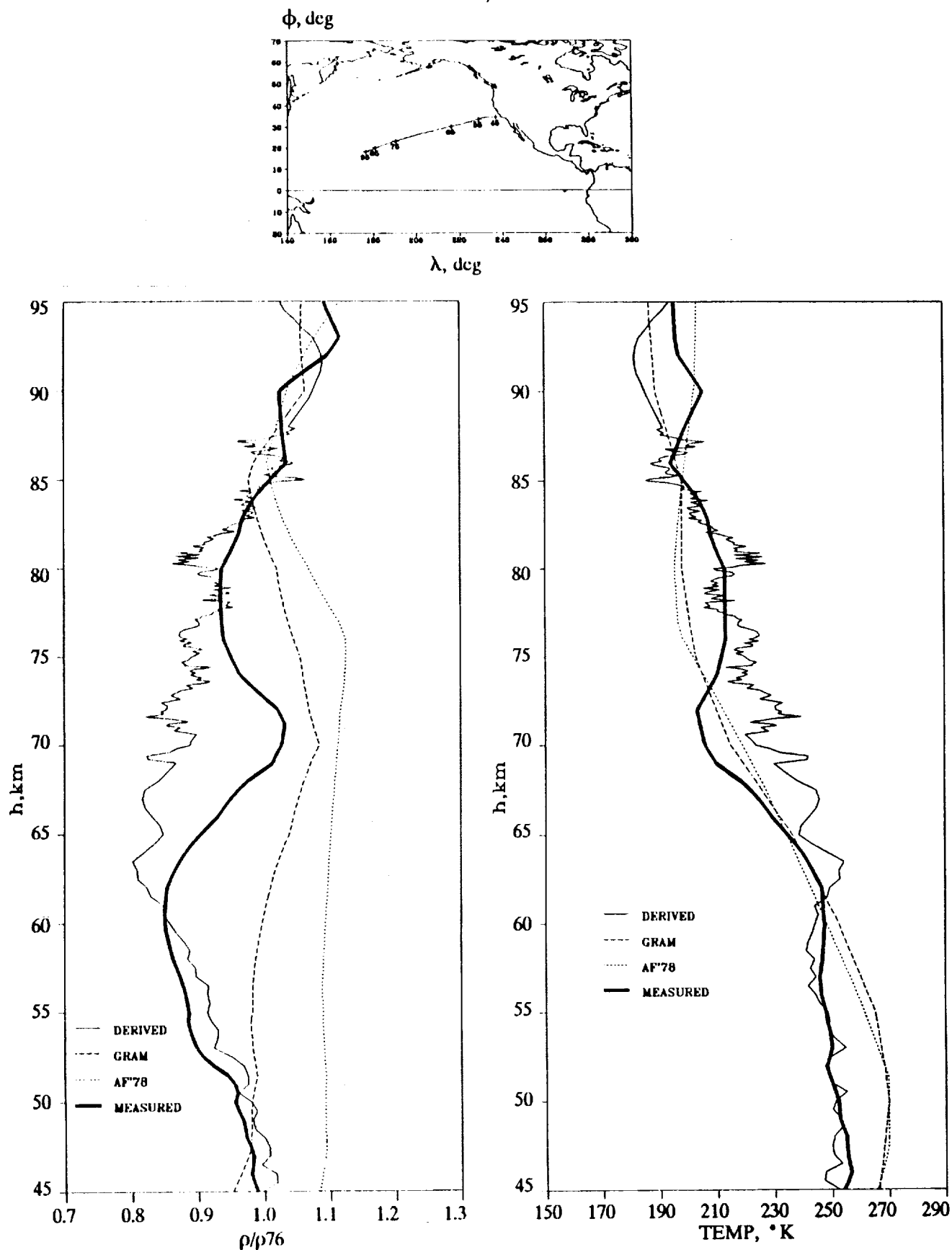


Figure II-5. STS-35 density and temperature comparisons.

### **III. AERODYNAMIC BET DEVELOPMENT**

The 218-word AEROBET for STS-35 was developed using the previously discussed Extended BET which was based on the FM&C reconstructed inertial trajectory and the JSC atmospheric data. As discussed in Part IV of Reference 1, this file is combined with the onboard measurements of the control surface deflections and RCS jet activity to define the in situ orbiter configuration; the final spacecraft mass and inertia properties; and the Shuttle aerodynamic databook (final pre-operational L7 version, Reference 7, rectified using the FAD26) to create the Aerodynamic BET. Given these data, interesting comparisons between flight-derived and predicted aerodynamic coefficients can be made. Readers are urged to peruse the previously noted reference for more details as to the AEROBET file contents, the various computations utilized, the Orbiter aerodynamic databook formulation, and, equally important, a discussion of the Shuttle control surface and RCS jet configuration.

Flight data are derived from the IMU measurements (in the body axes) and the associated air-relative information as discussed in the previous inertial and Extended BET development sections. Though the flight computations are straightforward, readers are reminded that the uppermost altitude for which meaningful performance computations can be made is restricted to approximately 280 kft due to IMU accelerometer (quantization) limitations. The quantization limitation of 1 cm/sec corresponds to approximately 1 mg. However, for appreciable signal, in situ measurements of the spacecraft accelerations, angular rates (and, equivalently, angular accelerations), the spacecraft mass and inertia properties, and the associated QBAR (see Table B-1 of Appendix B) define the flight data as indicated in Reference 1. Mass properties utilized for this flight are presented as Table 6 herein. The center-of-gravity data are given as inches in the structural reference system.

As one might expect, the resultant computations are "total" coefficients, consequently, the effects of the RCS jets must be removed. A measure of the RCS activity is derived from the so-called OI-2 file provided by LaRC. Figure III-1 shows the RCS firings which, at a 1 second spacing, are seen to be minimal.

The OI-2 file is also the source for the Shuttle control surface measurements necessary for the aerodynamic databook formulation. These data were reformatted for use at LaRC by Unisys. The nine-track reel was NX0562. This file was provided at 25 samples per second and thinned using the FM&C software utility, CONFIG, to 1 per second at times

commensurate with the other BET data. CONFIG nominally performs editing, to include selection of the best data channels where redundancy is available. However, for this flight, it was evident that the measurements in many of the channels of interest were extremely noisy. Consequently, the separate measurements of inboard and outboard elevon panel deflections on a given side were necessarily considered as one in the same rather than the usual averaging per side. For this purpose, FM&C adopted the cleanest channel available. On any given side, this approximation is of little concern. However, in some instances, left and right side elevon data had to be assumed equal across sides. This assumption negates computations of aileron deflection, an approximation of little consequence for performance investigations. Finally, rudder and speedbrake deflections were properly held stale for the first 1535 and 1285 seconds, respectively, despite the recorded implications. As noted, most if not all of the modifications required were of minimal importance. However, had these data been any noisier, the development of a contiguous AEROBET over the entire entry time frame might well have been prohibited. Final, edited control surface deflections for STS-35 are presented as Figure III-2.

Pursuant to the control surface measurement problems previously noted, FM&C discussed these anomalies with JSC, to include the concern that there seemed to be a more noticeable increase of erratic configuration data over the past few flights. The source for these erratic data has not been identified or isolated. To repeat, the control surface editing required on this particular flight did not present any particular problems for performance comparisons. The concern herein is that further degradations in the recorded data might well preempt (or, at least, degrade) such comparisons in the future.

The AEROBET generated for this flight is available on the CDC machines at LaRC as ABETF35, a semi-private file under UN=274885C. In this instance, due to size considerations, the file is a direct access file. The last section herein presents some summary results generated from the AEROBET.

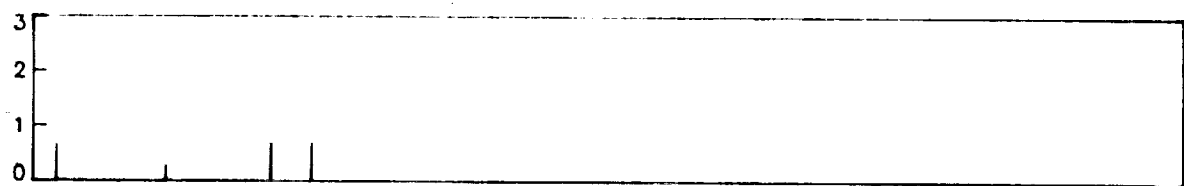
	Weight Lbs.	Center-of-gravity (inches)		
		X	Y	Z
Post deorbit	227706.2	1078.7	-0.5	371.4
Entry Interface	226613.2	1080.8	-0.5	371.4
EI + 3 minutes	226486.2	1080.2	-0.5	371.2
Mach 3	225531.2	1079.1	-0.5	370.8
Landing	225329.2	1080.5	-0.4	368.4

	Moments and products of inertia slug ft <sup>2</sup>					
	I <sub>xx</sub>	I <sub>yy</sub>	I <sub>zz</sub>	I <sub>xy</sub>	I <sub>xz</sub>	I <sub>yz</sub>
Post deorbit	946415	7352420	7640401	850	182210	868
Entry Interface	949754	7263416	7550845	1109	181057	451
EI + 3 minutes	947949	7245809	7534404	1162	176254	461
Mach 3	944545	7228591	7517573	1523	171229	533
Landing	973441	7249220	7513760	1783	163136	520

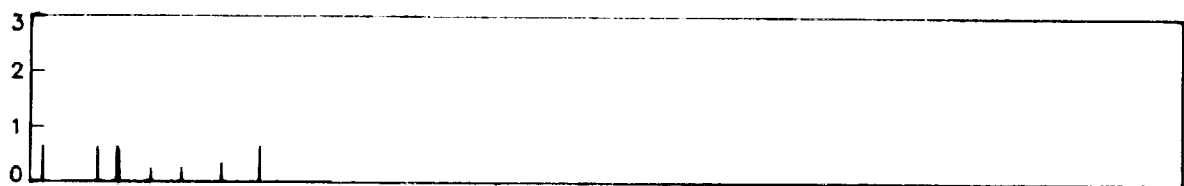
\* Approximate EI time is 19385 GMT seconds

**Table 6. STS-35 mass properties.**

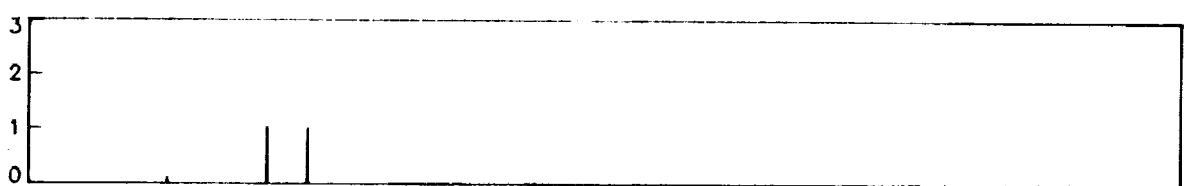
LHUF JETS



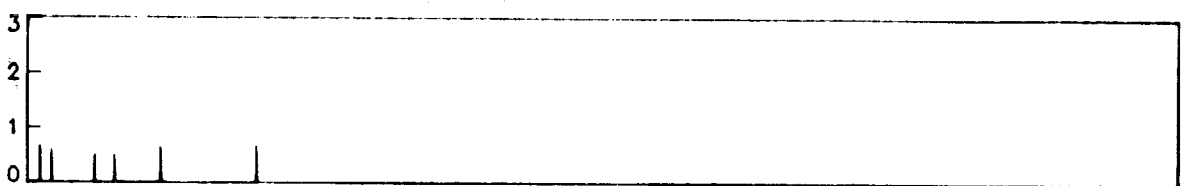
LHDF JETS



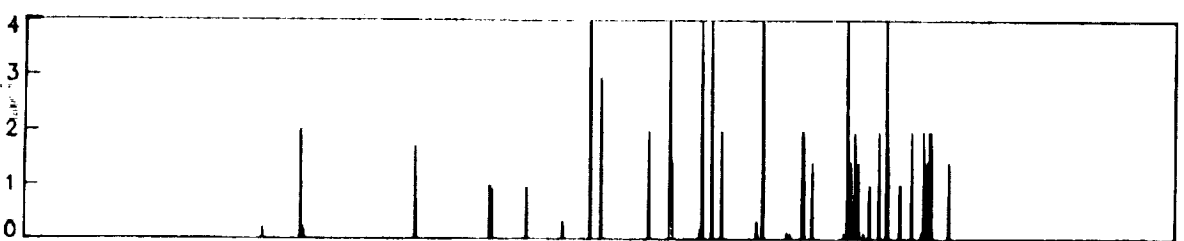
RHUF JETS



RHDF JETS



YAWP JETS



YAWN JETS

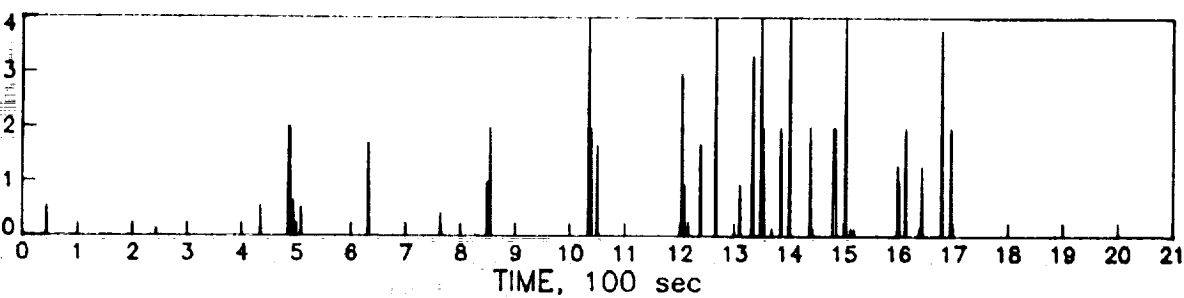
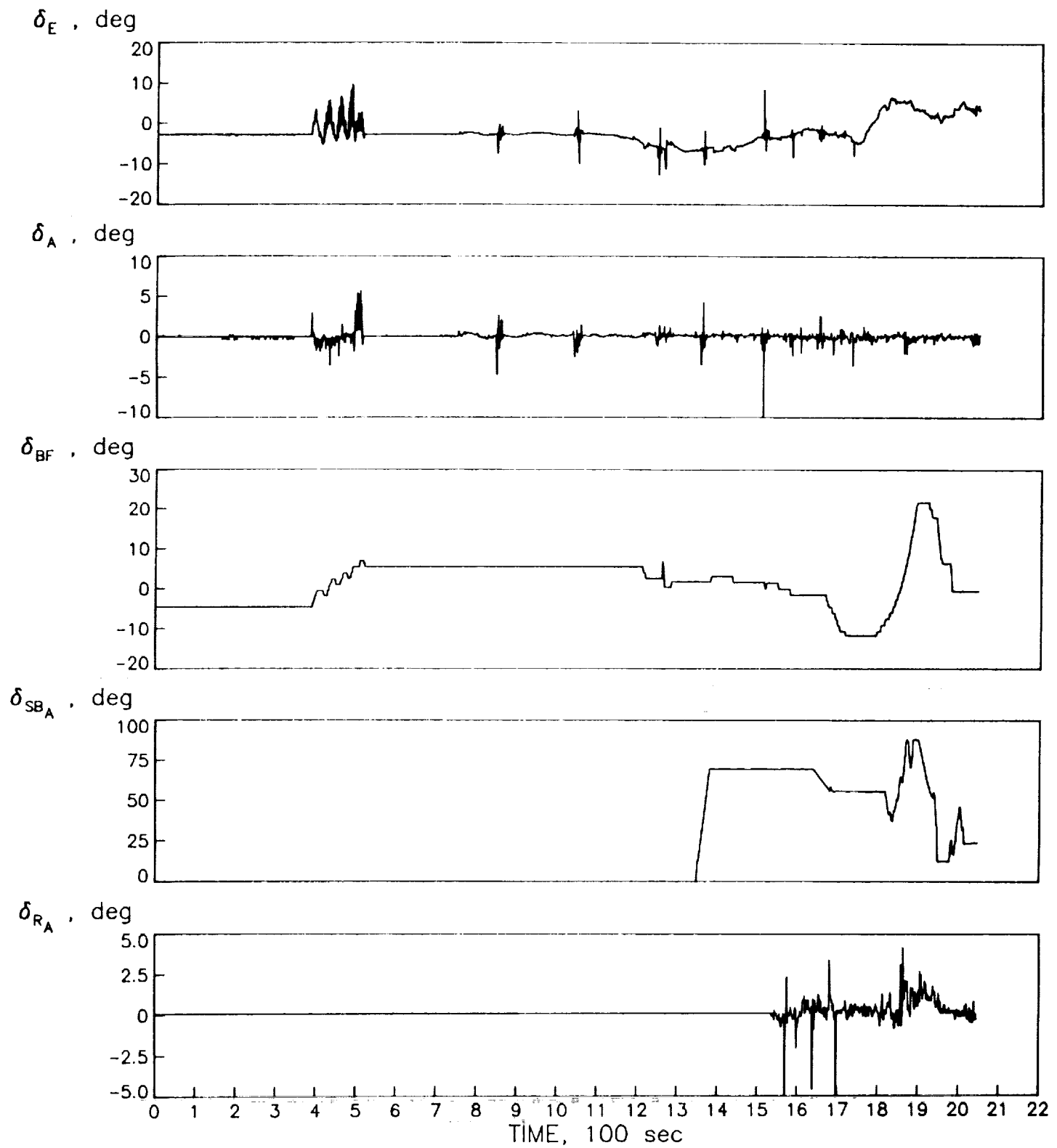


Figure III-1. STS-35 RCS jet activity during entry.



**Figure III-2. Time history of STS-35 control surface deflections.**

#### IV. SUMMARY RESULTS

Summary results showing aerodynamic performance comparisons for STS-35 are presented herein. Time histories of most of the elements necessary to determine flight coefficients and generate the necessary databook predictions have already been presented, either as figures within the report or included as part of the listing in Appendix B. In this section, some of this information will be re-plotted versus Mach number as a matter of interest prior to presenting the actual flight/databook differences. Though Mach number is utilized as the independent variable here, readers should note that the databook formulation incorporates table look-ups versus altitude, VBAR, and Mach number dependent upon the particular flight regime. Since altitude is used above 300 kft, and since this altitude is well above the threshold of the IMU accelerometer measurements, plots versus altitude, though interesting, will not be presented. VBAR is utilized for values of that variable between 0.08 ( $h \approx 300$  kft) and 0.005. The lowermost value translates to an approximate Mach number of 14.4 ( $h \approx 181$  kft). However, even though VBAR is utilized throughout much of the entry, plots versus Mach number are still considered the most relevant. To that extent, it should also be stated that these plots were initiated 410 seconds from epoch to assure that Mach number would be a monotonically decreasing variable thereafter. This time corresponds to an altitude of 282 kft.

Figures IV-1 and IV-2 show the spacecraft angular rates and linear accelerations versus Mach number. Control surface deflections are presented as Figure IV-3. The shaded band shown thereon provides for a measure of comparison versus the total range flown over an ensemble of 22 of the first 24 Shuttle entry flights, i. e., through and including STS 61-C. Obviously, the shaded region shown on this and other plots herein may no longer reflect a total spread since many later missions are not included in the compiled statistics.

Figure IV-4 presents the flight center-of-gravity plotted against Mach number. Again, the range associated with the earlier 22 flights is noted by the shaded region. As can be seen, the flight c.g. is somewhat forward of the previous subset of flights. This flight might well represent the extreme since it was one of the heaviest, if not the heaviest, Shuttle entry flights of record with its associated Astro payload.

The air-relative attitude angles included as part of the listing in Appendix B are re-plotted herein versus Mach number in Figure IV-5. Again, angle-of-attack excursions based on the

22-flight subset are indicated thereon. No comparable ranges were ever computed for the side-slip and roll angles. It can be observed that the excursions in the side-slip angle are quite small as one should expect, i. e., there are no steady-state departures from the inherent weather-vane stability of the Orbiter. This is an observation that supports the adequacy of the NOAA wind profile adopted from the JSC BET, at least over the subsonic environs where winds are more significant. On many past flights, large departures in side-slip and erroneous angle-of-attack computations were evident and had to be rectified by wind estimation methods and other supporting analyses. In any event, comparisons of both  $\alpha$  and  $\beta$  with the equivalent SEADS-derived quantities should be of interest.

The final summary results presented are the longitudinal aerodynamic performance comparisons. Aerodynamic differences are presented as a percentage of the flight-derived coefficient. The differences are defined as flight-extracted minus predicted values. Lift, drag, and L/D comparisons are shown in Figure IV-6. Similarly, axial, normal, and pitching moment coefficient comparisons are presented in Figure IV-7, the latter at the 65 percent moment reference center consistent with the databook. The statistical bands superimposed on these figures indicate the expected aerodynamic comparison accuracy, again based on the 22-flight subset. It should be understood that the predicted values herein were rectified using the FAD26 incrementals. These prediction corrections were derived based on consensus opinion of the various project aerodynamicists from analyses of flights through STS-26 (an August 1985 flight). Also, it can be observed that the major departure in the force coefficients (above Mach 20), which suggests a 20 percent over-prediction, coincides with the density bulge indicated in the measured density profile (refer back to Figure II-5 herein). The SEADS determined QBAR should substantiate that this discrepancy is in fact a limitation of the measured density.

The pitching moment comparisons do show considerable differences when compared with the expected results indicated by the statistical band. Though this is not completely understood, it was previously noted that the flight c. g. was further forward than on previous missions and, as can be seen in Figure IV-3, the elevon displacement is toward the lowermost boundary. Obviously, some of the pitching moment discrepancy may be related to density accuracy.

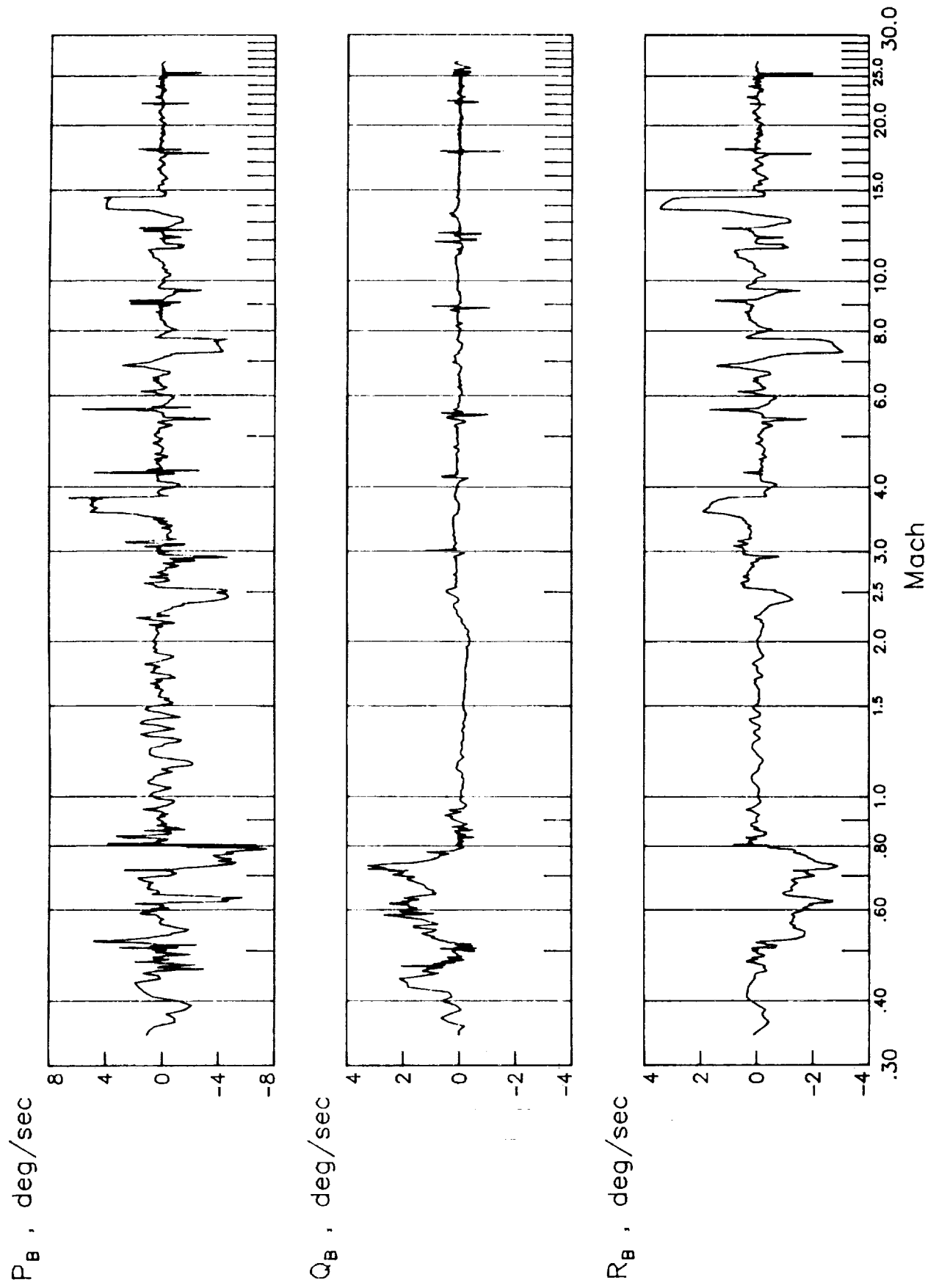


Figure IV-1. Spacecraft angular rates versus Mach number during STS-35 entry.

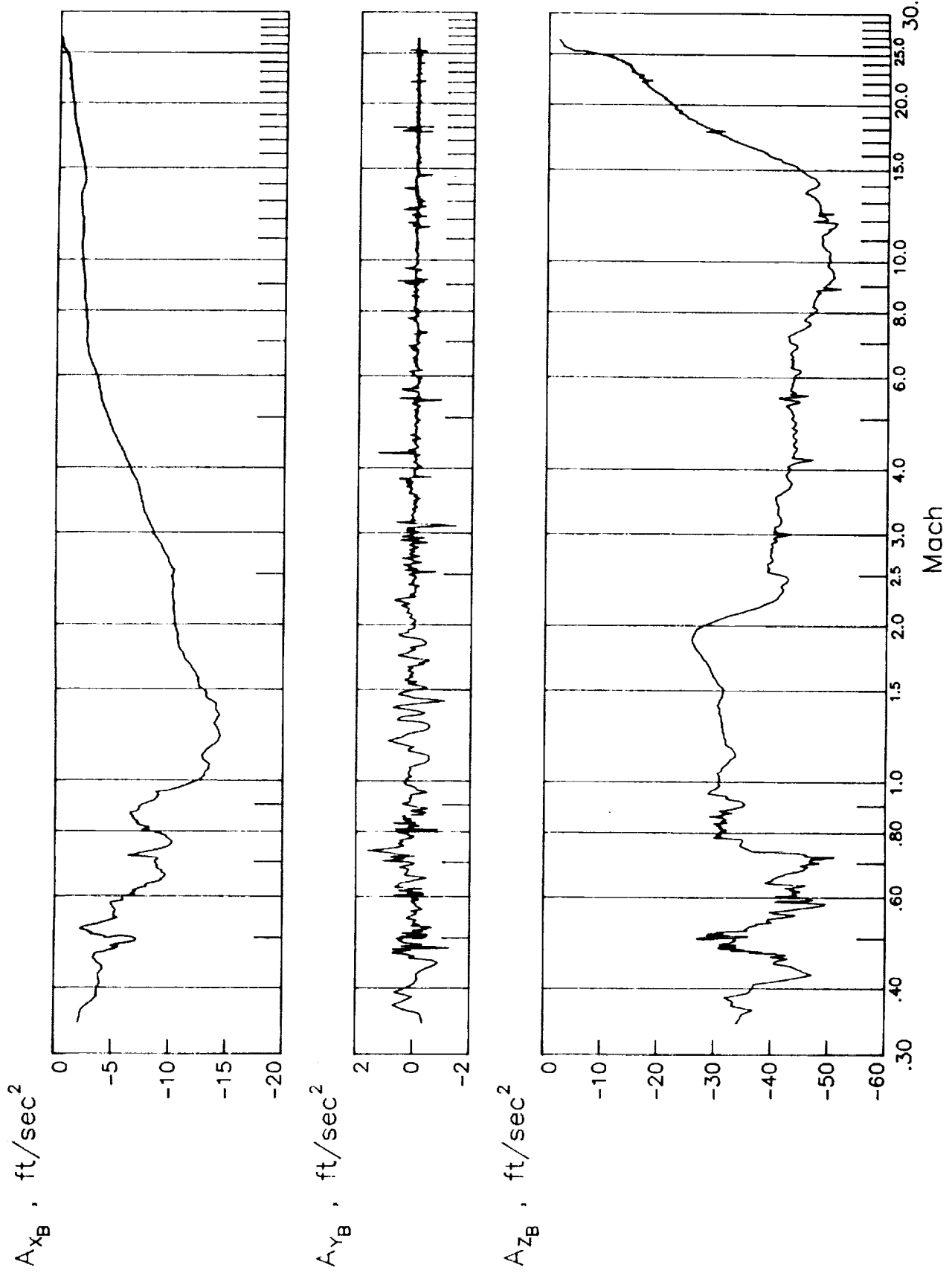


Figure IV-2. STS-35 body-axis accelerations versus Mach number.

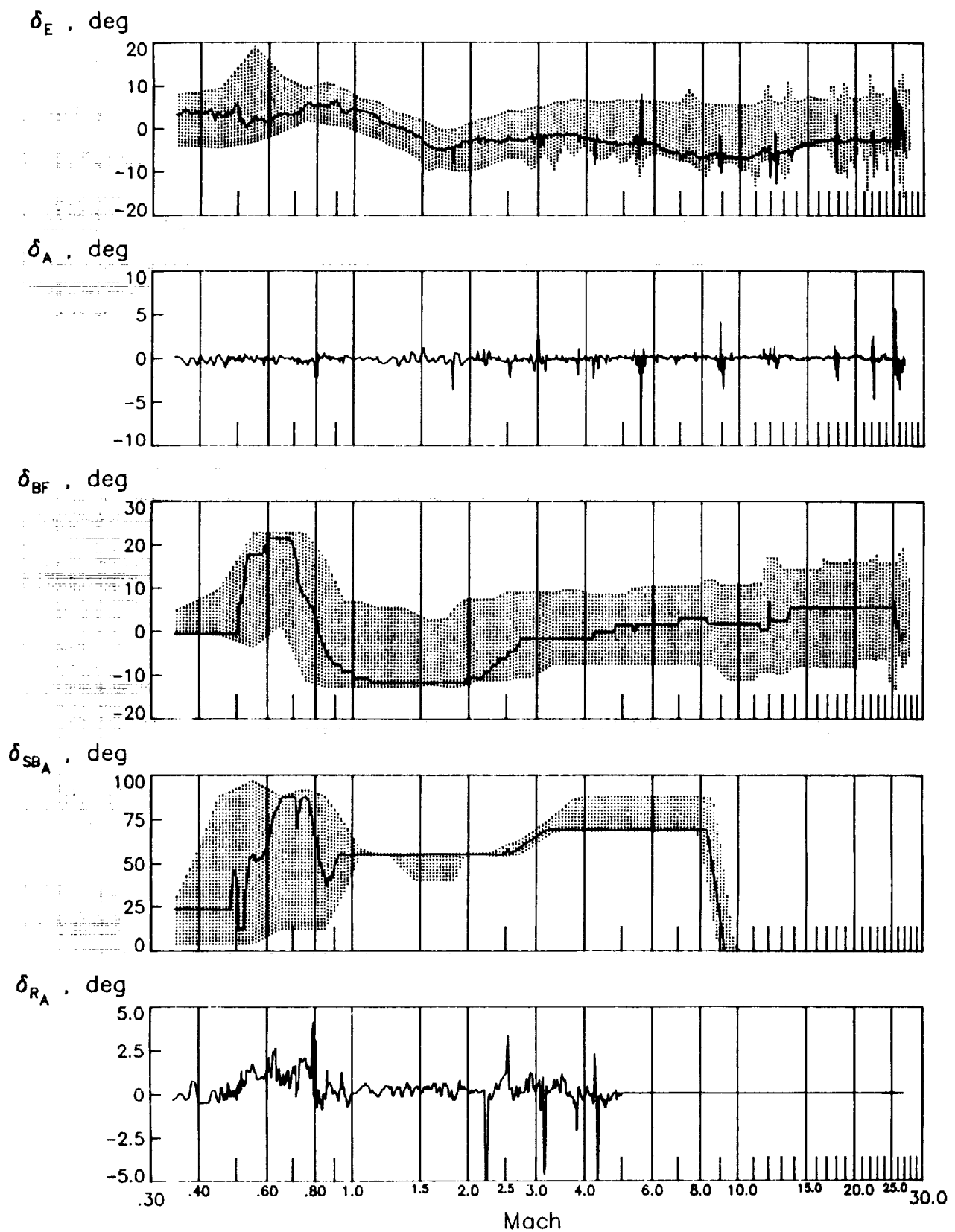
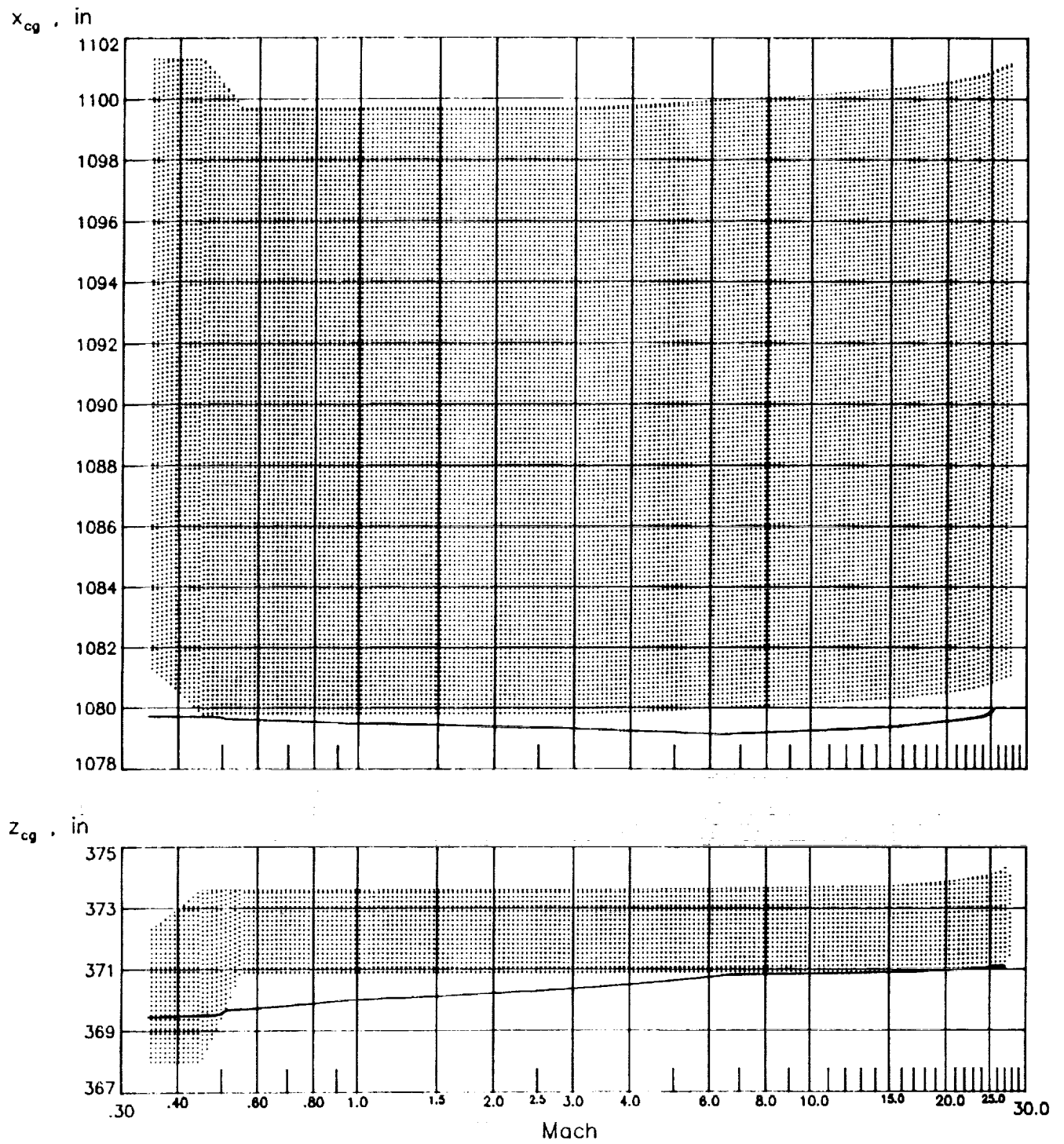
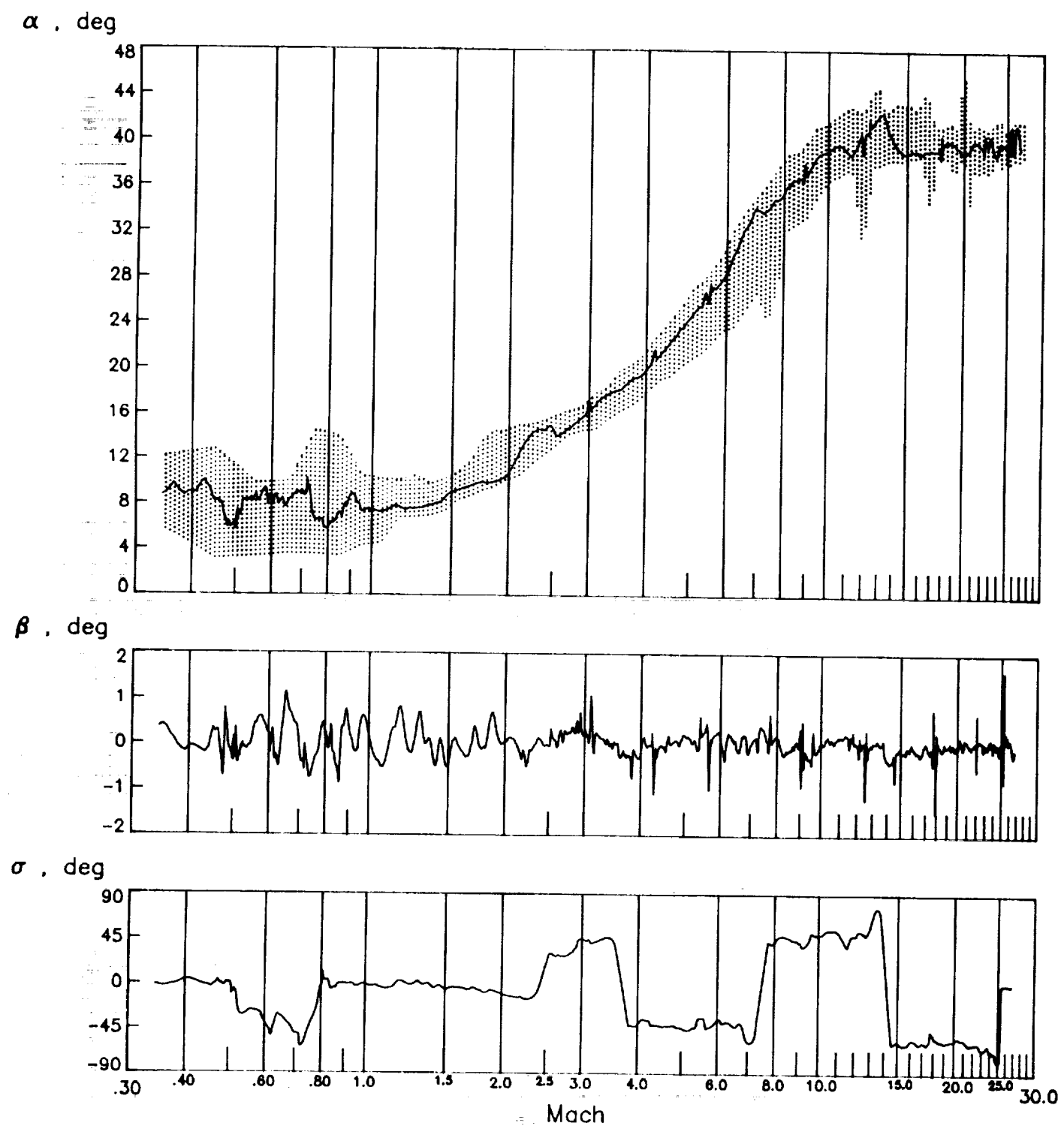


Figure IV-3. STS-35 control surface deflections versus Mach number.

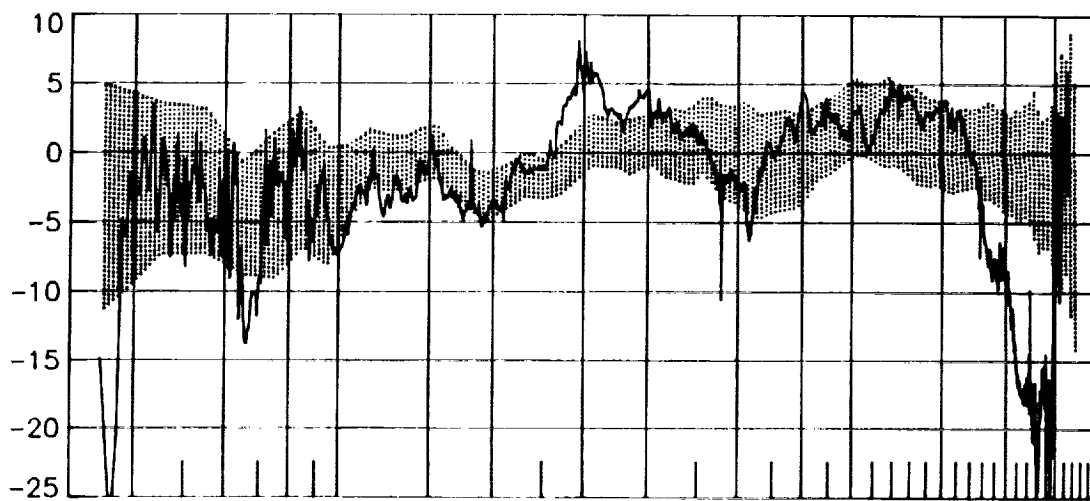


**Figure IV-4. STS-35 center-of-gravity versus Mach number.**

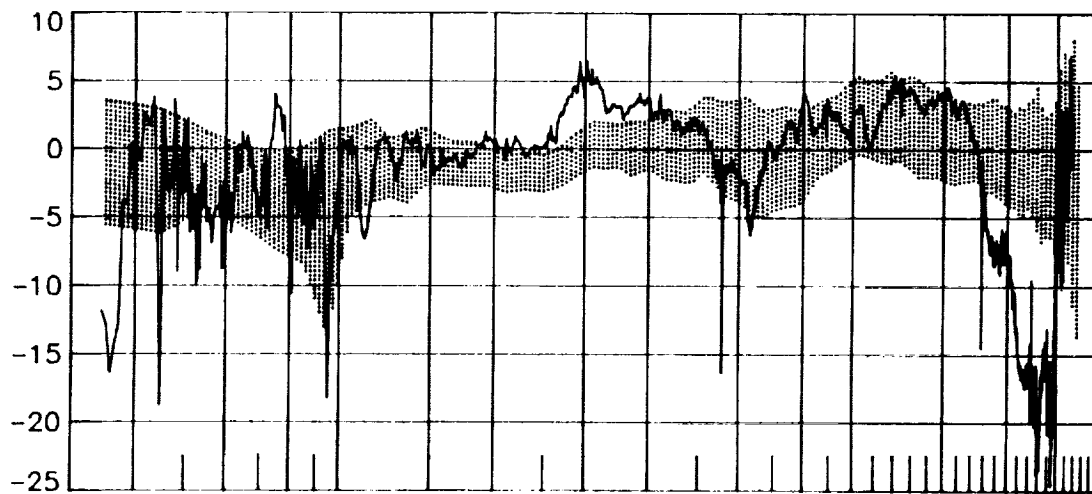


**Figure IV-5. STS-35 air-relative attitude angles versus Mach number.**

$\Delta C_L$ , percent



$\Delta C_D$ , percent



$\Delta(L/D)$ , percent

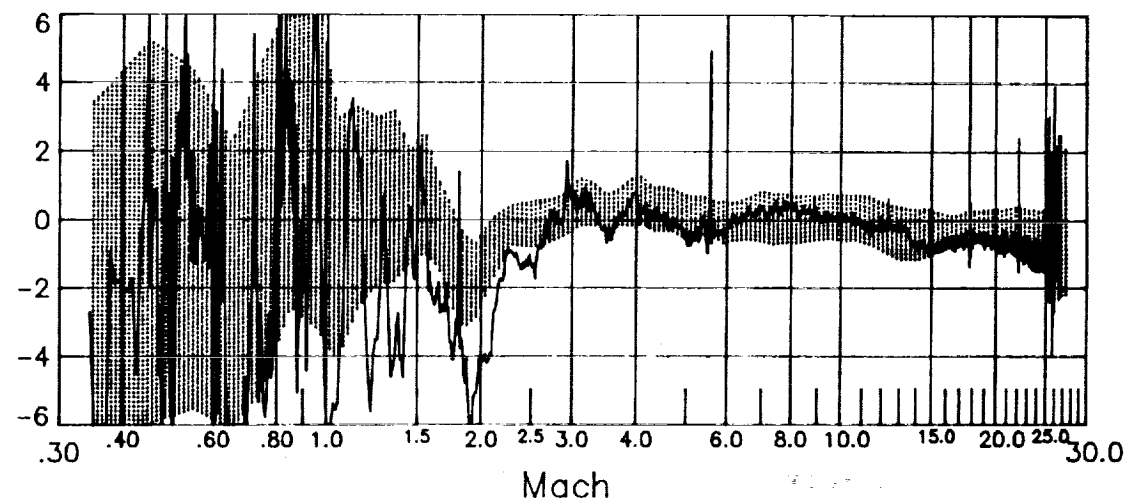
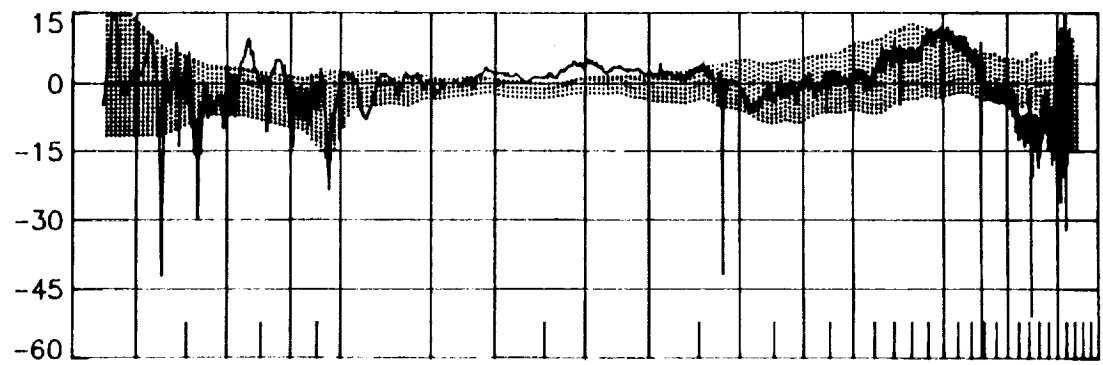
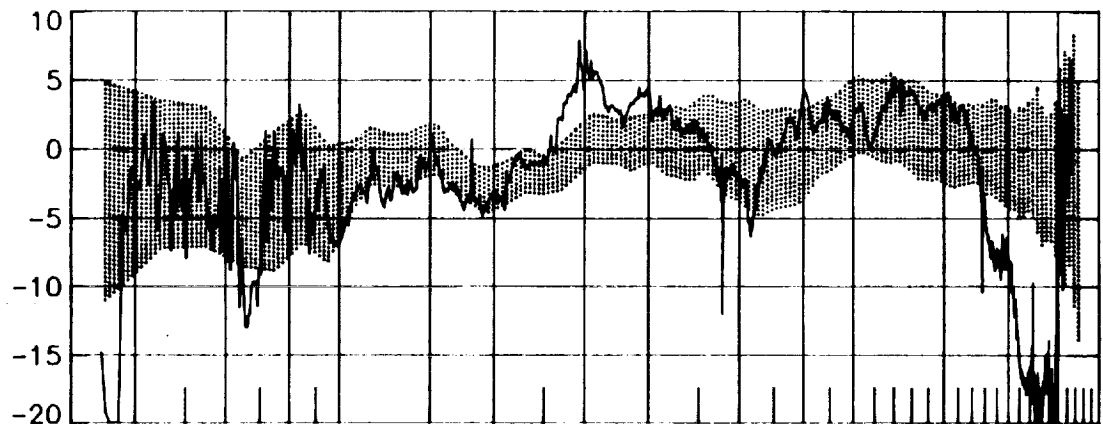


**Figure IV-6.** STS-35 flight/databook lift, drag and L/D comparisons for which the predicted values are rectified by the FAD26 incrementals.

$\Delta C_A$ , percent



$\Delta C_N$ , percent



$\Delta C_m$ , percent

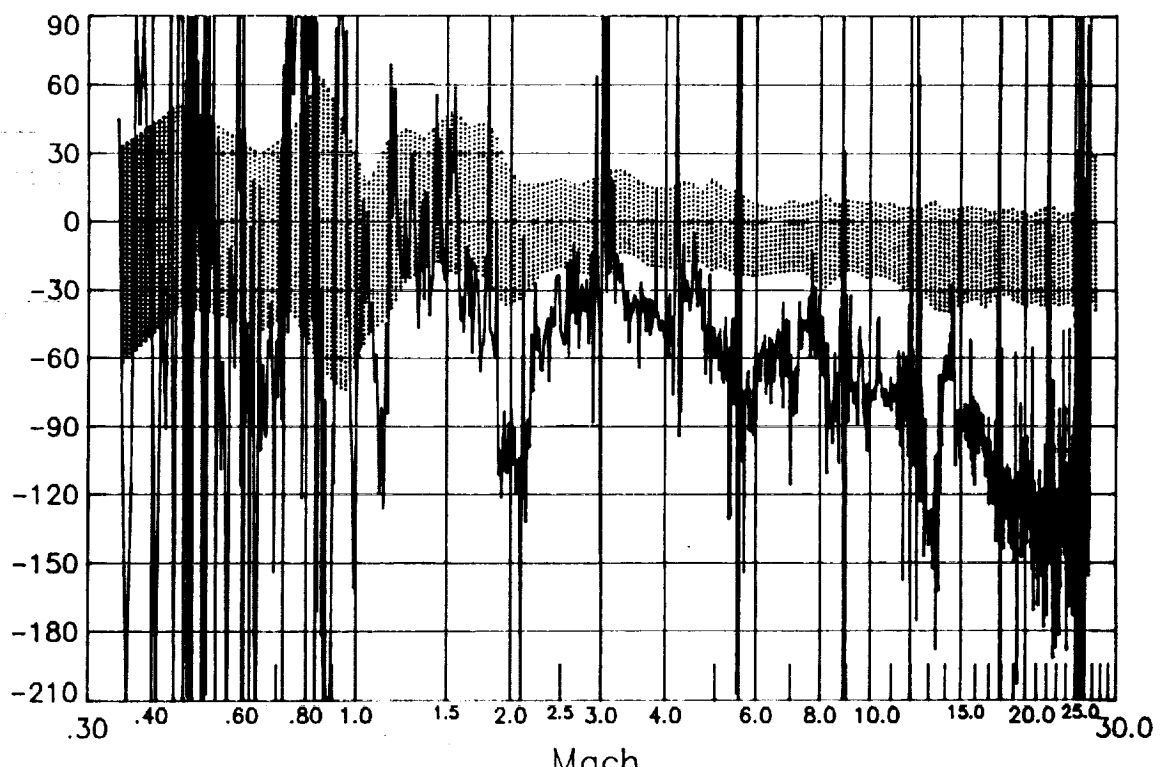


**Figure IV-7. STS-35 axial force, normal force and pitching moment comparisons.  
(databook rectified by FAD26,  $C_m$  referenced to 65% X/L)**

## REFERENCES

- (1) *Findlay, J. T., Oakes, K. F., Jasinski, R. A., and Wood, J. S.;*  
"The ENTRÉE System of Software; Parts I, III and IV," FM&C Report No. 89-R-3, May-June 1990.
- (2) *Oakes, K. F., and Findlay, J. T.;*  
"TDRSS Range and Doppler Observation Processing and Modeling for Inclusion in the ENTRÉE Program," FM&C Report No. 90-R-1, January 1990.
- (3) *Findlay, J. T., and Jasinski, R. A.;*  
"Final Shuttle-derived Atmospheric Database: Development and Results from Thirty-two Flights," NASA CR-185636, July 1990.
- (4) *Romere, P. O. (prepared by);*  
"Flight Assessment Package, Orbiter Aerodynamics, FAD26," JSC-22078, April 1986.
- (5) *Justus, C. G., et al;*  
"The NASA/MSFC Global Reference Atmospheres - Mod 3 (With Spherical Harmonic Wind Model)," NASA CR-3256, March 1980.
- (6) *Cole, A. E., and Kantor, A. J.;*  
"Air Force Reference Atmospheres," AFGL-TR-78-0051, Air Force Surveys in Geophysics, No. 382, February 1978.
- (7) *Schlosser, D. C. and Bornemann, W. E. (approved by);*  
"Pre-Operational Aerodynamic Design Data Book, Volume I, Orbiter Vehicle," Rockwell International Report SD72-SH-0060-1L-7, April 1982.

## **APPENDIX A**

### **FINAL C-BAND RESIDUALS FOR STS-35 TRAJECTORY RECONSTRUCTION**

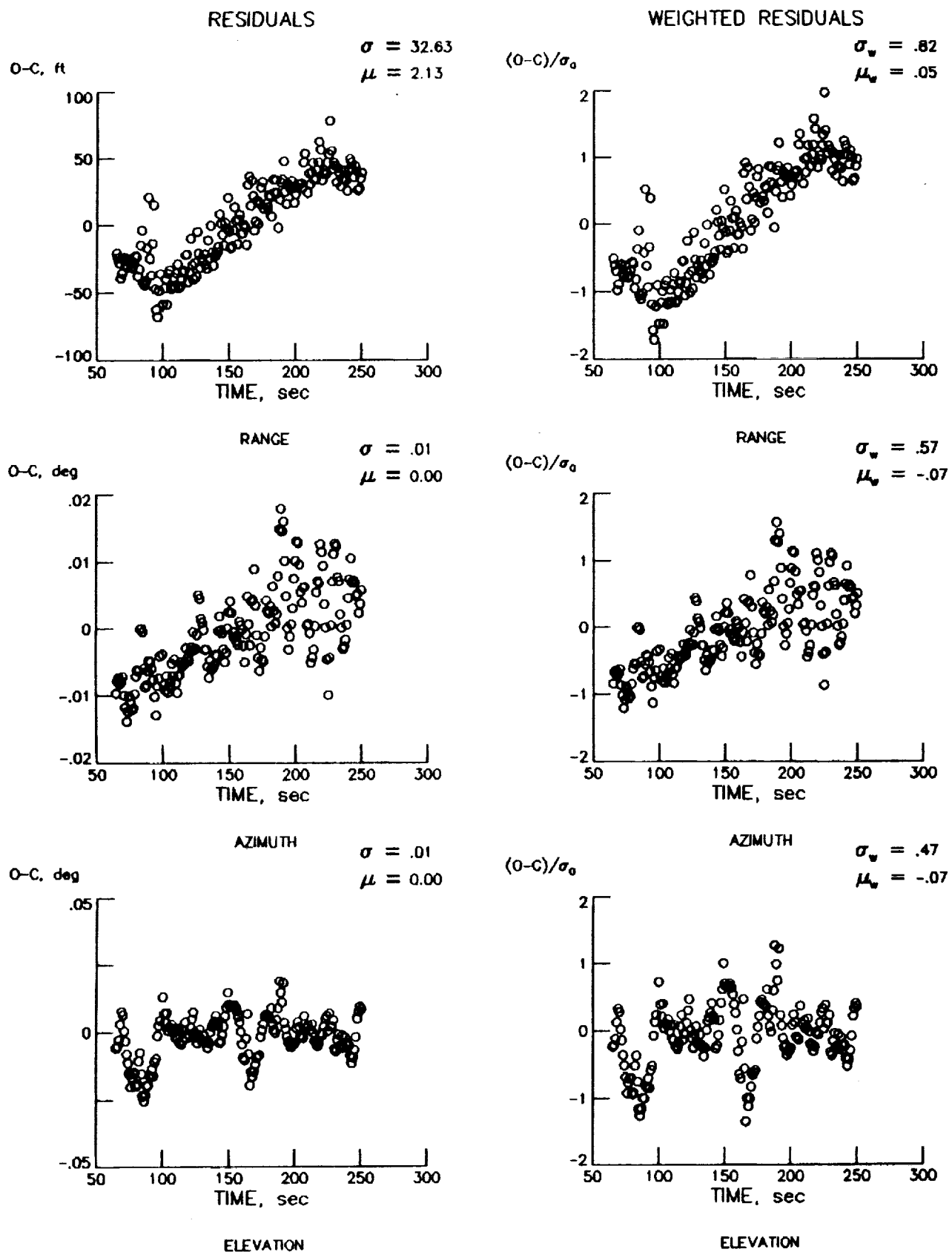


Figure A-1. Final residuals for high-rate Kwajalein station, KMACH.

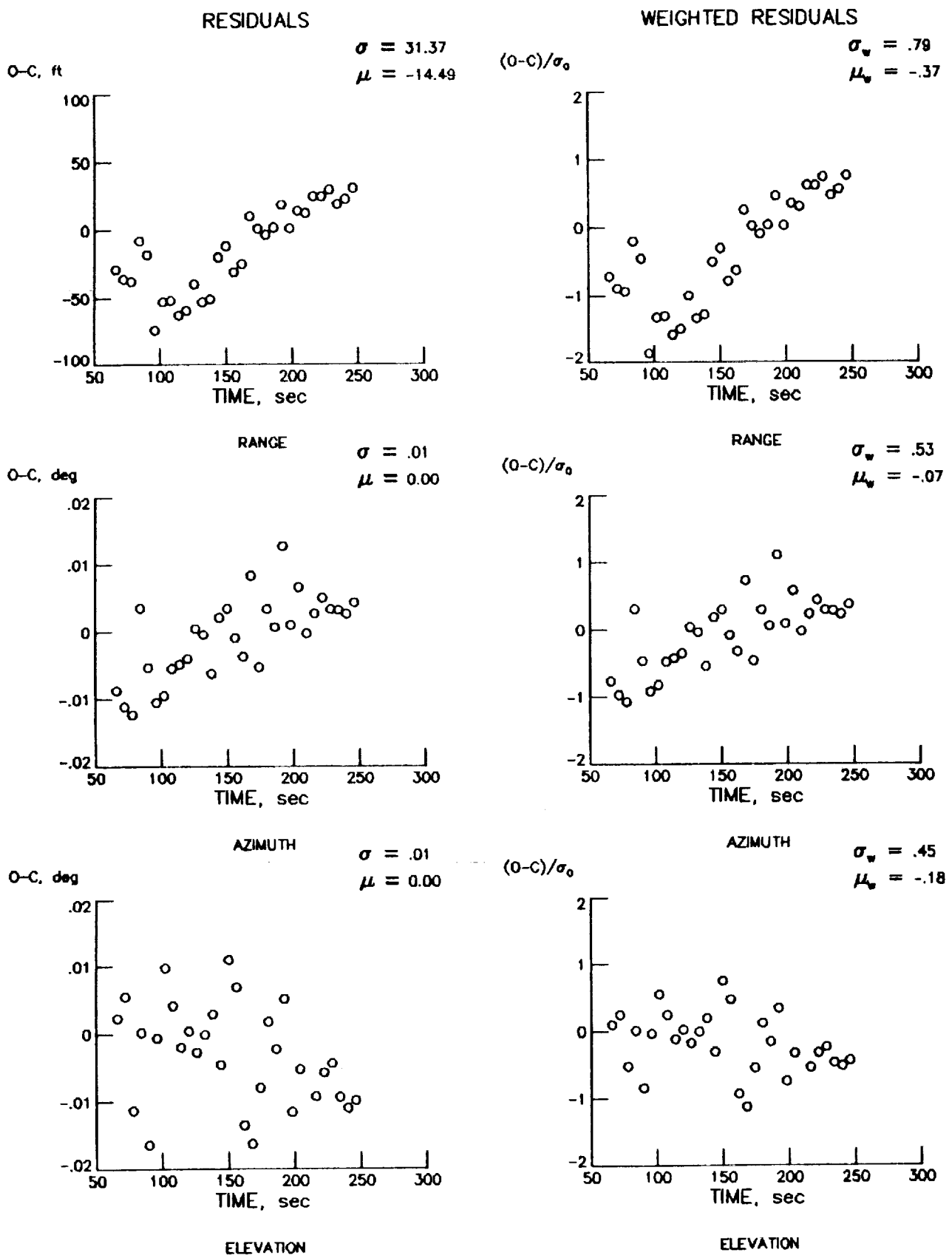


Figure A-2. Final residuals for low-rate Kwajalein station, KMACL.

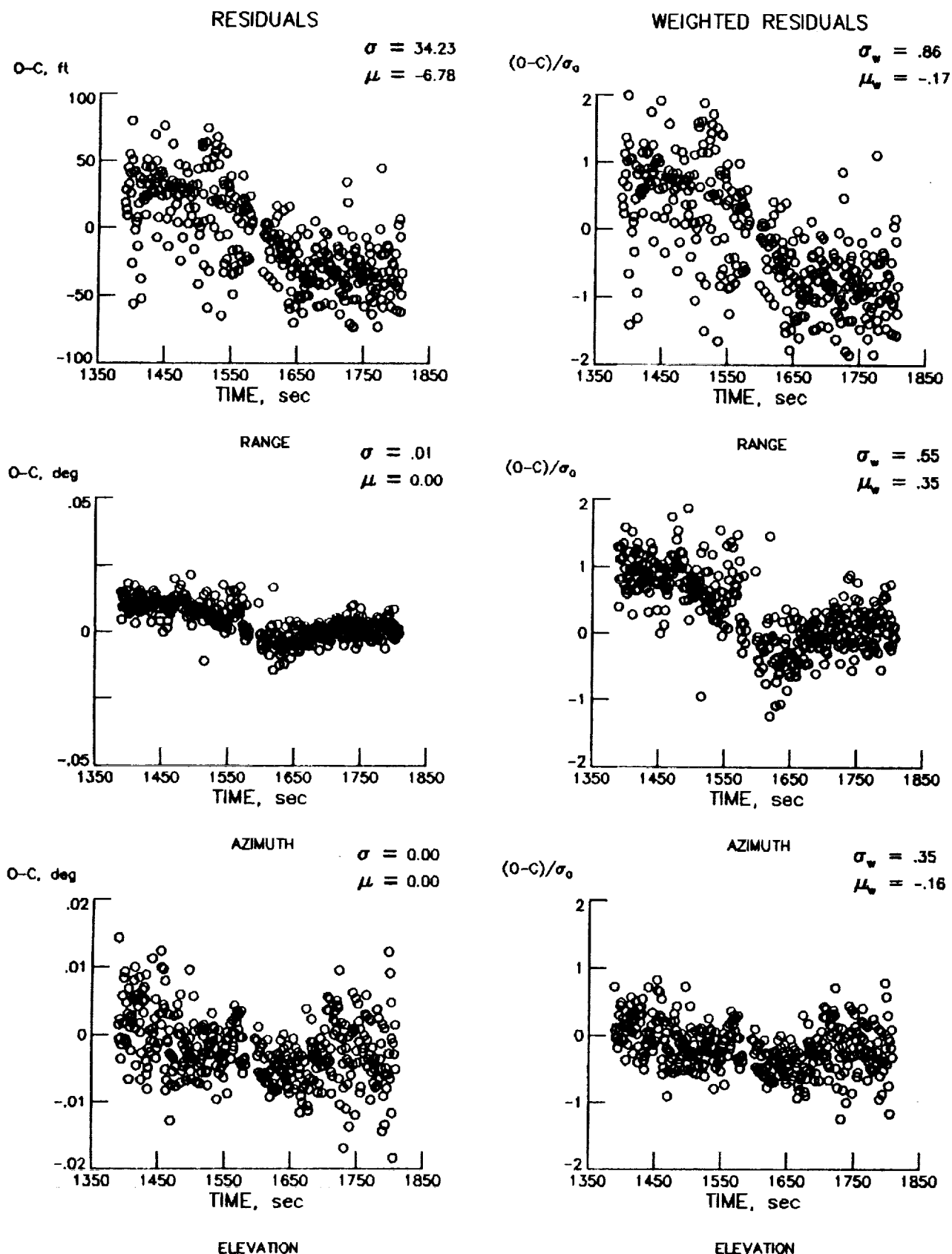


Figure A-3. Final residuals for Pt. Mugu, PMFC.

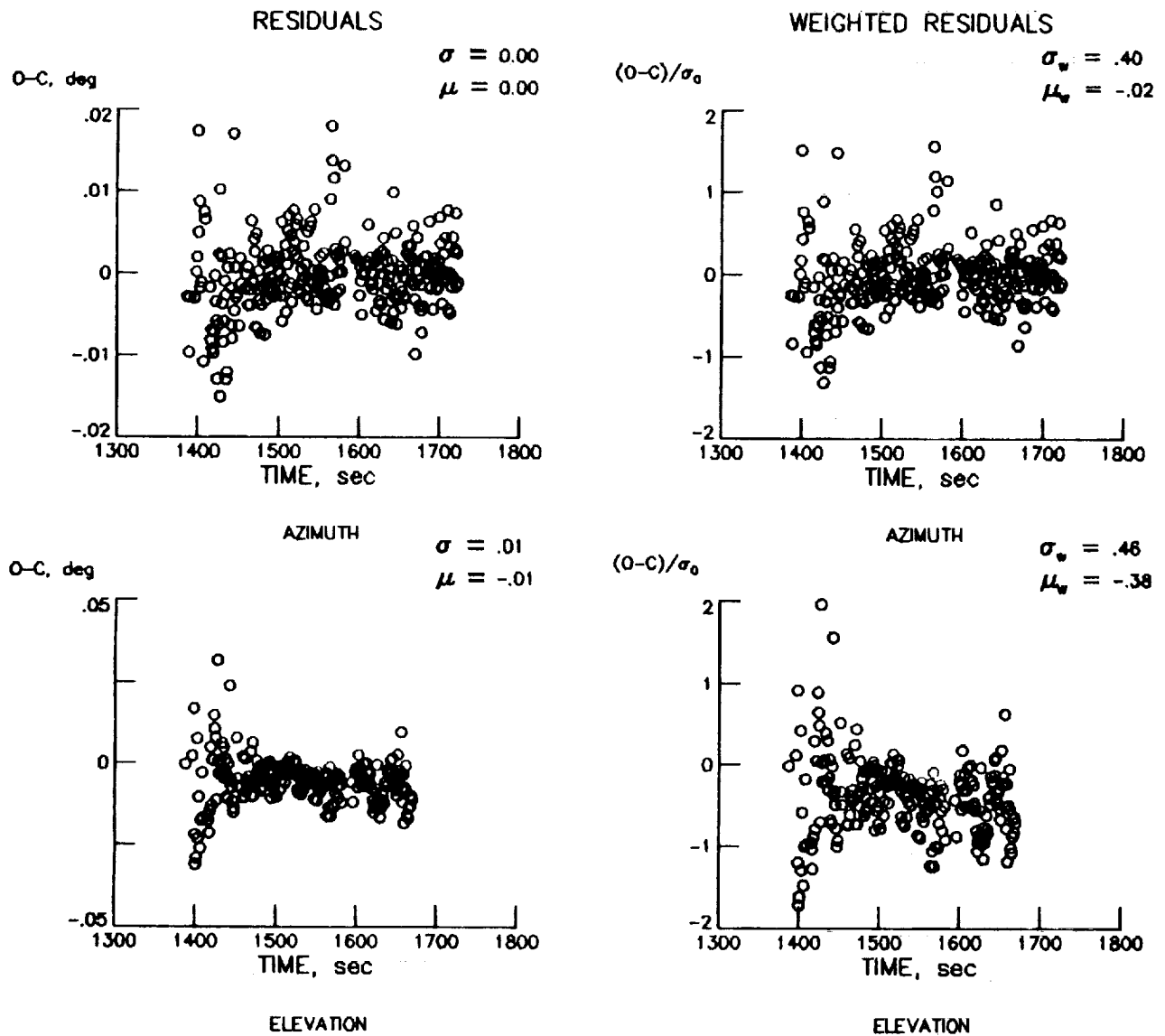


Figure A-4. Final azimuth and elevation residuals for SNFC.

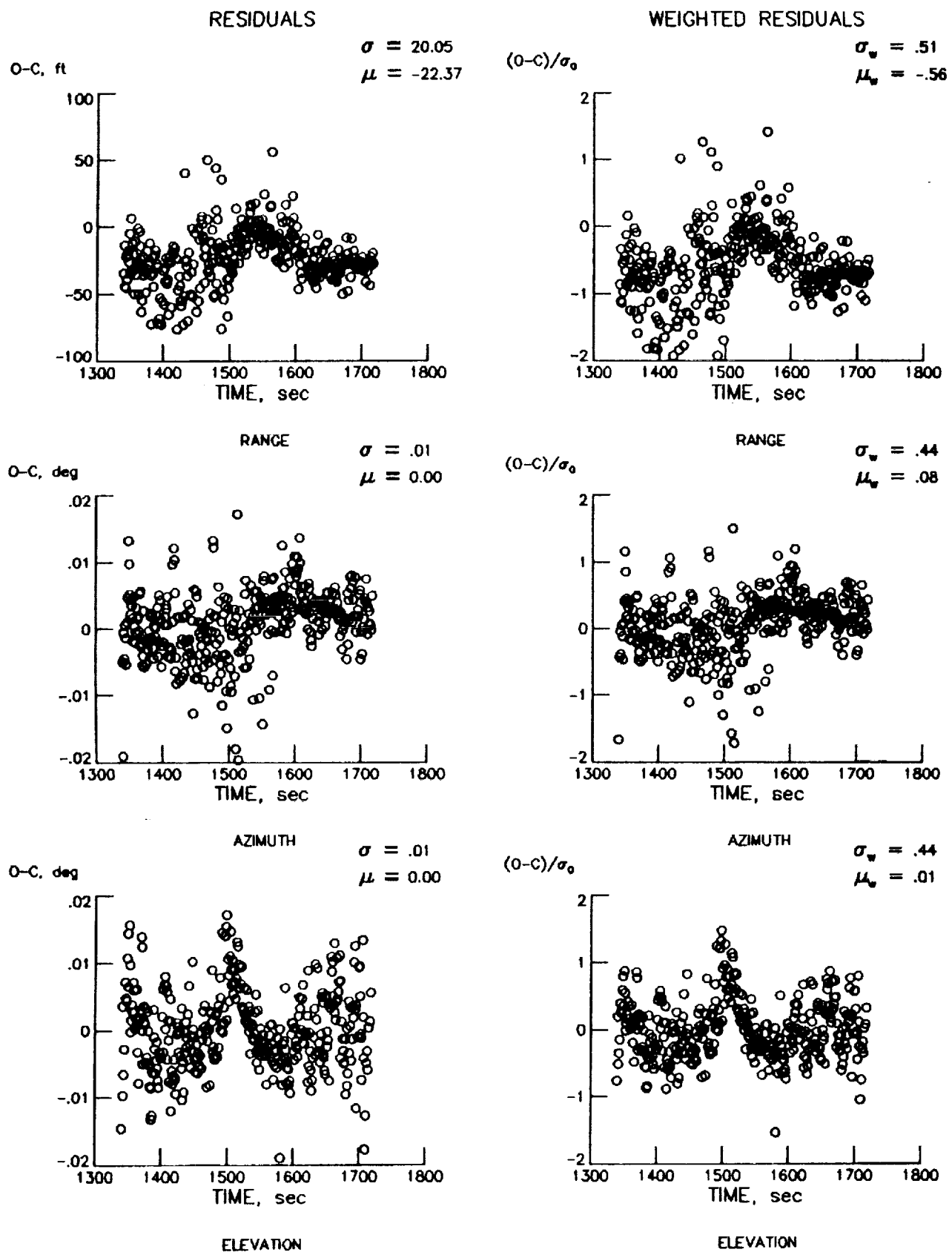


Figure A-5. Final Vandenberg residuals, VDBC.

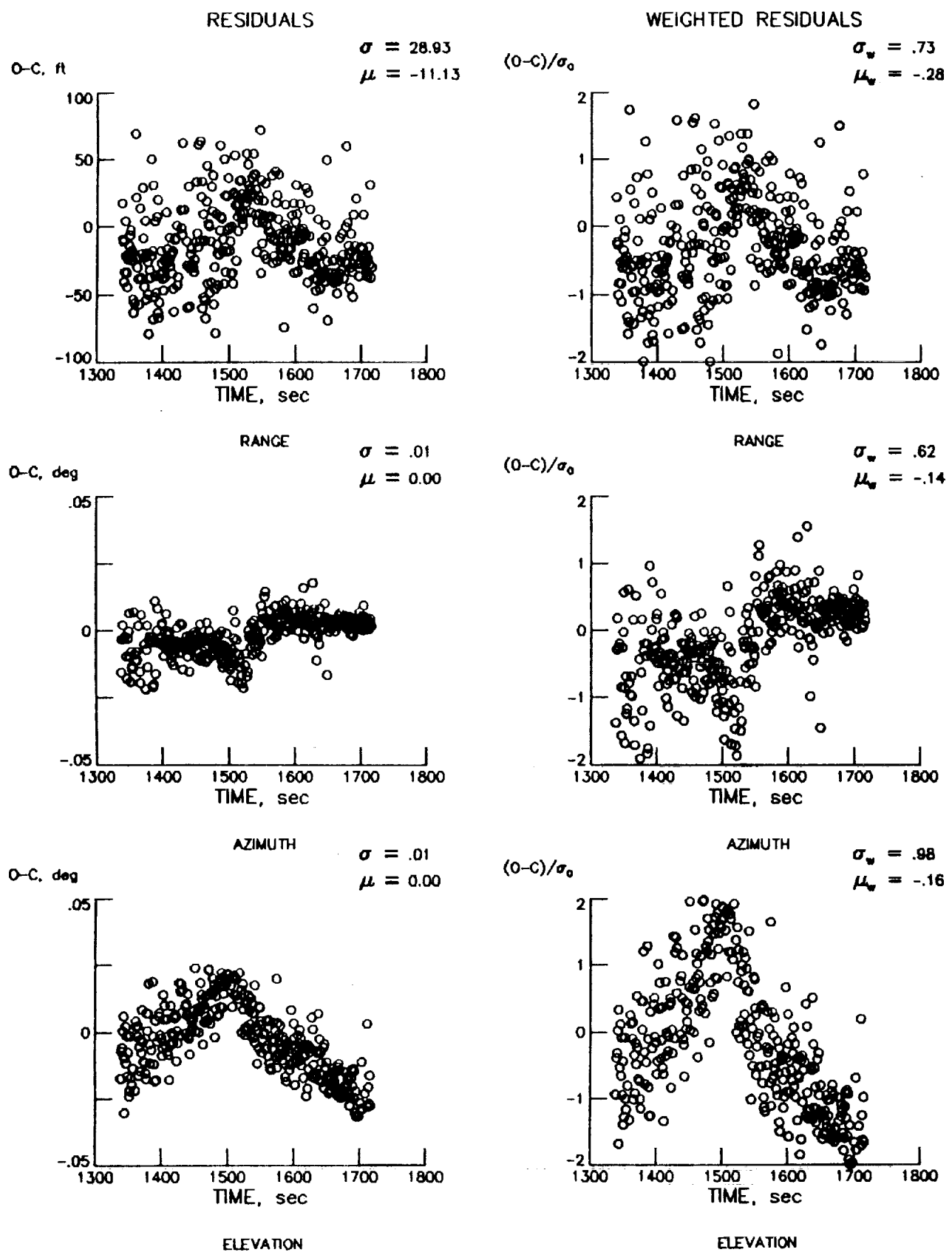


Figure A-6. Final Vandenberg residuals, VDFC.

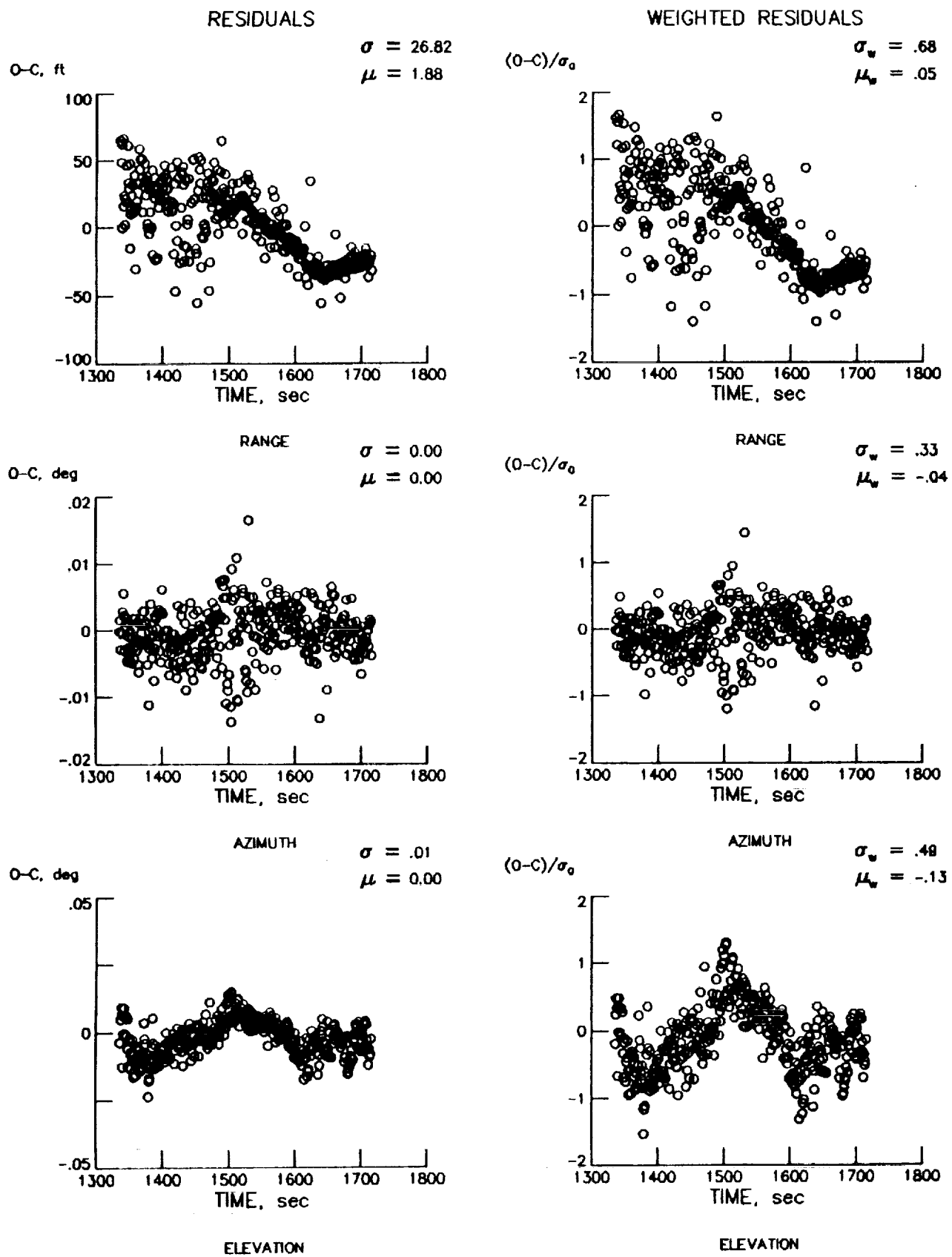


Figure A-7. Final Vandenberg residuals, VDHC.

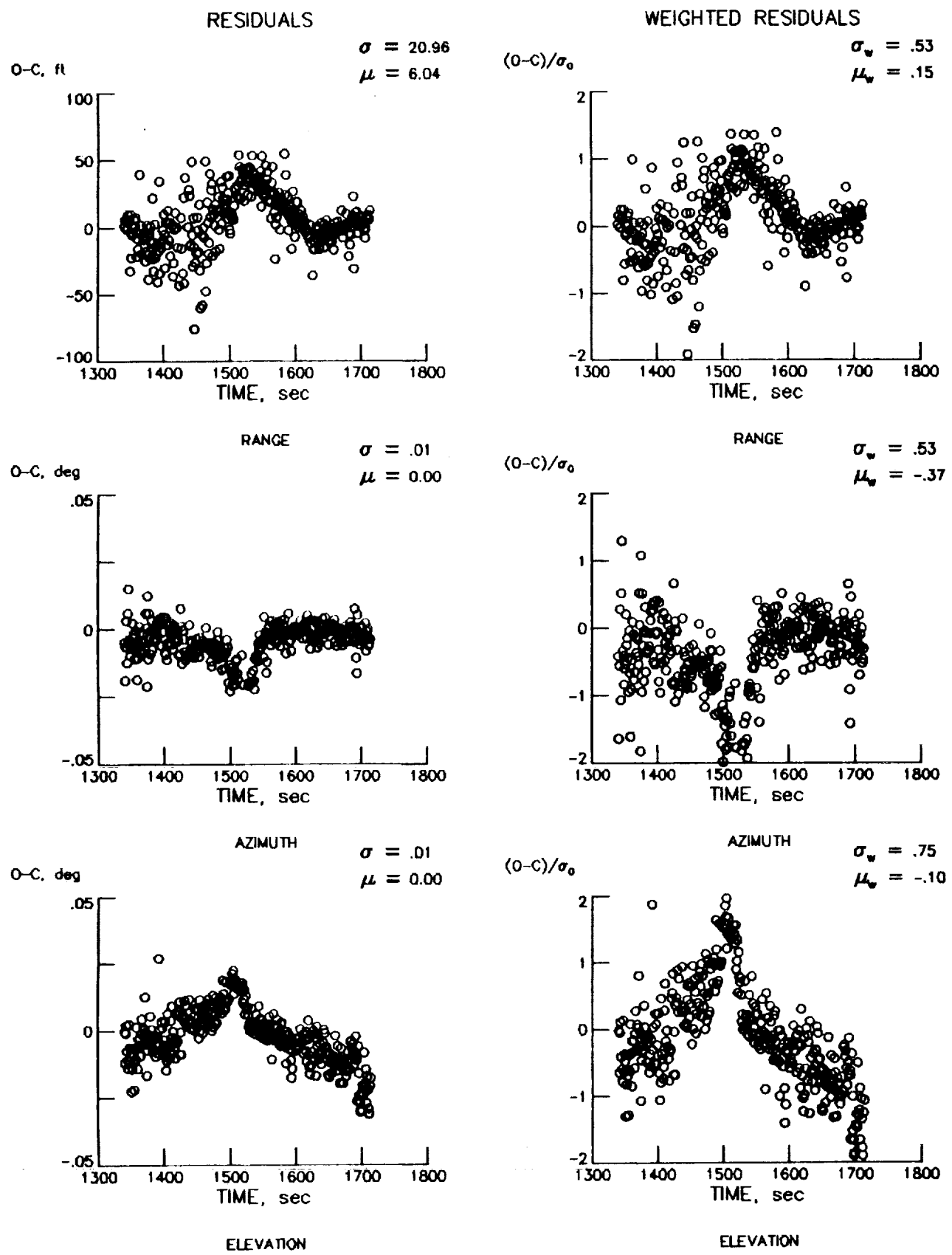


Figure A-8. Final Vandenberg residuals, VDSC.

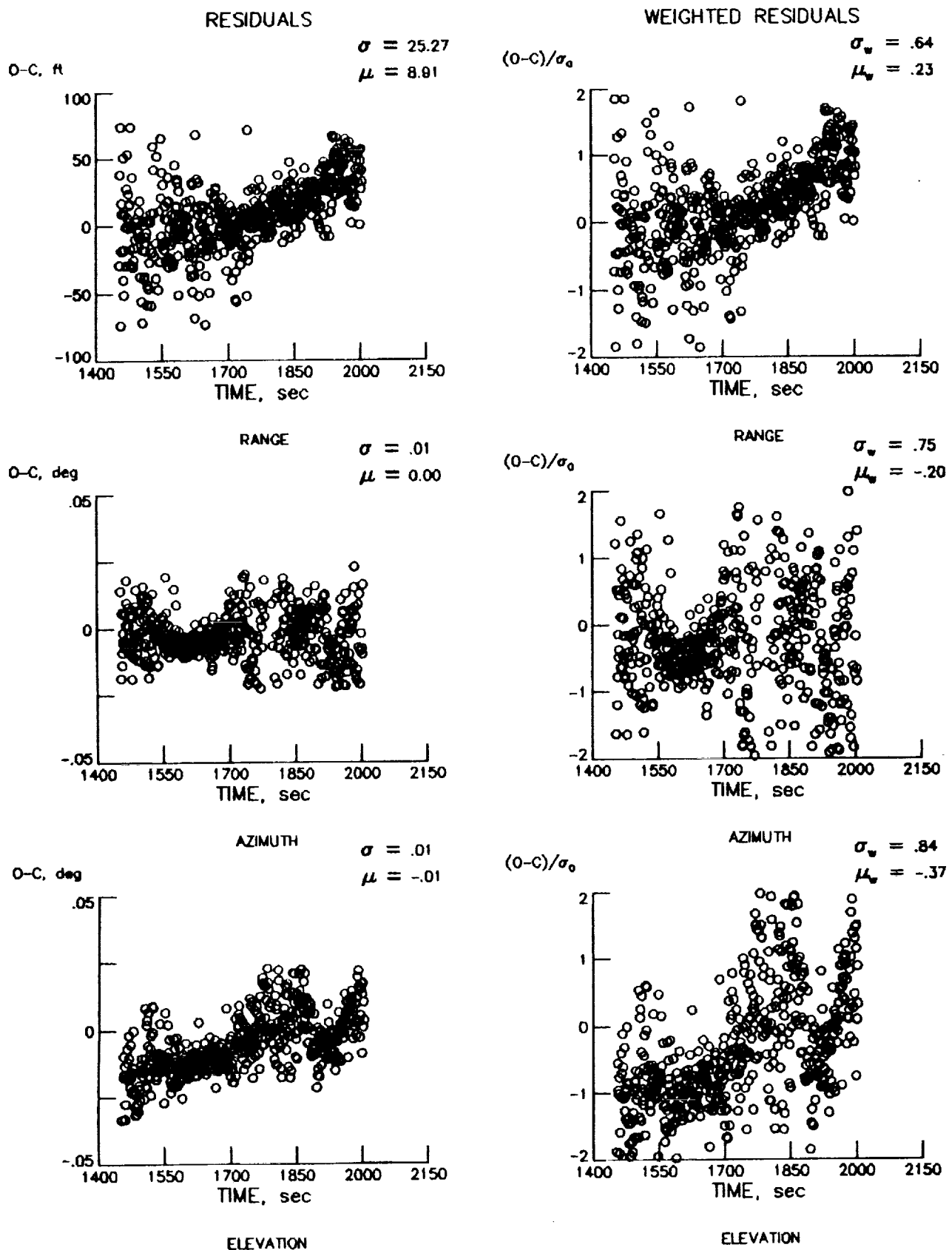


Figure A-9. Final Edwards residuals, EFFC.

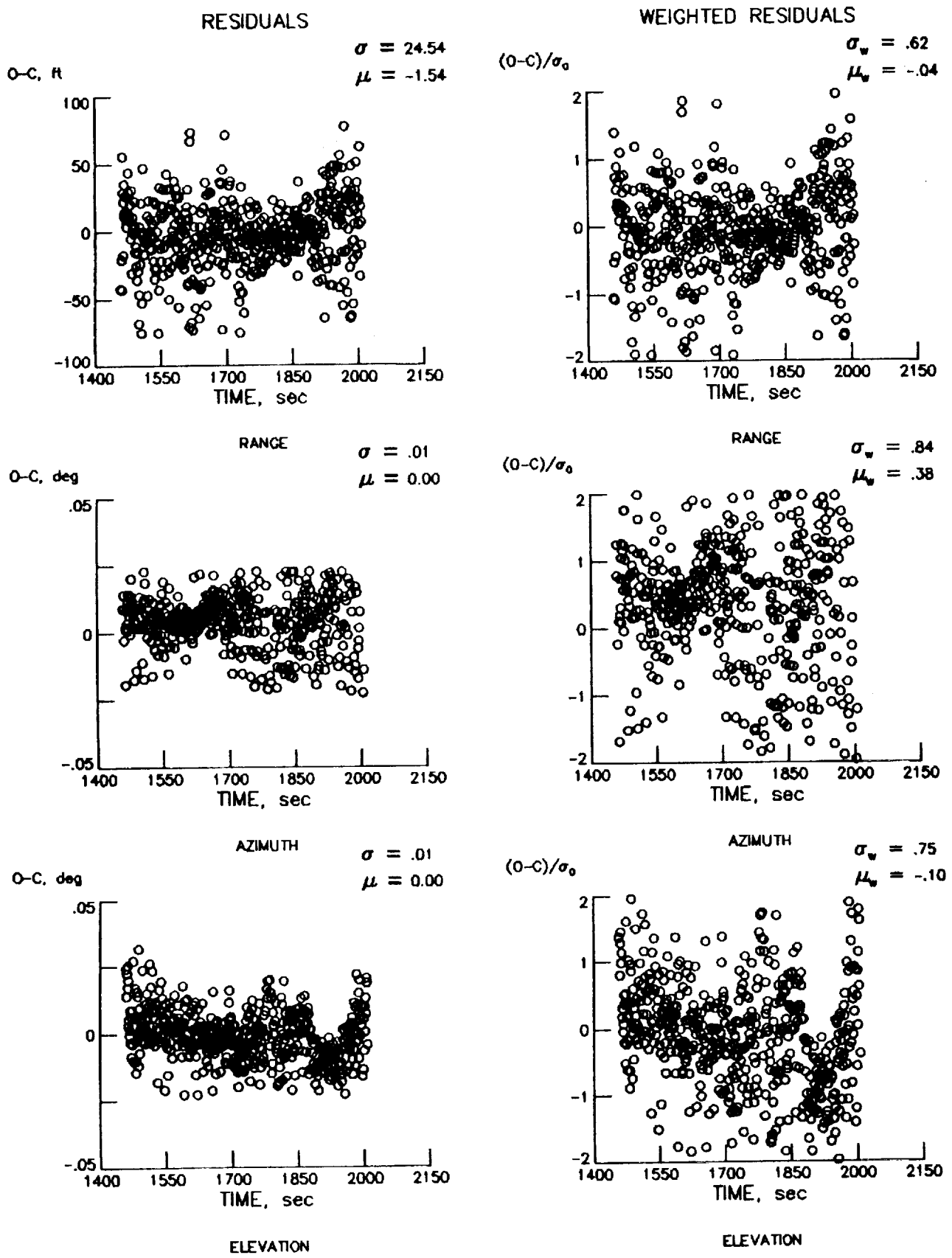


Figure A-10. Final Dryden residuals, FRCC.

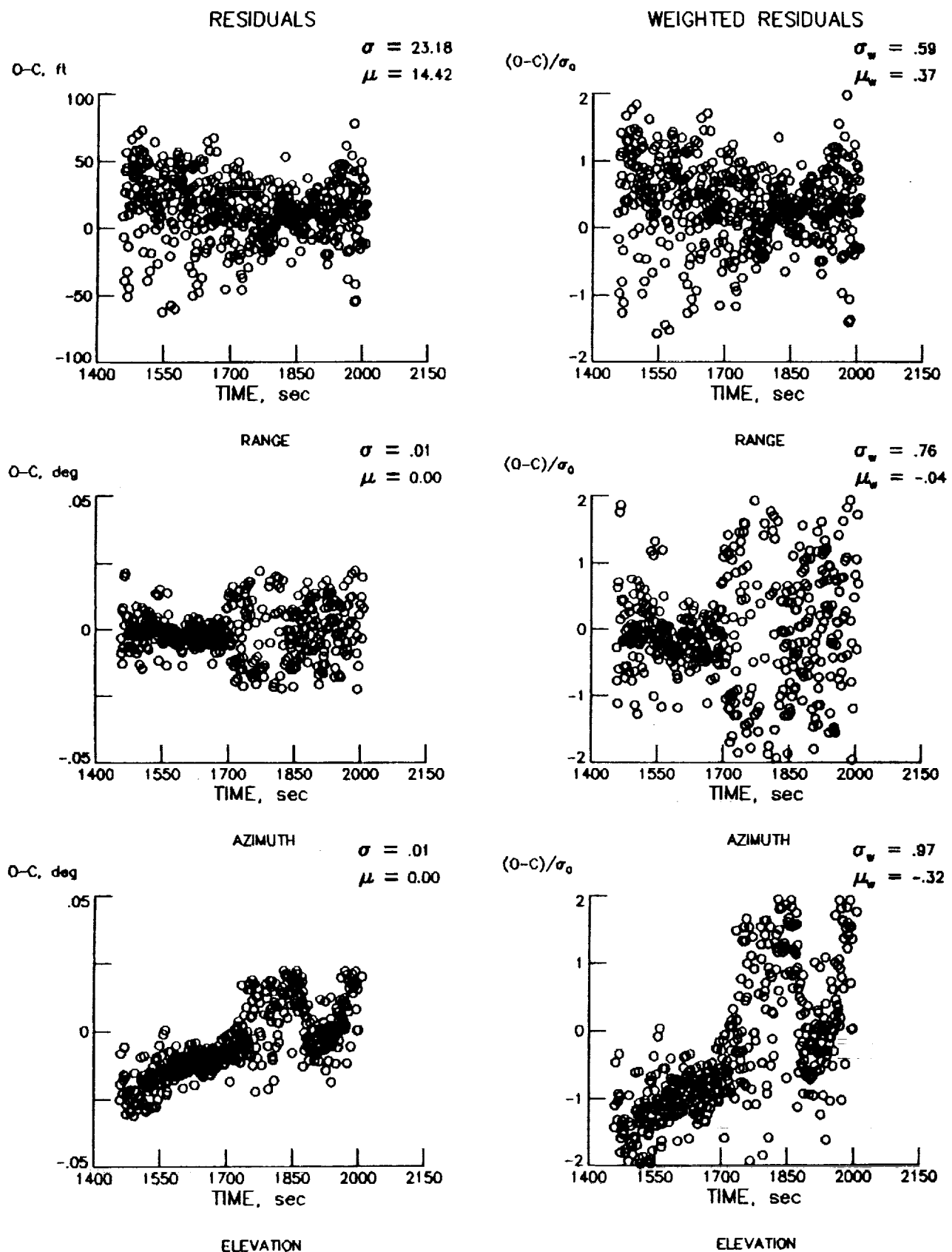


Figure A-11. Final Dryden residuals, FRFC.

## **APPENDIX B**

### **LISTING OF TRAJECTORY AND AIR-DATA PARAMETERS FOR THE STS-35 COLUMBIA OEX ENTRY MISSION**

TIME (sec)	ALTDE (ft)	VEL A (fps)	GAM A (deg)	HDG A (deg)	SIGMA (deg)	BETA (deg)	ALPHA (deg)	MACH	QBAR (psf)	VBAR	RNUM
0	513594	24357.7	-1.515	60.74	0.03	0.28	39.59				
2	512327	24359.3	-1.514	60.76	-0.11	0.16	39.67				
4	511062	24360.9	-1.513	60.78	-0.27	-0.01	39.77				
6	509797	24362.5	-1.512	60.80	-0.43	-0.18	39.86				
8	508533	24364.1	-1.511	60.82	-0.57	-0.35	39.96				
10	507270	24365.7	-1.510	60.84	-0.72	-0.50	40.08				
12	506008	24367.3	-1.509	60.86	-0.59	-0.41	40.23				
14	504746	24368.9	-1.508	60.87	-0.44	-0.29	40.39				
16	503486	24370.4	-1.508	60.89	-0.30	-0.18	40.56				
18	502226	24372.0	-1.507	60.91	-0.16	-0.06	40.74				
20	500967	24373.6	-1.506	60.93	-0.02	0.05	40.93				
22	499709	24375.2	-1.505	60.95	0.11	0.17	41.13				
24	498452	24376.7	-1.504	60.97	0.24	0.29	41.26				
26	497196	24378.3	-1.503	60.99	0.29	0.33	41.29				
28	495941	24379.9	-1.502	61.01	0.11	0.15	41.28				
30	494686	24381.4	-1.501	61.03	-0.08	-0.02	41.24				
32	493433	24383.0	-1.500	61.05	-0.26	-0.20	41.17				
34	492181	24384.6	-1.499	61.07	-0.44	-0.37	41.09				
36	490929	24386.2	-1.498	61.09	-0.57	-0.49	41.02				
38	489679	24387.8	-1.497	61.11	-0.36	-0.27	40.96				
40	488429	24389.3	-1.496	61.13	-0.14	-0.06	40.88				
42	487180	24390.9	-1.494	61.16	0.08	0.16	40.82				
44	485933	24392.5	-1.493	61.18	0.19	0.29	40.77				
46	484686	24394.0	-1.492	61.20	0.20	0.31	40.75				
48	483440	24395.6	-1.491	61.22	0.19	0.32	40.74				
50	482195	24397.1	-1.490	61.24	0.20	0.35	40.73				
52	480952	24398.7	-1.489	61.26	0.20	0.36	40.73				
54	479709	24400.3	-1.488	61.29	0.15	0.14	40.74				
56	478467	24401.8	-1.487	61.31	0.09	-0.08	40.75				
58	477226	24403.4	-1.486	61.33	0.03	-0.30	40.77				
60	475986	24404.9	-1.485	61.35	0.01	-0.31	40.81				
62	474748	24406.5	-1.484	61.38	-0.00	-0.29	40.84				
64	473510	24408.0	-1.482	61.40	-0.03	-0.28	40.87				
66	472273	24409.6	-1.481	61.42	-0.05	-0.26	40.93				
68	471038	24411.1	-1.480	61.44	-0.07	-0.24	40.98				
70	469803	24412.7	-1.479	61.47	-0.09	-0.23	41.05				
72	468569	24414.2	-1.478	61.49	-0.12	-0.22	41.03				
74	467337	24415.8	-1.477	61.51	-0.15	-0.20	40.99				
76	466106	24417.3	-1.475	61.54	-0.20	-0.19	40.97				
78	464875	24418.9	-1.474	61.56	-0.23	-0.18	40.92				
80	463646	24420.4	-1.473	61.59	-0.27	-0.17	40.85				
82	462418	24421.9	-1.472	61.61	-0.32	-0.17	40.79				
84	461191	24423.5	-1.471	61.63	-0.37	-0.16	40.74				
86	459965	24425.0	-1.469	61.66	-0.40	-0.15	40.69				
88	458740	24426.6	-1.468	61.68	-0.48	-0.15	40.65				
90	457516	24428.1	-1.467	61.71	-0.53	-0.15	40.62				
92	456294	24429.6	-1.466	61.73	-0.60	-0.15	40.59				
94	455072	24431.2	-1.464	61.76	-0.67	-0.15	40.58				
96	453852	24432.7	-1.463	61.78	-0.73	-0.14	40.57				
98	452633	24434.2	-1.462	61.81	-0.81	-0.15	40.58				
100	451415	24435.8	-1.461	61.83	-0.88	-0.15	40.58				
102	450198	24437.3	-1.459	61.86	-0.97	-0.16	40.60				
104	448982	24438.8	-1.458	61.89	-1.04	-0.16	40.62				
106	447768	24440.3	-1.457	61.91	-1.13	-0.17	40.66				
108	446554	24441.9	-1.455	61.94	-1.21	-0.17	40.70				
110	445342	24443.4	-1.454	61.97	-1.30	-0.17	40.75				

Table B-1. STS-35 trajectory and air-data parameters.

TIME (sec)	ALTDE (ft)	VEL A (fps)	GAM A (deg)	HDG A (deg)	SIGMA (deg)	BETA (deg)	ALPHA (deg)	MACH	QBAR (psf)	VBAR	RNUM
112	444131	24444.9	-1.453	61.99	-1.40	-0.19	40.80				
114	442921	24446.4	-1.451	62.02	-1.50	-0.27	40.86				
116	441712	24448.0	-1.450	62.05	-1.57	-0.44	40.94				
118	440505	24449.5	-1.449	62.07	-1.31	-0.32	41.02				
120	439299	24451.0	-1.447	62.10	-1.06	-0.18	41.06				
122	438094	24452.5	-1.446	62.13	-0.80	-0.05	41.04				
124	436890	24454.0	-1.444	62.15	-0.56	0.09	40.95				
126	435688	24455.5	-1.443	62.18	-0.32	0.21	40.87				
128	434487	24457.0	-1.441	62.21	-0.08	0.34	40.81				
130	433287	24458.5	-1.440	62.24	-0.10	0.22	40.78				
132	432088	24460.0	-1.439	62.27	-0.17	0.06	40.75				
134	430891	24461.5	-1.437	62.29	-0.23	-0.10	40.74				
136	429695	24463.0	-1.436	62.32	-0.31	-0.27	40.73				
138	428500	24464.5	-1.434	62.35	-0.38	-0.41	40.72				
140	427306	24466.0	-1.433	62.38	-0.41	-0.34	40.73				
142	426114	24467.5	-1.431	62.41	-0.44	-0.25	40.74				
144	424923	24469.0	-1.430	62.44	-0.47	-0.17	40.76				
146	423734	24470.5	-1.428	62.47	-0.51	-0.09	40.78				
148	422545	24472.0	-1.427	62.50	-0.54	-0.01	40.82				
150	421358	24473.5	-1.425	62.53	-0.60	0.06	40.86				
152	420173	24475.0	-1.424	62.56	-0.64	0.13	40.91				
154	418988	24476.4	-1.423	62.58	-0.70	0.15	40.96				
156	417805	24477.9	-1.421	62.61	-0.81	-0.03	41.03				
158	416623	24479.4	-1.419	62.64	-0.92	-0.21	41.04				
160	415443	24480.9	-1.418	62.68	-1.03	-0.39	40.99				
162	414264	24482.4	-1.416	62.71	-0.96	-0.37	40.95				
164	413087	24483.9	-1.415	62.74	-0.77	-0.26	40.90				
166	411910	24485.3	-1.413	62.77	-0.58	-0.14	40.85				
168	410736	24486.8	-1.412	62.80	-0.40	-0.03	40.82				
170	409562	24488.3	-1.410	62.83	-0.21	0.08	40.79				
172	408390	24489.7	-1.408	62.86	-0.04	0.20	40.76				
174	407220	24491.2	-1.407	62.89	0.13	0.30	40.75				
176	406050	24492.7	-1.405	62.92	0.24	0.35	40.75				
178	404883	24494.2	-1.404	62.95	0.19	0.26	40.77				
180	403716	24495.6	-1.402	62.99	0.15	0.18	40.80				
182	402551	24497.1	-1.400	63.02	0.11	0.09	40.83				
184	401388	24498.5	-1.399	63.05	0.06	-0.00	40.88				
186	400226	24500.0	-1.397	63.08	0.01	-0.09	40.92	18.45	0.01	0.8681	2.08E+02
188	399065	24530.0	-1.394	63.08	-0.05	-0.23	40.98	18.56	0.01	0.8536	2.17E+02
190	397906	24532.6	-1.392	63.11	-0.11	-0.32	41.04	18.68	0.01	0.8359	2.29E+02
192	396748	24535.2	-1.390	63.14	-0.16	-0.42	41.00	18.80	0.01	0.8186	2.41E+02
194	395592	24537.8	-1.388	63.18	-0.22	-0.50	40.96	18.93	0.01	0.8016	2.54E+02
196	394437	24540.3	-1.387	63.21	-0.25	-0.39	40.92	19.05	0.01	0.7850	2.67E+02
198	393284	24542.5	-1.385	63.25	-0.26	-0.23	40.89	19.18	0.02	0.7683	2.82E+02
200	392132	24544.6	-1.383	63.29	-0.29	-0.09	40.86	19.30	0.02	0.7515	2.97E+02
202	390982	24546.7	-1.382	63.33	-0.33	0.06	40.84	19.43	0.02	0.7352	3.14E+02
204	389833	24548.7	-1.380	63.37	-0.36	0.21	40.83	19.56	0.02	0.7192	3.31E+02
206	388686	24550.8	-1.378	63.41	-0.43	0.23	40.82	19.69	0.02	0.7035	3.50E+02
208	387540	24552.9	-1.376	63.45	-0.56	-0.01	40.82	19.82	0.02	0.6879	3.70E+02
210	386396	24554.9	-1.374	63.48	-0.68	-0.25	40.81	19.96	0.02	0.6721	3.91E+02
212	385253	24557.0	-1.373	63.52	-0.76	-0.45	40.83	20.09	0.02	0.6567	4.14E+02
214	384112	24559.1	-1.371	63.56	-0.49	-0.31	40.89	20.23	0.02	0.6417	4.38E+02
216	382972	24561.2	-1.369	63.59	-0.23	-0.17	40.95	20.36	0.02	0.6271	4.64E+02
218	381834	24563.6	-1.367	63.63	0.04	-0.01	41.02	20.50	0.02	0.6126	4.91E+02
220	380697	24568.1	-1.365	63.67	0.31	0.13	40.91	20.64	0.03	0.5981	5.21E+02

Table B-1. (continued)





























TIME (sec)	ALTDE (ft)	VEL A (fps)	GAM A (deg)	HDG A (deg)	SIGMA (deg)	BETA (deg)	ALPHA (deg)	MACH	QBAR (psf)	VBAR	RNUM
1762	60326	1358.8	-13.806	83.82	-2.14	0.14	8.38	1.44	222.61		1.21E+08
1764	59679	1338.6	-14.013	83.75	-3.87	-0.31	8.17	1.42	223.64		1.23E+08
1766	59031	1318.0	-14.239	83.77	-1.73	-0.46	8.06	1.40	224.44		1.26E+08
1768	58385	1297.1	-14.440	83.89	0.74	-0.05	7.99	1.38	224.80		1.28E+08
1770	57739	1276.2	-14.645	83.94	0.06	0.13	7.88	1.36	224.83		1.30E+08
1772	57096	1255.0	-14.832	83.94	-0.04	-0.01	7.86	1.33	224.64		1.32E+08
1774	56456	1234.3	-15.008	84.09	2.59	0.46	7.72	1.31	224.47		1.35E+08
1776	55820	1214.3	-15.168	84.25	1.51	0.69	7.60	1.29	224.39		1.37E+08
1778	55187	1192.9	-15.339	84.19	-0.60	0.18	7.61	1.27	223.56		1.39E+08
1780	54560	1171.1	-15.507	84.09	-0.25	-0.20	7.57	1.24	222.37		1.41E+08
1782	53937	1149.2	-15.654	84.10	1.59	-0.11	7.58	1.22	220.93		1.42E+08
1784	53321	1127.4	-15.783	84.26	3.18	0.37	7.52	1.20	219.32		1.44E+08
1786	52712	1106.4	-15.904	84.48	1.93	0.84	7.50	1.18	217.78		1.46E+08
1788	52111	1086.1	-15.913	84.46	-2.41	0.55	7.68	1.15	216.28		1.47E+08
1790	51523	1066.2	-15.864	84.30	-3.96	0.35	7.83	1.13	214.29		1.48E+08
1792	50947	1046.9	-15.830	84.12	-4.72	0.00	7.63	1.11	211.71		1.49E+08
1794	50381	1027.8	-15.889	83.92	-3.68	-0.41	7.45	1.09	209.03		1.49E+08
1796	49822	1008.4	-16.035	83.85	-1.80	-0.50	7.29	1.06	206.04		1.49E+08
1798	49268	989.6	-16.246	83.90	-1.64	-0.36	7.25	1.04	203.17		1.50E+08
1800	48716	971.9	-16.485	83.92	-1.70	-0.17	7.34	1.02	200.58		1.50E+08
1802	48166	955.9	-16.692	83.97	-0.16	0.18	7.39	1.00	198.25		1.50E+08
1804	47619	941.5	-16.896	84.11	0.07	0.57	7.49	0.98	196.50		1.50E+08
1806	47073	929.1	-17.120	84.16	-1.64	0.62	7.42	0.97	195.49		1.51E+08
1808	46524	919.3	-17.466	84.11	-2.16	0.39	7.28	0.96	195.54		1.52E+08
1810	45970	912.4	-17.807	84.03	-0.85	-0.11	7.52	0.95	196.82		1.53E+08
1812	45414	904.6	-17.819	84.13	0.51	-0.18	8.03	0.94	197.85		1.55E+08
1814	44864	896.8	-17.788	84.26	0.20	-0.11	8.20	0.93	198.88		1.56E+08
1816	44323	888.5	-17.506	84.39	-0.01	0.14	8.75	0.92	199.53		1.58E+08
1818	43797	880.2	-17.112	84.55	0.39	0.33	8.88	0.91	200.01		1.59E+08
1820	43288	872.3	-16.724	84.82	0.72	0.68	8.73	0.90	201.05		1.61E+08
1822	42793	865.5	-16.473	85.05	0.60	0.75	8.36	0.89	202.43		1.64E+08
1824	42306	859.6	-16.425	85.22	0.08	0.44	7.78	0.88	203.68		1.65E+08
1826	41820	854.7	-16.517	85.43	0.48	0.40	7.89	0.88	205.31		1.67E+08
1828	41338	850.3	-16.416	85.40	-0.97	0.25	7.69	0.87	207.10		1.69E+08
1830	40858	847.4	-16.444	85.21	-2.15	-0.22	7.50	0.86	209.60		1.71E+08
1832	40378	844.8	-16.651	84.77	-4.62	-0.80	6.78	0.86	212.35		1.73E+08
1834	39891	842.3	-16.901	84.35	-3.10	-0.69	7.08	0.86	215.26		1.76E+08
1836	39402	838.4	-16.940	83.99	-3.96	-0.54	7.21	0.85	217.29		1.78E+08
1838	38915	834.0	-16.928	83.54	-5.21	-0.46	7.10	0.84	219.00		1.80E+08
1840	38431	830.4	-16.995	83.19	-4.49	-0.22	6.86	0.84	221.06		1.81E+08
1842	37947	826.7	-17.000	83.11	0.33	-0.18	6.47	0.83	222.99		1.83E+08
1844	37462	823.5	-17.196	83.48	4.49	0.16	6.46	0.83	225.46		1.85E+08
1846	36975	820.6	-17.328	83.98	4.10	0.42	6.41	0.83	228.18		1.88E+08
1848	36487	817.7	-17.400	84.29	3.44	0.18	6.42	0.82	230.97		1.90E+08
1850	35999	814.6	-17.474	84.50	3.94	-0.08	6.26	0.82	233.60		1.93E+08
1852	35511	811.3	-17.483	84.80	4.57	-0.08	6.28	0.81	236.33		1.95E+08
1854	35026	808.7	-17.409	85.28	8.04	0.14	6.13	0.81	239.60		1.99E+08
1856	34542	807.3	-17.500	86.21	12.35	0.21	6.04	0.81	243.43		2.02E+08
1858	34057	806.2	-17.465	86.75	0.94	0.20	6.09	0.80	247.31		2.05E+08
1860	33576	803.4	-17.433	86.72	-1.64	0.21	5.85	0.80	250.04		2.07E+08
1862	33095	798.6	-17.526	86.51	-7.39	0.49	5.72	0.79	251.14		2.08E+08
1864	32614	791.7	-17.812	85.37	-21.55	0.35	5.84	0.78	250.96		2.09E+08
1866	32128	781.0	-18.091	82.98	-31.21	-0.17	6.58	0.77	248.51		2.09E+08
1868	31642	769.6	-18.594	79.85	-38.42	-0.31	6.51	0.76	245.54		2.09E+08
1870	31145	759.3	-19.490	76.10	-46.75	-0.59	6.59	0.75	243.05		2.09E+08

Table B-1. (continued)

TIME (sec)	ALTDE (ft)	VEL A (fps)	GAM A (deg)	HIDG A (deg)	SIGMA (deg)	BETA (deg)	ALPHA (deg)	MACH	QBAR (psf)	VBAR	RNUM
1872	30628	750.8	-20.725	71.62	-55.83	-0.75	7.41	0.74	241.81		2.10E+08
1874	30086	741.6	-22.035	65.58	-62.11	-0.28	9.32	0.73	240.67		2.11E+08
1876	29517	734.9	-23.484	58.79	-63.11	-0.01	9.86	0.72	242.61		2.15E+08
1878	28923	729.5	-24.583	51.45	-61.98	-0.31	9.75	0.72	247.43		2.22E+08
1880	28310	729.2	-25.279	44.32	-58.43	-0.51	9.36	0.72	253.26		2.27E+08
1882	27687	730.2	-25.460	37.88	-51.78	-0.40	8.88	0.72	259.18		2.31E+08
1884	27066	728.9	-25.222	31.70	-50.50	-0.39	8.80	0.71	263.54		2.34E+08
1886	26451	725.6	-25.144	25.91	-50.23	-0.41	8.68	0.71	266.31		2.36E+08
1888	25841	720.8	-25.059	20.27	-50.19	0.05	9.18	0.70	267.95		2.38E+08
1890	25237	715.0	-25.048	14.80	-46.93	0.42	8.87	0.69	268.81		2.39E+08
1892	24642	708.2	-24.677	9.81	-42.11	0.47	9.00	0.68	268.76		2.40E+08
1894	24064	699.7	-24.111	5.20	-39.06	0.68	8.75	0.67	267.01		2.40E+08
1896	23506	692.2	-23.613	1.16	-36.03	0.81	8.48	0.66	265.88		2.41E+08
1898	22964	685.5	-23.063	-2.43	-33.20	1.17	8.28	0.66	265.14		2.41E+08
1900	22439	678.9	-22.594	-5.98	-31.70	0.76	7.92	0.65	264.58		2.42E+08
1902	21929	672.9	-22.132	-9.40	-30.07	0.33	7.71	0.64	264.39		2.44E+08
1904	21434	666.9	-21.456	-13.30	-35.81	-0.29	8.49	0.63	263.80		2.44E+08
1906	20961	660.6	-20.888	-18.53	-44.09	-0.38	8.04	0.63	262.47		2.44E+08
1908	20493	656.7	-21.198	-24.47	-51.22	-0.26	7.89	0.62	263.19		2.46E+08
1910	20015	654.9	-21.845	-30.81	-51.38	-0.36	8.24	0.62	265.70		2.48E+08
1912	19529	652.8	-21.970	-36.91	-46.74	0.00	8.81	0.62	268.40		2.51E+08
1914	19046	650.3	-21.936	-42.55	-45.09	0.29	8.70	0.61	270.97		2.54E+08
1916	18564	647.6	-21.847	-48.13	-43.78	0.17	8.61	0.61	273.18		2.56E+08
1918	18088	645.0	-21.590	-53.74	-42.34	-0.07	8.07	0.61	275.14		2.58E+08
1920	17618	643.2	-21.453	-58.86	-39.97	0.01	8.01	0.60	277.75		2.61E+08
1922	17154	641.0	-20.941	-64.01	-38.18	0.27	8.61	0.60	280.07		2.63E+08
1924	16710	637.5	-19.904	-69.27	-35.90	0.25	8.71	0.60	281.08		2.65E+08
1926	16292	633.4	-18.617	-74.04	-32.08	0.38	8.16	0.59	281.21		2.66E+08
1928	15898	630.3	-17.764	-77.88	-28.99	0.45	8.51	0.59	282.04		2.68E+08
1930	15537	623.4	-15.767	-82.04	-27.69	0.60	9.41	0.58	279.08		2.67E+08
1932	15221	614.5	-13.976	-85.98	-27.10	0.59	8.84	0.57	274.03		2.66E+08
1934	14939	606.1	-12.905	-89.52	-26.37	0.44	8.10	0.56	269.04		2.64E+08
1936	14677	597.6	-12.082	-92.94	-26.87	0.31	8.78	0.56	263.81		2.63E+08
1938	14440	587.6	-11.159	-96.75	-29.99	-0.05	8.13	0.55	257.14		2.60E+08
1940	14216	578.7	-10.898	-100.71	-31.57	-0.13	8.38	0.54	251.34		2.58E+08
1942	13999	571.8	-10.886	-104.65	-30.74	-0.06	8.26	0.53	247.30		2.57E+08
1944	13783	567.3	-10.993	-108.26	-27.19	0.02	8.23	0.53	245.22		2.56E+08
1946	13566	564.4	-10.924	-111.39	-20.88	-0.02	8.26	0.52	244.60		2.57E+08
1948	13354	561.9	-10.598	-113.60	-11.80	-0.06	8.21	0.52	244.34		2.58E+08
1950	13152	559.0	-9.989	-114.80	-6.27	-0.30	8.10	0.52	243.57		2.58E+08
1952	12960	556.2	-9.885	-115.49	-4.78	-0.22	7.25	0.52	242.79		2.58E+08
1954	12765	553.8	-10.133	-116.17	-6.84	-0.42	7.25	0.51	242.46		2.59E+08
1956	12564	552.0	-10.736	-117.05	-8.64	-0.22	6.95	0.51	242.21		2.59E+08
1958	12353	550.8	-11.272	-117.88	-7.73	0.22	6.88	0.51	242.55		2.60E+08
1960	12129	550.2	-12.015	-118.73	-8.72	0.37	6.90	0.51	243.53		2.61E+08
1962	11892	550.2	-12.676	-119.80	-10.48	0.26	6.96	0.51	245.19		2.62E+08
1964	11644	550.8	-13.207	-120.95	-9.07	0.26	7.02	0.51	247.48		2.64E+08
1966	11387	551.6	-13.503	-122.01	-7.88	0.09	7.35	0.51	250.17		2.66E+08
1968	11127	552.0	-13.498	-123.00	-6.49	-0.14	7.40	0.51	252.48		2.67E+08
1970	10868	551.9	-13.414	-123.52	-1.09	-0.03	7.31	0.51	254.38		2.69E+08
1972	10610	551.5	-13.643	-123.55	0.52	0.07	6.61	0.51	256.04		2.71E+08
1974	10343	551.9	-14.159	-123.53	0.85	0.14	6.56	0.51	258.36		2.72E+08
1976	10066	552.5	-14.698	-123.56	0.92	-0.04	6.55	0.51	261.03		2.74E+08
1978	9783	552.1	-14.528	-123.45	1.60	-0.10	7.37	0.50	262.84		2.76E+08
1980	9512	549.7	-14.022	-123.21	1.63	0.05	6.67	0.50	262.75		2.77E+08

Table B-1. (continued)

TIME (sec)	ALTDE (ft)	VEL A (fps)	GAM A (deg)	HDG A (deg)	SIGMA (deg)	BETA (deg)	ALPHA (deg)	MACH	QBAR (psf)	VBAR	RNUM
1982	9243	548.2	-14.172	-123.07	1.19	-0.01	6.32	0.50	263.49		2.78E+08
1984	8969	547.9	-14.654	-122.97	1.03	-0.18	6.06	0.50	265.42		2.80E+08
1986	8684	548.7	-15.316	-122.85	0.58	-0.19	5.81	0.50	268.56		2.82E+08
1988	8384	550.6	-16.238	-122.79	0.31	-0.11	5.68	0.50	272.99		2.85E+08
1990	8068	552.6	-16.852	-122.75	0.39	-0.19	5.89	0.50	277.68		2.89E+08
1992	7739	554.2	-17.315	-122.55	1.26	0.16	6.24	0.50	282.16		2.92E+08
1994	7408	555.0	-17.269	-122.53	0.77	0.03	6.12	0.50	285.57		2.95E+08
1996	7079	554.9	-17.039	-122.57	0.60	-0.29	6.09	0.50	288.14		2.97E+08
1998	6755	553.5	-16.716	-122.50	1.11	-0.38	6.09	0.50	289.34		2.98E+08
2000	6439	549.9	-16.365	-122.38	1.79	-0.21	6.17	0.50	288.04		2.98E+08
2002	6132	545.9	-16.043	-122.25	0.12	-0.13	6.01	0.49	286.09		2.97E+08
2004	5831	542.9	-15.906	-122.46	-1.76	0.03	5.88	0.49	285.24		2.97E+08
2006	5531	541.0	-16.067	-122.52	-1.95	0.39	5.95	0.49	286.09		2.99E+08
2008	5232	539.4	-15.757	-122.55	-0.92	0.47	6.16	0.49	287.37		3.01E+08
2010	4940	537.5	-15.612	-122.40	-0.25	0.48	5.88	0.48	288.39		3.03E+08
2012	4649	536.7	-15.631	-122.24	0.30	0.60	6.27	0.48	290.44		3.06E+08
2014	4361	535.6	-15.386	-122.05	0.72	0.79	6.08	0.48	292.05		3.08E+08
2016	4076	534.4	-15.353	-122.12	-0.07	0.37	5.82	0.48	293.43		3.10E+08
2018	3790	533.0	-15.522	-122.22	0.69	-0.09	6.02	0.48	294.69		3.12E+08
2020	3505	530.1	-15.189	-122.25	1.82	-0.71	6.60	0.48	294.57		3.13E+08
2022	3230	527.2	-14.782	-121.80	3.59	-0.39	6.73	0.47	294.25		3.15E+08
2024	2971	523.1	-13.602	-121.35	1.50	-0.13	7.12	0.47	292.42		3.15E+08
2026	2736	517.1	-11.862	-121.27	-0.24	0.30	8.09	0.46	288.50		3.15E+08
2028	2539	507.3	-10.044	-121.59	-3.26	0.25	8.27	0.46	281.48		3.15E+08
2030	2381	495.4	-8.110	-122.14	-1.22	0.17	8.20	0.45	271.48		3.12E+08
2032	2259	479.2	-5.747	-122.54	-0.13	-0.21	9.56	0.43	256.38		3.06E+08
2034	2189	459.1	-2.722	-122.32	3.10	-0.09	9.52	0.42	236.60		2.95E+08
2036	2156	441.2	-1.518	-121.71	3.91	-0.07	8.96	0.40	218.87		2.85E+08
2038	2137	424.0	-0.958	-121.29	0.14	-0.13	8.63	0.38	202.40		2.74E+08
2040	2121	408.6	-1.026	-121.32	-1.18	0.10	9.30	0.37	188.35		2.65E+08
2042	2109	393.0	-0.326	-121.63	-2.74	0.36	9.26	0.36	174.75		2.56E+08
2044	2107	378.1	0.150	-122.07	-1.02	0.37	8.68	0.34	161.88		2.46E+08

Table B-1. (concluded)

REPORT DOCUMENTATION PAGE			Form Approved OMB No. 0704-0188
<p>Public reporting burden for this collection of information is estimated to average 1 hour per response, including the time for reviewing instructions, searching existing data sources, gathering and maintaining the data needed, and completing and reviewing the collection of information. Send comments regarding this burden estimate or any other aspect of this collection of information, including suggestions for reducing this burden, to Washington Headquarters Services, Directorate for Information Operations and Reports, 1215 Jefferson Davis Highway, Suite 1204, Arlington, VA 22202-4302, and to the Office of Management and Budget, Paperwork Reduction Project (0704-0188), Washington, DC 20503.</p>			
1. AGENCY USE ONLY (Leave blank)	2. REPORT DATE November 1991	3. REPORT TYPE AND DATES COVERED Contractor Report	
4. TITLE AND SUBTITLE  Final STS-35 "Columbia" Descent BET Products and Results for LaRC OEX Investigations		5. FUNDING NUMBERS  C NAS1-18937 WU 506-48-11-01	
6. AUTHOR(S)  Kevin F. Oakes, John T. Findlay, Rachel A. Jasinski, and James S. Wood			
7. PERFORMING ORGANIZATION NAME(S) AND ADDRESS(ES)  Flight Mechanics & Control, Inc. 47 East Queen's Way Hampton, VA 23669		8. PERFORMING ORGANIZATION REPORT NUMBER	
9. SPONSORING/MONITORING AGENCY NAME(S) AND ADDRESS(ES)  National Aeronautics and Space Administration Langley Research Center Hampton, VA 23665-5225		10. SPONSORING/MONITORING AGENCY REPORT NUMBER  NASA CR-189569	
11. SUPPLEMENTARY NOTES  Langley Technical Monitor: Paul M. Siemers III			
12a. DISTRIBUTION/AVAILABILITY STATEMENT  Unclassified - Unlimited  Subject Category 19		12b. DISTRIBUTION CODE	
13. ABSTRACT	<p>Final STS-35 "Columbia" descent Best Estimate Trajectory products have been developed for LaRC Orbiter Experiments investigations. Included are the reconstructed inertial trajectory profile; the Extended BET, which combines the inertial data and, in this instance, the National Weather Service atmospheric information obtained via Johnson Space Center; and the Aerodynamic BET. The inertial BET utilized IMU dynamic measurements for deterministic propagation during the ENTREE estimation process. The final estimate was based on the considerable ground-based C-band tracking coverage available as well as TDRSS Doppler data, a unique use of the latter for endo-atmospheric flight determinations. The actual estimate required simultaneous solutions for the spacecraft position and velocity, spacecraft attitude, and six IMU parameters - three gyro biases and three accelerometer scale-factor correction terms. The anchor epoch for this analysis was 19,200 GMT seconds (December 11, 1990) which corresponds to an initial Shuttle altitude of approximately 513 kft. The atmospheric data incorporated were evaluated based on Shuttle-derived considerations as well as comparisons versus the GRAM and AF78 reference models. The AEROBET was developed based on the Extended BET, the measured spacecraft configuration information, final mass properties, and the final Orbiter pre-operational databook. The latter was updated based on aerodynamic consensus incrementals defined by the latest published FAD. The rectified predictions were compared versus the flight computed values and the resultant differences were correlated versus ensemble results from twenty-two previous STS entry flights.</p>		
14. SUBJECT TERMS	15. NUMBER OF PAGES 93		
Orbiter Experiments; Best Estimate Trajectory; Endo-atmospheric Flight; Trajectory Reconstruction; Atmospheric Evaluations; Aerodynamic Comparisons; TDRSS Doppler; C-Band Tracking		16. PRICE CODE A05	
17. SECURITY CLASSIFICATION OF REPORT Unclassified	18. SECURITY CLASSIFICATION OF THIS PAGE Unclassified	19. SECURITY CLASSIFICATION OF ABSTRACT	20. LIMITATION OF ABSTRACT

